# Investigation of Ferromagnetic / Antiferromagnetic Interfaces

## with Magnetization-Induced Second Harmonic Generation

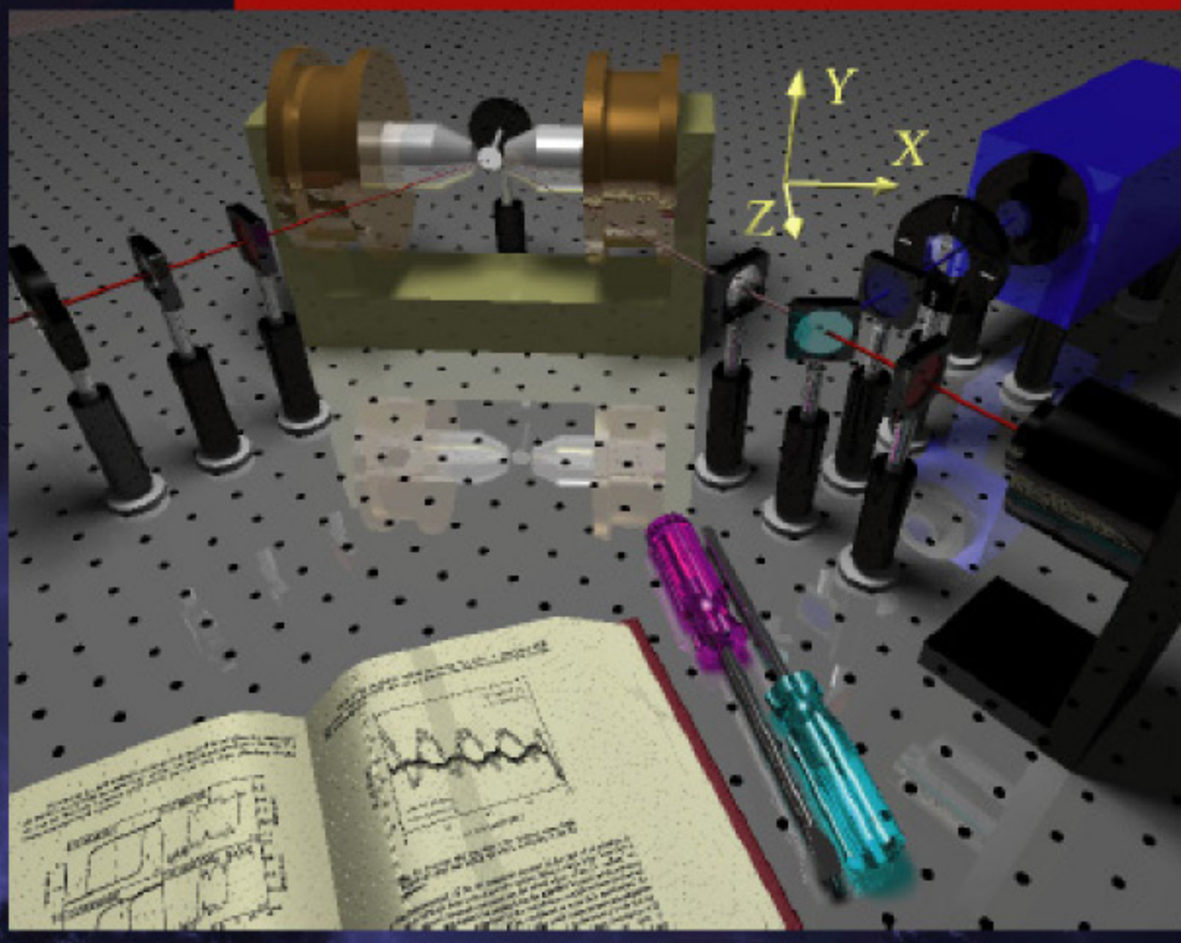


V. K. Valev

Printed by PrintPartners Ipskamp, Enschede
ISBN-10: 90-9021353-8
ISBN-13: 978-90-9021353-8

Illustrated with references
Cover design by V. K. Valev
An electronic version of this thesis can be found at:
http://www.valev.org

# Investigation of Ferromagnetic/Antiferromagnetic Interfaces with Magnetization–Induced Second Harmonic Generation

een wetenschappelijke proeve op het gebied van
de Natuurwetenschappen, Wiskunde en Informatica

Proefschrift

ter verkrijging van de graad van doctor
aan de Radboud Universiteit Nijmegen
op gezag van de Rector Magnificus prof. dr. C.W.P.M. Blom,
volgens besluit van het College van Decanen
in het openbaar te verdedigen op
woensdag 6 december 2006,
des namiddags om 15.30 uur

door

Ventsislav Kolev Valev

geboren op 31 Augustus 1976
te Silistra, Bulgarije

**Promotor:** Prof. dr. Th. Rasing

**Co-promotor:** Dr. A. Kirilyuk

**Manuscriptcommisie:**

| | |
|---|---|
| Prof. dr. J. Ferré | Laboratoire de Physique des Solides<br>Université Paris-Sud XI<br>Orsay, France |
| Prof. dr. G. Luepke | Department of Applied Sciences<br>College of William and Mary<br>Williamsburg, VA, USA |
| Prof. dr. E. Vlieg | |

This work was supported by the Dutch organization for Fundamental Research on Matter (FOM) and in part by NanoNed and the EU projects DYNAMICS and ULTRASWITCH.

"*When you use new technology, new things are **bound** to happen!*"

Nicolaas Bloembergen
*October 2001, Nijmegen*
*The Netherlands*

На моите родители,
които несъзнателно ме насочиха към физиката,
и на Биляна, с всичката ми любов

# Acknowledgements

Fifteen years ago, I decided to become a doctor in physics. This was the time when I first arrived in France and started struggling with the French school system. It wasn't easy since I knew very little of French history, geography, literature, etc. However, there were a few things that I knew as well as the local kids and sometimes even better: the sciences. Mathematics quickly became the easiest discipline for me because I didn't have to learn a list of new French words in addition to every lesson. Physics and chemistry followed closely. Among these, physics had a very special place in my heart for it was the science of starships, teleportation, lasers, time travel and of course... lightsabers!

Science fiction has been a constant companion of my love for physics and has followed me throughout my studies in Brest (France), Cardiff (UK), Nijmegen (the Netherlands) and now Leuven (Belgium). In all these places, physics has allowed me to explore strange new things, to seek out new people and new civilizations, and in a few privileged moments... to boldly go where no one has ever been before.

Of course, this journey would not have been possible without the help of some persons, which I would like to thank here.

First of all, I am grateful to Prof. John Inglesfield who directed me towards Nijmegen. Dear John, your contagious enthusiasm for physics has been an inspiration for me since our very first encounter.

Upon my arrival in Nijmegen, I was greatly helped by our secretaries Riki and Marilou. I am especially thankful to Marilou for all the discussions we had together, her friendship and of course… for her help in the lab.

Many of my colleagues who were present in the beginning of my Ph.D. are now gone and others have arrived since then. To all of them, Markus, Sergiy, Florian, Daniel, Marina, Stephanie, Toyo, Christelle, Erich, Grzegorz, Oleg, Roman, Gabriela, Sasha, Lucian, etc. I wish to express my appreciation. Thanks also to Dr. Kimel who taught me the basics of Faraday rotation and provided a challenging environment for my studies. Special thanks to Thomas Gerrits, Kürşat Bal and Arata Tsukamoto who are among the most thought provoking people I ever met.

I am indebted to Albert van Etteger for teaching me how to operate the lasers as well as to Wiesiek Szweryn who taught me everything I know about UHV and showed a great deal of patience in doing so. Additionally, I am grateful to Tonnie Toonen for all his help and for the wonderful person that he is.

Furthermore, I wish to thank Yelle Wouters from K.U. Leuven for helping me with the Dutch translation of this thesis' summary.

None of the work presented in this thesis would have been possible without the help of my collaborators. I wish to start with Dr. Markus Gruyters who has provided me with carefully prepared samples, very helpful scientific expertise and whose encouragements have kept me going in times of doubt. Next, I wish to acknowledge the assistance of Dr. Jürgen Kohlhepp and Prof. Bert Koopmans for their samples and their insightful comments and suggestions. Last but not least of the collaborators, I wish to thank Prof. Igor Lybchanskii for our discussions on MSHG. I especially cherish his friendship and our conversations in Russian.

This thesis has been prepared under the supervision of Dr. Andrei Kirilyuk. Dear Andrei, some lessons are easier to learn than others and our relation hasn't always been very simple. In the beginning of my Ph.D. I found your constant criticism irritating and confusing. I spent quite some time complaining about what I called "lack of supervision" and about how unfair it all was. During this period I was getting on the nerves of a lot of people and for that I wish to apologize. I guess that most Ph.D. students go through a similar phase. It is a moment of darkness and pain when one has to learn to trust oneself and grow up to become an independent scientist. When finally, I made the transition, I started to appreciate your criticism and our discussions are one of the things which I will miss the most. Thank you for your patience and all your help!

Doubtlessly, the most important person for the completion of my thesis was Prof. Theo Rasing. Dear Theo, I am grateful to you for giving me the opportunity to work and study in your wonderful group. Coming from a rather theoretical background, I had some difficulties starting an experimental Ph.D. Soon after, I had some problems with the UHV that no one really knew how to operate, then there was some bad luck when the construction workers outside the university cut a power cable and the UHV filaments all burned out, and finally I made some mistakes in my interaction with most of the group members. Starting a new research project and overcoming all this has been a great challenge for me. However, of all my personal achievements during the last five years, having earned your trust and your friendship has been the highest point for me. I am indebted to you for your guidance and for something else which is more difficult to explain. Up until the beginning of my Ph.D. I loved what I thought was "physics" and "science", but I didn't really understand these words. What I knew was text book physics and the popularized Legend of Science. The *real* physics is a complexes social activity that, in addition to spending sleepless nights making experiments and studying, involves giving talks, presenting posters, a lot of writing (proposals, articles) and even more re-writing, interacting with other scientists at conferences, grants, referee reports, setting up networks of collaboration, etc. It was through you, Theo, that I saw the "big picture" and since then my love for science has become even stronger. So most of all, I thank you Dear Professor for your example!

I believe that many Ph.D. students experience a time when their long experiments appears to be going nowhere and when they have the distinct feeling that they are wasting their lives. Throughout these moments, the love of my parents Anélia Véléva and Kolyo Valev, as well as that of my good friends Dr. Zlatka Zasheva and Capt. Patrice Fath have been of great comfort to me.

Finally, I wish to thank my wife Bilyana for her unfailing support. Ever since that distant past, fifteen years ago, when I was first trying to impress her with my knowledge and dreams of science, to the present days, when she never ceases to impress me. While pursuing her own studies of business and administration, Bilyana has often assisted me in the lab, aligning optical components, handling the liquid helium equipment and keeping me company throughout entire nights to prevent me from falling asleep during the experiments.

Ventsislav K. Valev
Leuven, September 2006
Belgium

# Contents

# Chapter one

# Introduction

Unique magnetic properties are revealed as we lower the dimensions of matter, from bulk materials to single monolayer interfaces and beyond. Exchange bias is one of the many remarkable discoveries of the last fifty years, which also include giant magnetoresistance, tunneling magnetoresistance, interface anisotropy and interlayer exchange coupling. Together, these phenomena have revolutionized the field of data storage as they find applications in both random-access memories and hard drives. With the addition of the applications for new magnetic sensors, this revolution is in turn about to transform our daily lives as computers are no longer confined to desktops but are built in cars, stereos and even toasters.[1]

The very first studies of thin films are believed to have been done by August Kundt in 1884, in Germany. He made use of linear magneto-optical techniques to study cobalt, iron and nickel. Today, more than a hundred years later, these techniques are still being employed in combination with the much more recent nonlinear magneto-optical ones. Magnetization-induced Second Harmonic Generation is one of these new techniques and its high sensitivity to monolayer-thin surfaces and interfaces makes it an exciting tool for both fundamental and application-driven research.

## 1.1. Magnetic order

There are two main types of magnetic order in nature: ferromagnetic and antiferromagnetic.

### 1.1.1. Ferromagnetism

Ferromagnetism occurs in materials such as nickel, iron, cobalt etc. It is characterized by a positive coupling ($J>0$) between the electron spins ($S$) at neighboring atoms, which causes them to align parallel to each other. The exchange energy between the spins is then:

$$E = -J\sum_{i,j}^{i<j} \mathbf{S}_i \cdot \mathbf{S}_j \qquad (1.1)$$

Usually, the bulk of a magnetic material appears nonmagnetic because it breaks up in many domains. However, under the influence of a small external magnetic field (**H**), the domains can be aligned collectively along the direction of that field and the material is magnetized. If then the external field is removed, ferromagnets retain their magnetization to some extent. This tendency to "remember their magnetic history" is called a hysteresis (see Fig. 1.1). It is important to notice that the hysteresis curve is centered at **H** = 0.

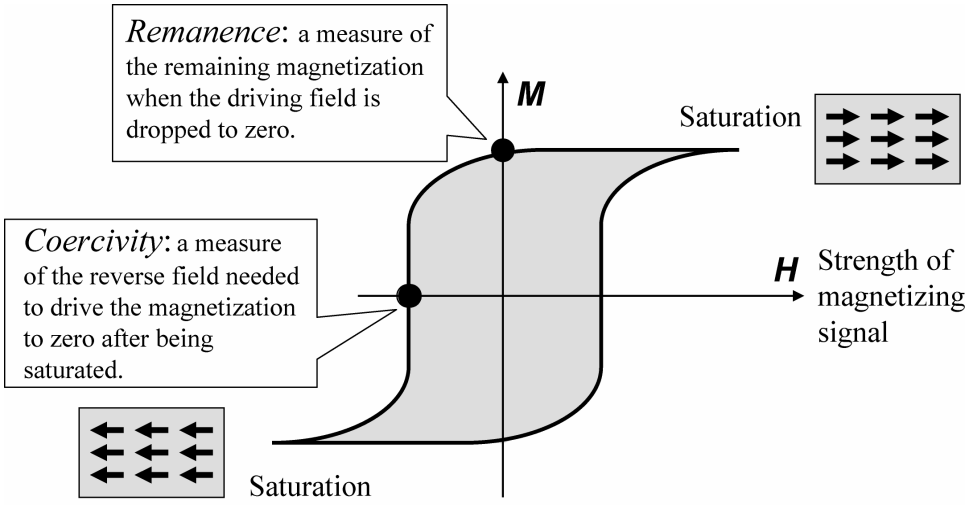


**Fig. 1.1** The hysteresis loop in a ferromagnetic material. Note that the loop is centered at H=0.

The ferromagnetic order has a limiting temperature, above which the order disappears. It is called the Curie temperature $T_C$ and typical values are: Co (1388 K), Fe (1043 K) and Ni (627 K).

## 1.1.2. Antiferromagnetism

Antiferromagnetism occurs in metal oxides such as NiO, FeO, CoO but also in metals such as Mn and Cr. It is characterized by a negative coupling ($J$<0) between the electronic spins ($S$) at neighboring atoms. The exchange energy between the spins is then:

$$E = -J\sum_{i,j}^{i<j}\mathbf{S}_i \cdot \mathbf{S}_j \tag{1.2}$$

As a consequence, all the spins cancel each other and the total magnetization is zero. Antiferromagnets as a whole are not influenced by moderate magnetic fields, although the situation may be different at surfaces. Fig. 1.2 shows the two types of antiferromagnetic surfaces that we can distinguish depending on the manner neighboring spins are oriented with respect to each other. At the uncompensated antiferromagnetic surface all the spins are aligned along the same direction, similarly to a ferromagnetic

surface, while at the compensated antiferromagnetic surface the individual spins within the topmost layer are oriented in such a way as to cancel each other.

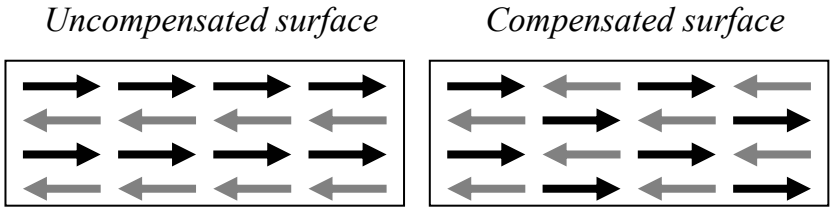


**Fig. 1.2** Antiferromagnetic order: the two types of antiferromagnetic surfaces. At the uncompensated surface, all the spins at the top most layer of the material are aligned in the same direction.

The antiferromagnetic order also has a limiting temperature, above which the order disappears. It is called the Néel temperature $T_N$ and typical values are: CoO (290 K) and NiO (520 K).

## 1.2. Exchange bias

An antiferromagnetic (AFM) material has no net magnetic moment. Yet, when placed in contact with a ferromagnet (FM), the magnetic properties of the latter can be significantly modified. This phenomenon has puzzled scientists since its discovery in 1956 by Meiklejohn and Bean.[2,3] It has been named *exchange anisotropy* and is more often referred to as *exchange bias*. In order to elucidate the specific role of the antiferromagnet, the research in this field is focused mainly on the AFM/FM interface.

Initially, exchange bias was discovered in partially oxidized Co particles. The interface in these structures was between the ferromagnetic Co core and an antiferromagnetic CoO "envelope". However, the phenomenon is much more widely studied in thin-films, since this facilitates the characterization and control of the interface.

For an uncompensated AFM interface one could indeed expect such an exchange bias since it presents a spin polarized layer that can interact with the adjoining ferromagnet. However, it has been discovered that exchange bias also exists for compensated AFM interfaces (see Fig. 1.3). Moreover, in some cases, the phenomenon was more pronounced for compensated AFM interfaces than for uncompensated ones![4]

The nature of the interface magnetic structure itself is still under discussion. Some of the current theories include random uncompensated spins, domain walls, partial domain walls and canted perpendicular spins. Interestingly, even though the pioneering work of Meiklejohn and Bean has become very frequently cited in the scientific literature, and even though its important applications (which will be discussed later in this Chapter) have driven an abundant amount of research, the overwhelming majority of papers on the topic begin by saying something like: "Although exchange bias has been discovered almost 50 years ago, there is still no complete theoretical explanation for this phenomenon."

There are many open questions regarding exchange bias and knowledge of the interface is clearly at the heart of the problem.[4–6]

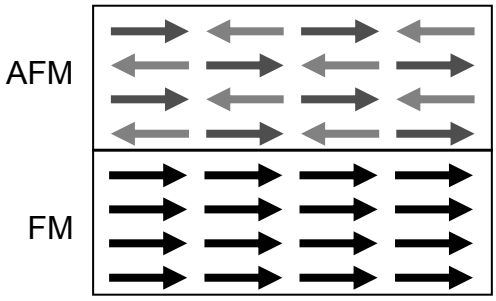


**Fig. 1.3** Exchange bias appears at the interface between antiferromagnetic (AFM) and ferromagnetic (FM) materials. The figure is a schematic representation of a compensated AFM/FM interface.

Another major reason for studying exchange bias in thin-films is that most technological applications are based on this form of the effect.

### 1.2.1. Applications of exchange bias

In the year 2000, near 90% of all recording heads for computer hard disk drives manufactured in the industry were estimated to make use of exchange bias in combination with the giant magnetoresistance effect (GMR).[7] GMR was discovered in 1987 by the German P. Grünberg[8] and by the Frenchman A. Fert.[9] It was observed that when the current flows through two FM thin-layers separated by a nonmagnetic conductive spacer, the value of the electrical resistance depends on the relative magnetization direction in the ferromagnets. Because of electrons scattering at the interfaces, the resistance is higher when the FM layers are in an antiparallel configuration, while for parallel configurations the resistance drops (see Fig. 1.4).

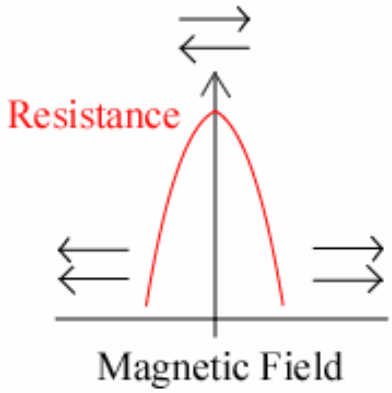


**Fig. 1.4** Schematic representation of the Giant Magnetoresistance Effect. The electrical resistance is higher when the two ferromagnetic layers are in an antiparallel configuration.

There are several types of GMR reading heads, however the most widespread one is the spin valve which makes use of the exchange bias effect. In fact, IBM, Hitachi and Western Digital all use the term “spin valve” as synonymous to “GMR reading head” on their websites.

#### 1.2.1.1. Spin valves

In Fig. 1.5, the schematic configuration of a spin valve sensor is presented. As the reading head flies over the magnetically oriented bits on the surface of the hard disk, the *sensing layer* (a soft magnetic layer) orients its magnetization along the magnetization direction of the bits. While this is occurring, the *pinned layer* provides a reference by remaining along its original direction. This pinned layer is a ferromagnet, usually of the same material as the sensing layer, that has been hardened by the presence of an antiferromagnet (the *exchange layer*) through exchange bias.

The GMR effect is then measured as electrical current flows across the entire structure.

In order to ensure high signal-to-noise levels, it is important that the reference from the pinned layer remains as constant as possible. For that reason, materials with strong exchange bias values are sought after by the industry.

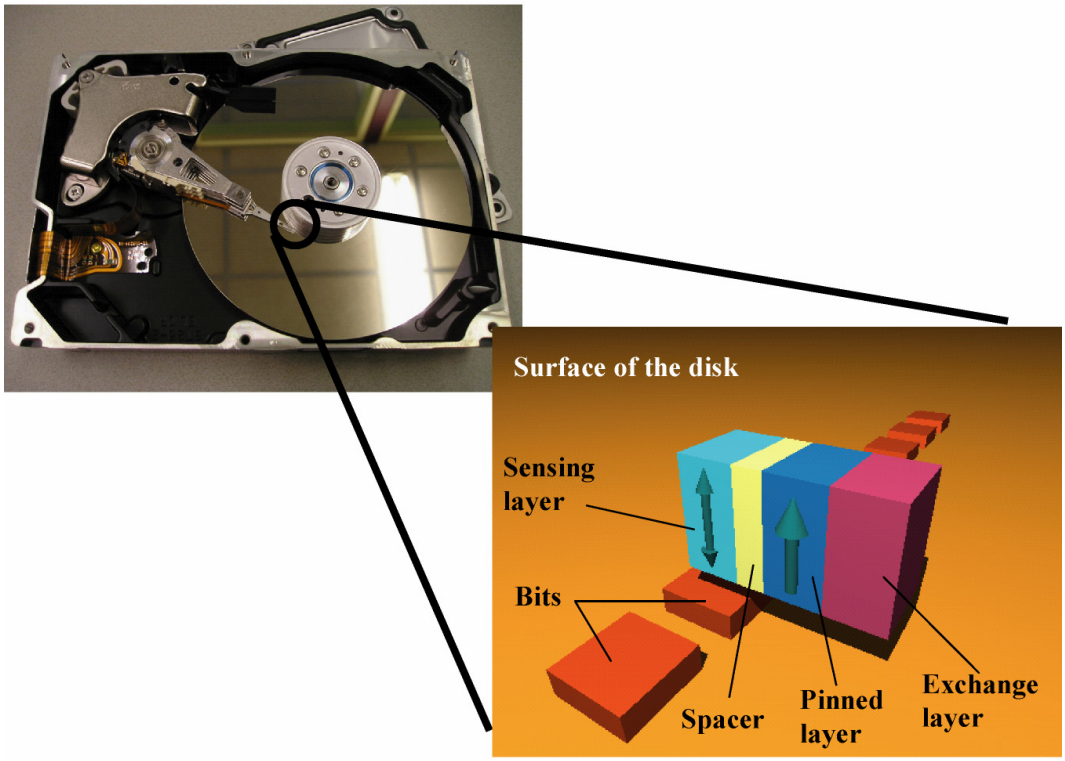


**Fig. 1.5** Schematic of the spin valve that is situated in computer hard disk drives. Exchange bias is used between the FM *pinned layer* and the AFM *exchange layer*.

Another important effect concerning magnetization in thin films that has been mentioned in the introduction is the tunneling magnetoresistance (TMR). TMR has features similar to those of GMR. Again a current is flowing across two FM layers with varying relative magnetization directions and again the current is higher for parallel configurations than it is for antiparallel. However, in the case of TMR the nonmagnetic layer that separates the FM layers is an electric isolator and therefore the current has to tunnel from one FM layer to the other.

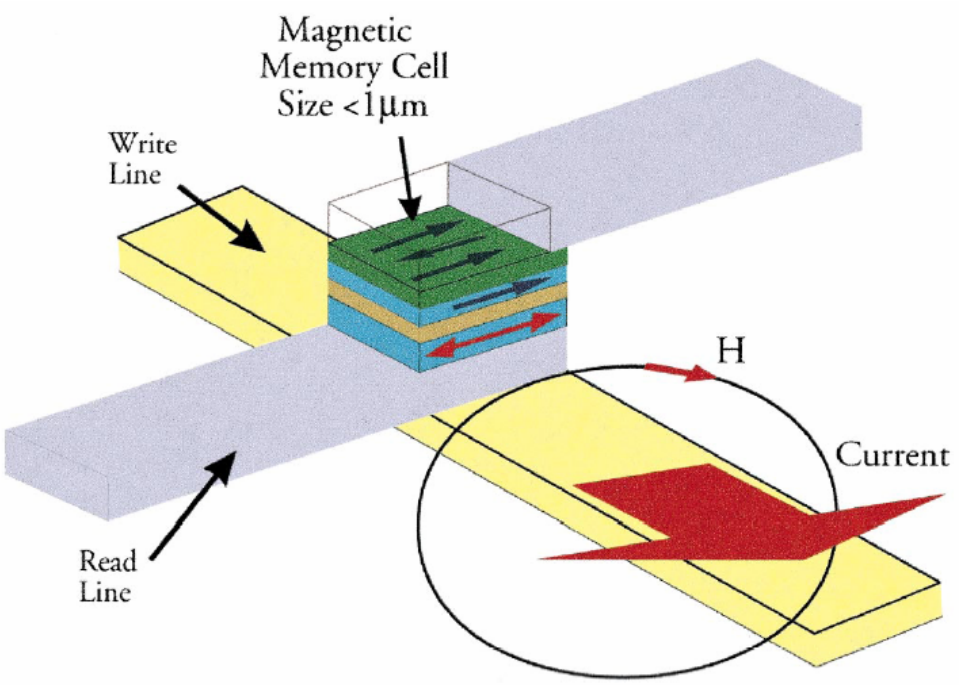


**Fig. 1.6** "The ideal memory", MRAM, is expected to be on the computer market by 2007. It uses spin valves as recording elements and an AFM layer for exchange bias.[10]

Instead of scattering from the interfaces, as it is in the case of GMR, the electrical current in TMR depends on the electronic density of states for the different spin directions of the FM layers. And just as GMR spin valves are at the heart of the computer hard disk drives reading heads industry, TMR spin valves are at the center of a new type of random access memory (RAM) technology that is expected to arrive on the markets in 2007.

MRAM (Magnetoresistive or Magnetic Random Access Memory) is expected to display at the same time the speed of SRAM (Static Random Access Memory), the density of DRAM (Dynamic Random Access Memory) and the non-volatility of FLASH memory. It will be able to withstand high radiation and extreme temperatures while keeping low power consumption. In short, MRAM has been described as "the ideal memory".

Fig. 1.6 shows a schematic of MRAM. It is a nanoscopic grid of horizontal and perpendicular power strips and at each intersection a data storage element is situated, which is in fact a spin valve. Bits are written by switching the soft layer with the help of an in-plane magnetic field pulse, generated by an appropriate current pulse through the

write line. Once again, exchange bias ensures the stability of the reference layer's magnetization direction.

#### 1.2.1.2. Other applications

With decreasing dimensions magnetic particles entering the nanoscale range tend to loose their magnetization to temperature fluctuations. In so doing these nanoparticles are said to encounter the superparamagnetic limit which is an obstacle to their otherwise potentially useful applications in medicine and ultra-high density recording. The unidirectional anisotropy connected with exchange bias, can provide these particles with an additional anisotropy that stabilizes their magnetization and allows further miniaturization.[11,12]

Besides the extra source of anisotropy provided by exchange bias, another main feature of the effect is an increase of the coercivity (see Chapter two). This characteristic finds use in the fabrication of permanent magnets.[13]

Finally, it should be noticed that GMR sensors can be employed whenever a small magnetic field is to be measured. Exchange bias could then play a role in motion sensors participating in the development of modern cars and robotics, in geophysical exploration, in finances (magnetic ink character recognition) and in many medical applications (from magneto-encephalographs to DNA recognition).[14]

## 1.3. Second Harmonic Generation

Light is an electromagnetic wave. When it propagates through mater, the oscillating electric and magnetic fields interact with the charged particles that constitute the material. This interaction gives rise to sinusoidally oscillating electric dipoles, since the contribution form the magnetic field part of the wave and the electric quadrupoles is much weaker and is usually neglected. This is called the *electric-dipole approximation* (ED).

Generally, the electric field associated with light is much smaller that the strength of the internal atomic fields and it can be treated as a small perturbation to the atom. However, the discovery of mode-locked femtosecond lasers has lead to the development of very high peak intensities corresponding to extremely strong electromagnetic fields. These have become comparable to the internal atomic fields and the resultant light-matter interaction can lead to electromagnetic oscillations in the nonlinear regime.

Compared with linear optics, nonlinear optical phenomena reveal new and complementary information, partly as a result of the different experimental degrees of freedom and the higher-order susceptibilities involved,[15,16] In 1981, the Dutch physicist Nicolaas Bloembergen received the Nobel Prize for developing its theoretical framework.

In the vast field of nonlinear optics, *Second Harmonic Generation* (SHG), as the lowest-order nonlinear process, plays a very important role. Since in the leading ED order SHG is allowed only in noncentrosymmetric materials, it is very sensitive to surfaces and interfaces of centrosymmetric materials, due to the breaking of inversion symmetry at these boundaries. Furthermore, the penetration depth of light allows us to apply the same

sensitivity in order to investigate buried interfaces in multilayer systems. The SHG technique has therefore been used widely for studies of surfaces and interfaces.

### 1.3.1. Frequency conversion

Second Harmonic Generation is a particular case of the effect called *Sum Frequency Generation* (SFG) in which two or more light waves are mixing.

$$I(\omega_1 + \omega_2) \propto I(\omega_1) \cdot I(\omega_2) \tag{1.1}$$

In the case of SHG, two coherent light waves of the same frequency act together in generating a third light wave that is of the double frequency (or half the wavelength).

$$I(2\omega) \propto \left(I(\omega)\right)^2 \tag{1.2}$$

Choosing the initial wavelength to be 800 nm, which corresponds to near infra-red, the generated second harmonic light wave has a frequency of 400 nm, which corresponds to blue. Although conversion factors from $\omega$ to $2\omega$ of up to 80% have been claimed for some specific crystals,[17] a typical value for this factor after reflection from a centrosymmetric material is only $10^{-15}$.

### 1.3.2. Observation of SHG

Experimentally, SHG was first observed by Franken et al. in 1961.[18] This was made possible because of the fabrication of the pulsed laser in 1960. Lasers have several important characteristics that play a role in SHG: they provide well defined monochromatic light (this is important for Eq. 1.2), coherent waves and high intensities.[19]

Typically, in order to observe SHG, peak light intensities of a few hundreds of MW/cm$^2$ are required.

Coherent waves are necessary to insure the efficiency of SHG by fulfilling the *phase match condition* (that derives from the conservation of momentum). However, because of their very small sizes, this condition is not particularly important when light is reflected from multilayered thin films, such as, for instance, spin valves and other exchange biased systems.

### 1.3.3. Magnetization-induced SHG (MSHG)

Magnetism influences second harmonic generation because it is related to the breaking of time-reversal symmetry.[20-22] We can consider the magnetic moments of atoms in a magnetic material to be the result of small electric current loops around the atoms. Switching the magnetization in the opposite direction is then equivalent to reversing the

direction of time so that the current in the electric loops starts flowing in the opposite way.

In order to observe MSHG, both structural symmetry breaking and time reversal are necessary. In other words, in centrosymmetric materials MSHG is produced mainly by the surface and interfaces of the magnetic material and therefore it is a useful tool for investigating surface and interface magnetism.

Although the first predictions for MSHG can be traced back to the 1960s,[23-25] it was only thirty years later that the field of nonlinear magneto-optics really started developing, after the observation of huge magneto-optical effects from magnetic surfaces and interfaces.[26-28] Both the advances in solid-state, mode-locked, femtosecond lasers and the huge interest in the study and applications of magnetic multilayers and nanostructures have strongly stimulated the development of nonlinear magneto-optics.[29]

One of the most important achievements of MSHG was the demonstration that it offers the possibility to distinguish between the magnetic contributions from different buried interfaces.[30] Another one is that it allows the observation of even a tiny increase in the magnetization of the surface/interface layers.[31]

By illustrating both of those capabilities, it is precisely this physical phenomenon – the generation of magnetization-induced second harmonic light from interfaces – that will be at the center of the physics studied in this thesis.

## 1.4. Overview of this thesis

We have seen that the exchange biasing at the AFM/FM interface is an intellectually challenging problem with many important practical applications. On the other hand, MSHG is a very interesting technique that is particularly suited for studies of interface magnetism.

After introducing in greater detail the phenomenon of exchange bias and the MSHG technique in Chapters two and three respectively, we will direct our attention to the practical considerations behind realizing the experimental investigation of the exchange bias phenomenon using MSHG, in Chapter four. In particular, in Chapter five, we will see that measurements have to be done very carefully in order to avoid a nonlinear dependence on the magnetization in the MSHG signal.

In Chapter six we will demonstrate the usefulness of MSHG for observing spin polarization at the antiferromagnetic/spacer interface when a thin nonmagnetic spacer is inserted between the AFM and the FM and we will discuss its potential for providing new insights into the exchange bias phenomenon.

In Chapter seven, we will compare the magnetic properties of a Co surface with those of an exchange biased Co/Mn interface. Similarities and differences concerning the behavior of the net magnetic moment and the magnetization reversal will be discussed.

Finally, in Chapter eight we will focus our attention on a rather special antiferromagnetic/ferromagnetic interface, namely NiO(111) grown on the surface of a Ni(001) single crystal.

## References:

[1] Source: http://www.research.ibm.com/research/gmr.html

[2] W.H. Meiklejohn, C.P. Bean, Phys. Rev. **102,** 1413 (1956).

[3] W.H. Meiklejohn, C.P. Bean Phys. Rev. **105,** 904 (1957).

[4] J. Nogués, I. K. Schuller, J. Magn. Magn. Mater. **192**, 203 (1999).

[5] A.E. Berkowitz, K. Takano, J. Magn. Magn. Mater. **200**, 552 (1999).

[6] M. Kiwi, J. Magn. Magn. Mater. **234**, 584 (2001).

[7i] Source: http://www.hitachigst.com/hdd/research/recording_head/headmaterials/

[8] G. Binasch, P. Grünberg, F. Saurenbach and W. Zinn, Phys. Rev. B **39**, 4828 (1987).

[9] M.N. Baibich, J.M. Broto, A. Fert, F. Nguyen Van Dau, F. Petroff, P. Etienne, G. Greuzet, A. Friederich and J. Chazelas, Phys. Rev. Lett. **61**, 2472 (1988).

[10] J. B. Kortright, D. D. Awschalom, J. Stöhr, S. D. Bader, Y. U. Idzerda, S. S. P. Parkin, I. K. Schuller, and H.-C. Siegmann, J. Magn. Magn. Mater. **207**, 7 (1999).

[11] V. Skumryev, S. Stoyanov, Y. Zhang, G. Hadjipanayis, D. Givord and J. Nogués, Nature **423**, 850 (2003).

[12] K. Liu, I.V. Roshchin, I.K. Schuller, J. Nogués, C. Leighton, C. Londergan, C. Kubiak, K. Nishio, H. Masuda, App. Phys. Lett. **81**, 4434 (2002).

[13] J. Sort, J. Nogues, S. Surinach, J.S. Munoz, M.D. Baro, E. Chappel, F. Dupont, and G. Chouteau, Appl. Phys. Lett. **79**, 1142 (2001).

[14] Source: http://www.sensorsmag.com/articles/0999/76/main.shtml

[15] Y. R. Shen, The Principles of Nonlinear Optics (Wiley, New York, 1984).

[16] R. W. Boyd, Nonlinear Optics (Academic, London, 1992).

[17] Potassium Titanyl Phosphate KTiOPO4 (KTP) crystal from Coretech, source: http://www.coretech.com.cn/products-KTP.pdf

[18] P. A. Franken, A. E. Hill, C. W Peters, and G. W Weinreigh, Phys. Rev. Lett. **7**, 118 (1961).

[19] A.C. Newell and J.V. Moloney, “Nonlinear Optics”, ed. by Addison-Wesley Publishing Company, 1992

[20] Ru-Pin Pan, H.D. Wei and Y.R. Shen, Phys. Rev. B **39**, 1229 (1989).

[21] A. Kirilyuk and Th. Rasing, J. Opt. Soc. Am. B **22**, 148 (2005).

[22] M. Fiebig, V. V. Pavlov, and R. V. Pisarev, J. Opt. Soc. Am. B **22**, 96 (2005).

[23] P. S. Pershan, Phys. Rev. **130**, 919 (1963).

[24] E. Adler, Phys. Rev. **134**, A728 (1964).

[25] J. Lajzerowicz and M. Vallade, C.R. Acad. Sci. Paris **264**, 1819 (1967).

[26] J. Reif, J. C. Zink, C. M. Schneider, and J. Kirschner, Phys. Rev. Lett. **67**, 2878 (1991).

[27] J. Reif, C. Rau, and E. Matthias, Phys. Rev. Lett. **71**, 1931 (1993).

[28] G. Spierings, V. Koutsos, H. A. Wierenga, M. W. J. Prins, D. Abraham, and Th. Rasing, Surf. Sci. **287**, 747 (1993).

[29] Th. Rasing, Appl. Phys. B **68**, 477 (1999).

[30] A. Kirilyuk, Th. Rasing, M. A. M. Haast, and J. C. Lodder, Appl. Phys. Lett. **72**, 2331 (1998).

[31] Q. Y. Jin, H. Regensburger, R. Vollmer, and J. Kirschner, Phys. Rev. Lett. **80**, 4056 (1998).

# Chapter two

# Exchange bias

Although antiferromagnetic (AFM) materials do not possess a net magnetic moment, their coupling to a ferromagnetic (FM) thin film can dramatically affect the magnetic properties of the latter. When an AFM/FM bilayer is cooled in the presence of an external magnetic field (this process is called *field-cooling*) from a temperature T, above the Néel temperature ($T_N$) of the antiferromagnet but below the Curie temperature ($T_C$) of the ferromagnet, a new magnetic symmetry is induced in the system: a *unidirectional anisotropy*. In the literature, this term is sometimes used as synonymous to "exchange bias".

In most cases, the role of the external magnetic field during field-cooling is to fix the direction of the FM magnetization. As a result, the antiferromagnet orders in a manner that minimizes the coupling energy with the ferromagnet. Once the AFM order is set, it "keeps in memory" the initial FM direction and acts on the FM reversal as an additional biasing field ($H_E$), i.e. a field that makes it easier to orient the FM film along its initial direction and harder along the opposite. This directional preference results in a shifted or "biased" hysteresis loop.

In this Chapter, the Meiklejohn and Bean intuitive model for exchange bias will be presented. Then, after discussing the characterization of the phenomenon, some of the most important theoretical works will be introduced.

## 2.1 Meiklejohn and Bean's intuitive model

Fig. 2.1 shows a simple but intuitively very appealing model. Here it is assumed that the antiferromagnet consists of alternating layers of spins. Within each layer, the spins have the same direction and from one layer to the next the direction is opposite so that the overall net magnetic moment is zero.

For a temperature T such that $T_N<T<T_C$, when an external magnetic field $\mathbf{H_0}$ is applied to the system, the FM spins orient along the direction of $\mathbf{H_0}$, while the AFM ones remain random (i). As the system is field-cooled, because of the exchange interaction, the AFM order forms in a way that the first layer of AFM spins are locked to the FM magnetization. The second layer then points in the opposite direction, the third is again parallel to the FM magnetization, etc. (ii). Now, if $\mathbf{H_0}$ is reversed, (part of) the magnetization in the FM material will attempt to switch, however because of the exchange interaction with the AFM spins at the interface, this reversal will be made more

difficult. Effectively, the AFM spins pin the magnetization at the interface (iii). However, after sufficiently increasing $\mathbf{H_0}$, this pinning can be overcome and the magnetization switches (iv). During the second reversal, the exchange coupling is again present, however this time it acts in the direction of the reversal, i.e. it facilitates the switching (v). As a result, the hysteresis loop is shifted away from the zero field position. This is the most well known feature of exchange bias.

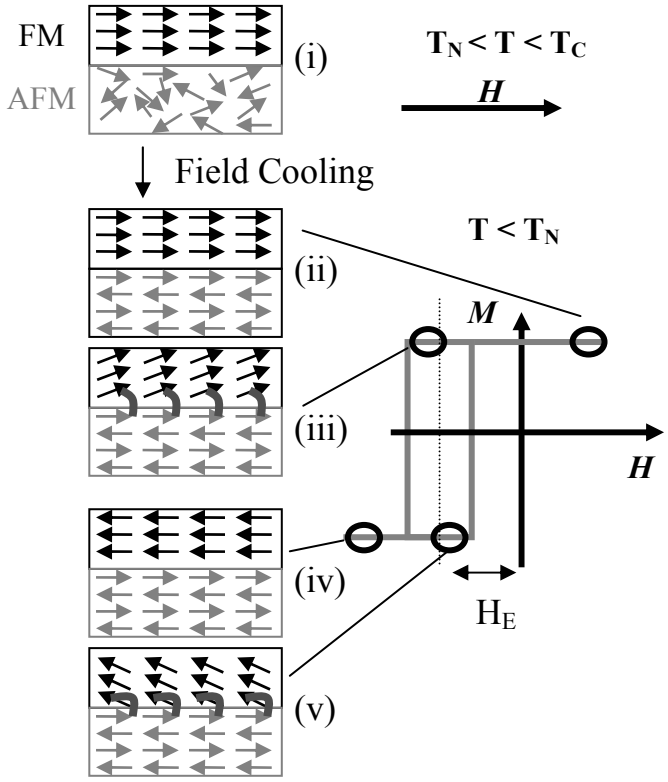


**Fig 2.1** Magnetization reversal in ferromagnetic/antiferromagnetic bilayer after field-cooling from a temperature above the Néel temperature but below the Curie temperature. Figure from reference [1].

Assuming coherent rotation of the magnetization, the energy per unit area of the exchange bias system is given by the formula:

$$E = H_0 M_{FM} t_{FM} \cos(\theta - \beta) + K_{FM} t_{FM} \sin^2(\beta) + K_{AFM} t_{AFM} \sin^2(\alpha) - J_{INT} \cos(\beta - \alpha) \tag{2.1}$$

where $H_0$ is the applied field, $M_{FM}$ the saturation magnetization, $K_{FM}$ the anisotropy of the FM layer, $K_{AFM}$ the anisotropy of the AFM layer, $t_{FM}$ the thickness of the FM layer, $t_{AFM}$ the thickness of the AFM layer and $J_{INT}$ the interface coupling constant. $\alpha$, $\beta$ and $\theta$ are the angles between the AFM anisotropy axis and the direction of the axis along which the AFM spins are actually situated, the magnetization and the FM anisotropy axis, and the applied field and the FM anisotropy axis respectively. Neglecting the FM anisotropy,

since it is usually true that $K_{FM} << K_{AFM}$, and minimizing with respect to $\alpha$ and $\beta$, the loop shift becomes:

$$H_E = \frac{J_{INT}}{M_{FM} t_{FM}} \tag{2.2}$$

Note that although this formula takes into account some important physical parameters of the AFM/FM coupling, it assumes, among other factors, a lack of domain structure in the FM and the AFM, co-linearity of the FM and the AFM easy axis and absence of structural defects at the interface. Additionally, it assumes an uncompensated AFM interface and neglects the effect that the magnetic field may have on the AFM spins. Finally, taking $J_{INT}$ to be similar FM exchange interaction, the calculated loop shift is several orders of magnitude larger than the experimental results.

## 2.2 Characteristics

Besides the hysteresis loop shift, the other main characteristic of exchange bias is the increase of the coercivity.

### 2.2.1 Shift of the hysteresis $H_E$ and increase of the coercivity $H_C$

The exchange anisotropy was first revealed in 1956 by W. H. Meiklejohn and C. P. Bean.[2-4] They discovered that this anisotropy was the result of an interaction between an antiferromagnetic material and a ferromagnetic material. The material that exhibited this exchange anisotropy was a compact of fine particles of cobalt with a cobaltous oxide shell. The effect occurred only below the Néel temperature of the antiferromagnetic material, which is essentially room temperature for the cobaltous oxide. A displaced hysteresis loop and an asymmetrical coercive force which occurred when the specimen was cooled in the presence of a magnetic field were observed. The maximum displacement was 1600 Oe at the temperature of 77 K (see Fig. 2.2).

In 1961, the effect was confirmed by J. S. Kouvel. He noticed that magnetic hysteresis loops that are displaced from their symmetrical positions about the origin are observed when alloys of about 5–30 per cent Mn in Cu and 10–25 per cent Mn in Ag are cooled to 1.8 K in a magnetic field.[5,6] The two remanent magnetizations from each loop were equal both in magnitude and direction and represented a ferromagnetic alignment of a significant fraction of the Mn atomic moments. For each alloy, the hysteresis loop displacement decreased with increasing temperature and its disappearance was accompanied by large hysteresis losses.

In the intuitive model described in the previous section, the loop shift is due to a pinning by uncompensated AFM spins at the interface. Recent work suggests that actually, there is only a small number of AFM spins that remain pinned during the FM magnetization reversal.[7] In fact, most of the AFM interfacial spins couple strongly to the

ferromagnet and they follow its magnetization, thereby contributing to the enlargement of the coercivity.

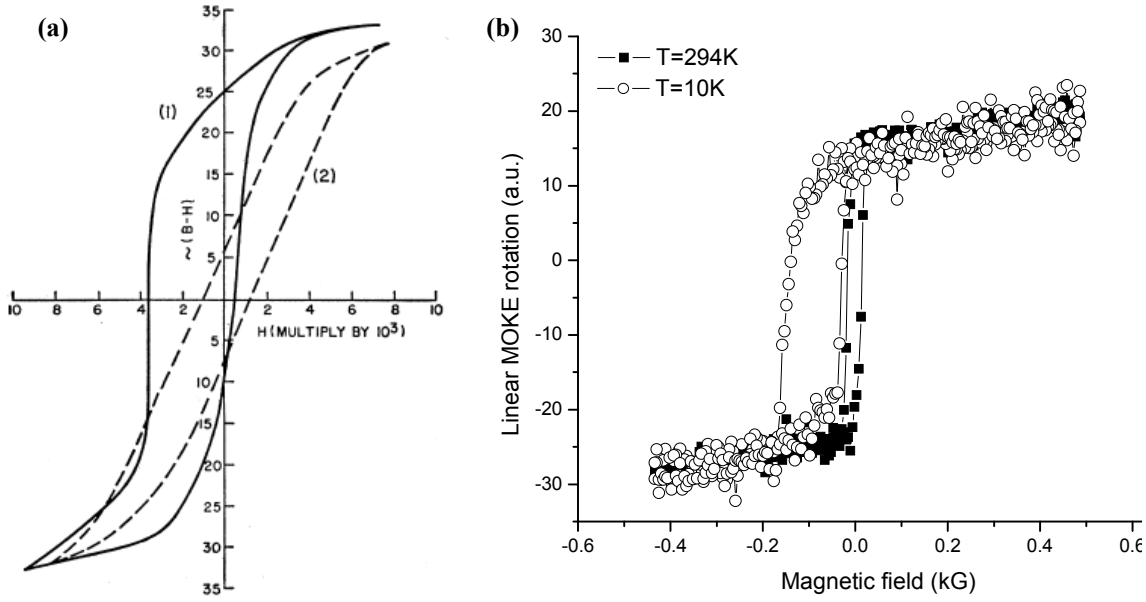


**Fig 2.2** a) Meiklejohn and Bean's hysteresis loops at 77 K of oxide-coated cobalt particles. Solid line curve results from cooling the material in a 10 000 Oe field. The dashed line curve shows the loop when cooled in zero field. b) Our own hysteresis curves measured with linear MOKE from Si(111)/Fe(6 nm)/Cu(2.5 nm)/CoO(2 nm)/Au(6 nm) at room temperature and at 10 K after field cooling. The loop shift and the increase of coercivity are clearly visible.

## 2.2.2 Temperature dependence

It has been found that thermal instabilities can strongly affect the exchange bias behavior in polycrystalline AFM films. Here we will discuss two important features of exchange bias: the blocking temperature and the peak in the coercivity.

### 2.2.2.1 Blocking temperature $T_B$

It is often observed that exchange bias occurs well below the Néel temperature. For instance, $T_N$ of CoO is 291 K, however Fig 2.3 shows that the loop shift appears below 200 K. This value is almost 100 K lower! By definition, the temperature below which $H_E$ appears is called the *blocking temperature* $T_B$.

One of the first observations of $T_B$ was reported by C. Schlenker.[8] He studied the temperature dependence of the ferromagnetic-antiferromagnetic coupling between -190° and 20°C in polycrystalline thin films of Co or Ni oxidized superficially. He found that the unidirectional anisotropy vanishes at a transition temperature below the Néel temperature and was related to the average thickness of the antiferromagnetic film.

In 1999, M. D. Stiles and R. D. McMichael proposed a model which explained the temperature dependence of the exchange bias and related effects that result from coupling a ferromagnetic thin film to a polycrystalline antiferromagnetic film.[9] In this model, an important source of temperature dependence comes from thermal instabilities of the antiferromagnetic state in the antiferromagnetic grains, much as occurs in superparamagnetic grains. At higher temperatures (above $T_B$), the antiferromagnetic state remains stable on short time scales, but becomes unstable on longer time scales, due to thermal excitations. At low enough temperatures (below $T_B$), the antiferromagnetic state in each grain is stable as the ferromagnetic magnetization is rotated and the model predicts the unidirectional anisotropy that gives rise to the observed exchange-bias loop shift.

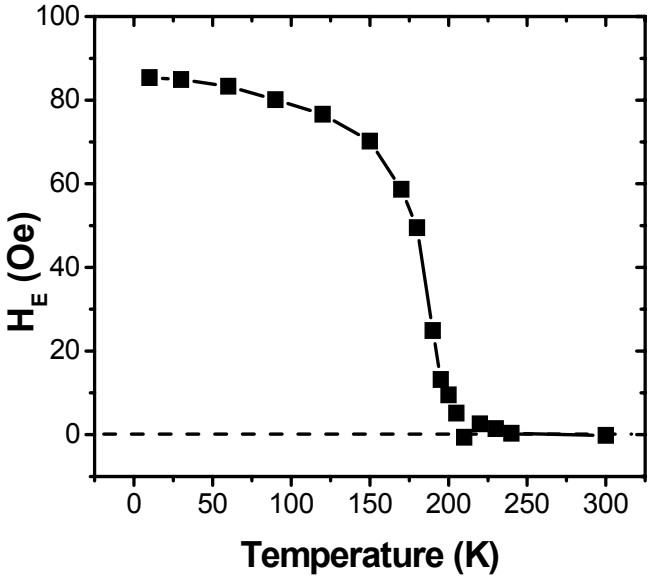


**Fig 2.3** Our results showing the temperature dependence of the loop shift from a Si(111)/Fe(6 nm)/Cu(2.5 nm)/CoO(2 nm)/Au(6 nm) exchange biased sample, measured with linear MOKE.

The blocking temperature in CoO is of particular interest to us since this material was used in our experiments. Many studies have found that, for small antiferromagnetic layer thickness $t_{AFM}$, $T_B$ is reduced below the bulk $T_N$ of the AFM material.[10-12] In addition, it has been reported that the ordering temperature of ultrathin antiferromagnetic oxide films is lower than the bulk $T_N$ for $t_{AFM} \leq 10$ nm.[13,14] Hence, it was widely believed that $T_B$ follows $T_N$ in AFM/FM exchange biased systems and that the reduction of $T_B$ for small $t_{AFM}$ arises from finite-size scaling, see Fig. 2.4.

P. J. van der Zaag et al. described the effect of the variation of the $t_{AFM}$ on $T_B$ for the *single-crystalline* $Fe_3O_4$/CoO system. They have studied this system as CoO has a comparatively simple AFM spin structure and has been studied extensively.[15] To test the finite-size scaling hypothesis, they performed neutron diffraction measurements of the ordering temperature for CoO layers with small $t_{AFM}$ in exchange biased samples, for which they have also determined the blocking temperature by bulk magnetization

techniques. They found from neutron diffraction measurements that, for small $t_{AFM}$ at which $T_B$ is *reduced*, the ordering temperature of CoO in $Fe_3O_4$/CoO exchange biased systems is *higher* than the bulk $T_N$. Thus it was established that the reduction in $T_B$ is *not* the result of finite-size scaling.

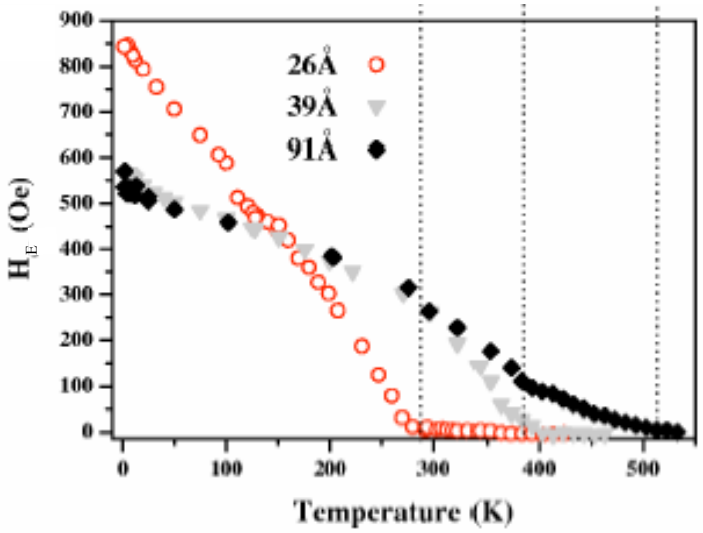


**Fig 2.4** Temperature dependence of the exchange bias field $H_E$ for selected IrMn thicknesses in a IrMn/Co system. Samples were initially field cooled in 0.4 T field to 2 K before commencing measurements. The vertical dashed lines indicate the blocking temperatures of the three samples.[16]

### 2.2.2.2 Coercivity peak at $T_B$

It is sometimes observed that a peak in $H_C$ appears at the blocking temperature (see Fig 2.5).

The increase of the coercivity below $T_B$, seems to be related to the AFM anisotropy. It has been discussed above how the FM spins drag some of the AFM spins at the interface during magnetization reversal. It is the strength of the AFM anisotropy that determines how "easily" this dragging occurs.

Above $T_B$, the magnetic order in the antiferromagnet is not yet set (see previous paragraph) and therefore the AFM spins offer little resistance to the FM reversal. At $T_B$, the AFM order is fixed and this results in an increase of the coercivity. Then, as the temperature decreases, the AFM anisotropy increases and this makes it more and more difficult for the ferromagnet to drag AFM spins. As a consequence, the coercivity decreases again.

It appears that the width of the peak depends on the inhomogeneity of the sample. In polycrystalline AFM films, the size of the grains follows some distribution and consequently so does their anisotropy. Hence, since the peak in the coercivity is related to the anisotropy, it also relates to the sample inhomogeneity.

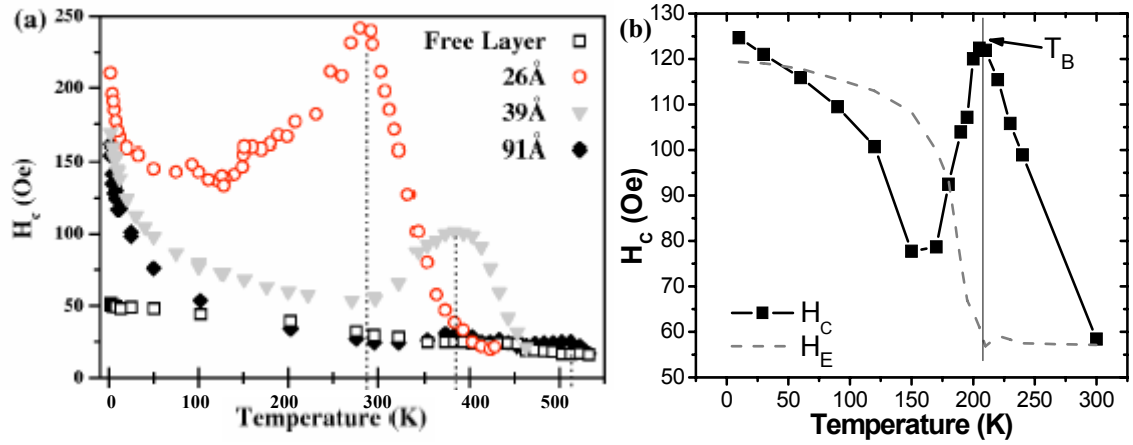


**Fig 2.5** a) Temperature dependence of the coercivity $H_C$ for selected IrMn thicknesses in a IrMn/Co system (the temperature scale is the same as in Fig. 2.3a). The open square symbols represent the coercivity of a free Co layer. Samples were initially field cooled in 0.4 T field to 2 K before commencing measurements. The vertical dashed lines indicate the blocking temperatures of the three samples.[16] b) Our results showing the temperature dependence of the coercivity from a Si(111)/Fe(6 nm)/Cu(2.5 nm)/CoO(2 nm)/Au(6 nm) exchange biased sample, measured with linear MOKE.

### 2.2.3 Training effect

The *training effect* describes the decrease of the EB field when cycling the system through several consecutive hysteresis loops (see Fig. 2.6).

With $n$ being the number of such hysteresis loops, it is often observed[17,18] that the EB field after $n$ loops, $H_E^n$ , can be obtained by the equation $H_E^n - H_E^\infty \propto \frac{1}{\sqrt{n}}$ (although some deviations have been reported[19]). The training effect in general has its origin in the reorientation of AFM domains and/or the diminishing of the number of AFM uncompensated spins at the AFM/FM interface which takes place during each magnetization reversal of the FM top layer. As described by Nogués and Schuller, a pronounced training effect has been found in heterosystems involving polycrystalline AFM pinning layers,[20-22] while in single-crystalline pinning systems this effect is expected to be small.[23-25] The grain size of a polycrystalline AFM pinning substrate is an upper boundary for the correlation length of the AFM order parameter. Hence polycrystallinity limits the long-range AFM order and favors a metastable domain configuration. However, there are various other mechanisms, like structural disorder at the interface or impurity induced random fields, which give rise to AFM domain formation and AFM uncompensated spins and hence make a training effect possible in heterostructures involving singlecrystalline AFM pinning layers.

A. Hochstrat et al. have studied the training effect of a NiO(001)/Fe(110) heterostructure from magnetic hysteresis loops measured by superconducting quantum interference device magnetometry (SQUID).[26] Consecutive hysteresis loops were found

to exhibit a decreasing exchange bias effect. This training effect was assumed to reflect the dependence of the exchange bias field on the antiferromagnetic interface magnetization. In order to support this conjecture, the authors studied the decrease of the total saturation magnetization of the heterostructure for an increasing number of hysteresis cycles. Assuming proportionality between the interface magnetization and the total saturation magnetization, the description of the data was consistent within the phenomenological Meiklejohn-Bean approach.

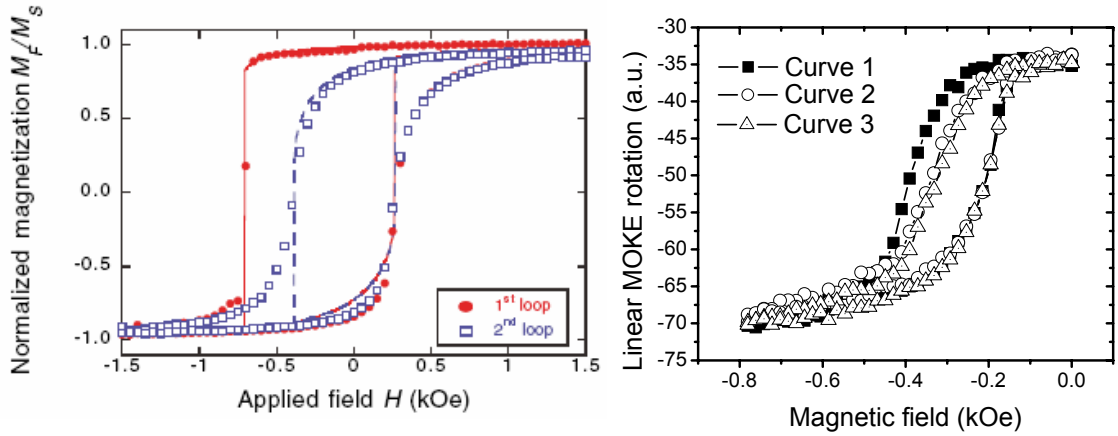


**Fig 2.6** a) Field dependence of the magnetization of a polycrystalline Co/CoO bilayer showing the first (solid symbols) and second (open symbols) hysteresis loop after field cooling. The magnetization $M_F$ is normalized by the saturation value $M_S$. The solid and dashed lines show calculated hysteresis loops for comparison.[27] b) Our results showing consecutive hysteresis loops from the sample Si(111)/Fe(6 nm)/Cu(2.5 nm)/CoO(2 nm)/Au(6 nm) measured at temperature of 10 K with linear MOKE after field-cooling.

A more recent model by C. Binek provides a further quantitative explanation of the training effect.[28] This model is based on an expansion of the energy at the interface in a power series and it successfully derives the simple phenomenological expression that is observed experimentally.[29,30]

## 2.2.4 Thickness dependence

In the following paragraphs we will discuss the thickness dependence of the exchange bias for both the ferromagnet and the antiferromagnet, as well as the effects of inserting a nonmagnetic spacer of varying thickness between these materials.

### 2.2.4.1 FM thickness

In a systematic study of ferromagnetic-antiferromagnetic coupling in Co-CoO evaporated thin films with thicknesses from 30 to 140 nm, M. Takahashi et al. have measured the

hysteresis loops and torque curves in the temperature range from 77 to 630 K.[31] They have found that exchange bias is roughly inversely proportional to the FM thickness:

$$H_E \propto \frac{1}{t_{FM}}, \tag{2.3}$$

which is consistent with the idea that exchange bias is an interface effect.

In another study, L Smardz et al. have investigated the temperature and thickness dependence of the exchange-induced unidirectional anisotropy field and coercive field in Co/CoO bilayers using a Faraday balance.[32] They have also observed that the unidirectional exchange anisotropy field shows the predicted proportionality to the inverse of the ferromagnetic layer thickness.

In general, as pointed out by Nogués and Schuller, this formula has been verified for thicknesses up to several hundreds of nm and is believed to be generally true for rather thick ferromagnets.[33] It appears that for thin ferromagnets the relationship is no longer true, probably because the ferromagnetic film ceases to be continuous. The limit of validity for Eq. 2.3 is different for different systems and is related to the conditions of growth and the microstructure.

### 2.2.4.2 AFM thickness

The situation regarding the AFM thickness dependence of $H_E$ is more complex.

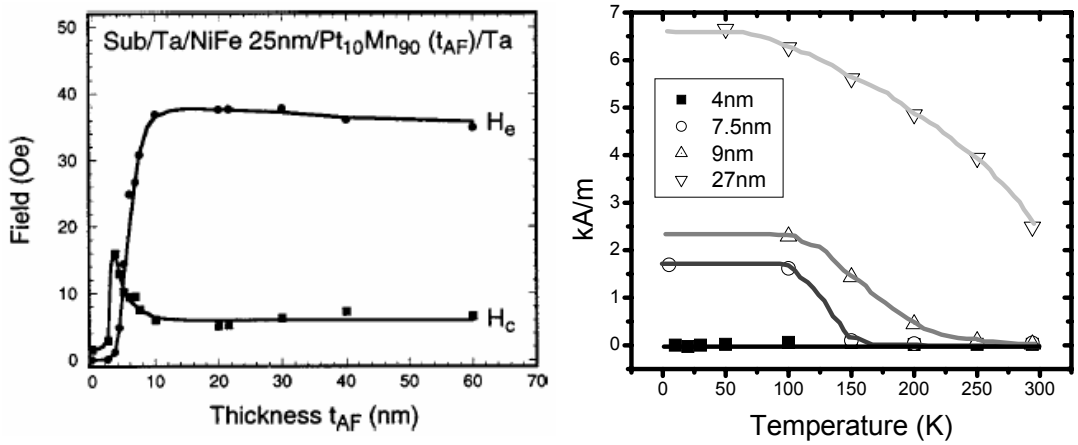


**Fig 2.7** (a) AFM layer thickness dependence of the exchange field and coercivity in the $Ni_{81}Fe_{19}$(25 nm)/$Pt_{10}Mn_{90}$ (from Ref. 36) and (b) Our results showing the temperature dependence of the loop shift from different MnPt thicknesses in Glass/Ta(10 nm)/$Ni_{81}Fe_{19}$(18 nm)/ $Pt_{40}Mn_{60}$ exchange biased samples measured with linear MOKE.[i]

[i] Samples were grown by Dr. D. Spenato, Laboratoire de Magnetisme de Bretagne CNRS UBO, Brest, France.

Usually, for thin antiferromagnets (a few nm) there is no exchange bias. Then there is a sharp increase until a maximum value of $H_E$ is achieved at around 20 nm and subsequently the exchange bias value remains constant. Intuitively, this can be understood in terms of the stability of the AFM order. When the antiferromagnet is too thin the ferromagnetic spins that couple at the interface are able to drag the AFM spins during the magnetization reversal. For thicker AFM layers, the AFM order stiffens the interface and this leads to the appearance of a loop shift. Finally, after the AFM order is established there are no variations with increasing AFM thickness.

In addition, a coercivity peak, similar to the one in Fig. 2.5 is often observed (see Fig. 2.7a). Its explanation has been addressed in terms of an interfacial uniaxial anisotropy induced by a higher order exchange coupling terms,[34] a spin flop state in the AFM layer,[35] and calculations based on reversible and irreversible transitions of the magnetic moments in this FM/AFM system.[36,37]

Fig. 2.7b shows that the AFM thickness dependence is strongly influenced by the different Néel temperatures, and therefore blocking temperatures, for the varying AFM thicknesses.

### 2.2.4.3 Spacer thickness dependence and long-range exchange bias

Similarly to the exchange coupling of two ferromagnetic layers across a non-magnetic spacer, it has been established that the exchange bias interaction can also propagate through a non-magnetic spacer layer. Effectively, the spacer decouples the AFM and FM spins at the interface and it has been often observed that $H_E$ decreases with increasing spacer thickness.

However, unlike FM/spacer/FM systems that show an oscillatory behavior as a function of space thickness, using trilayers of FM/spacer/AFM with Ag, Au, and Cu as spacer layer materials, Gökemeijer et al. have found that the strength of the observed exchange coupling decays exponentially and extends over as much as 5 nm (see Fig. 2.7a).[38] Our own measurements of a Fe/Cu/CoO system, presented on Fig. 2.7b, revealed a similar decrease and a limit of 3.5 nm.

Gruyters et al. found that the decrease of exchange bias was even sharper than the one observed by Gökemeijer et al.[39]. However, although these findings indicate a possible RKKY[ii]-like nature for exchange bias, no oscillations of the effect were observed.

Three years later, oscillations *were* observed by Thomas et al. however those were not monotonic and were attributed to interface roughness.[40]

The first oscillatory exchange bias effect in FeNi/Cu/FeMn and FeNi/Cr/FeMn trilayer systems, were reported by Mewes et al. The authors found that the period of the oscillatory exchange bias field is half of the period of the oscillatory interlayer coupling in the corresponding FM/spacer/FM systems with the same spacer, indicating that the observed effect is caused by an analogous coupling mechanism, being, however, sensitive to the absolute value of the coupling strength and not to its sign.[41]

In another FM/spacer/AFM trilayer system (NiO/Cu/NiFe), Lin et al. have observed a strong temperature dependence of the characteristic behavior of the interlayer exchange bias coupling. The oscillation of the interlayer exchange bias coupling was

[ii] Ruderman, Kittel, Kasuya and Yosida.

found to be *thermally* assisted. At low temperature, the exchange bias field decreased monotonically with the Cu spacer thickness. Increasing the temperature close to the Néel temperature, the interlayer exchange bias field became oscillatory with the Cu spacer thickness. A simple picture of the temperature-dependent competition between the RKKY-like coupling and the antiferromagnetic coupling within the antiferromagnetic layer as well as the interlayer dipolar interaction was proposed to explain these results.[42]

Y.-J. Lee et al. produced a theoretical framework for these results. They calculated the long-range exchange bias between a ferromagnet and an antiferromagnet separated by a nonmagnetic metal spacer. The RKKY interaction and dipolar interaction were used to analyze the temperature effects and thickness dependence in the trilayer structure. The experimental observed oscillatory exchange bias through the metal spacer was in good agreement with the calculated results.[43]

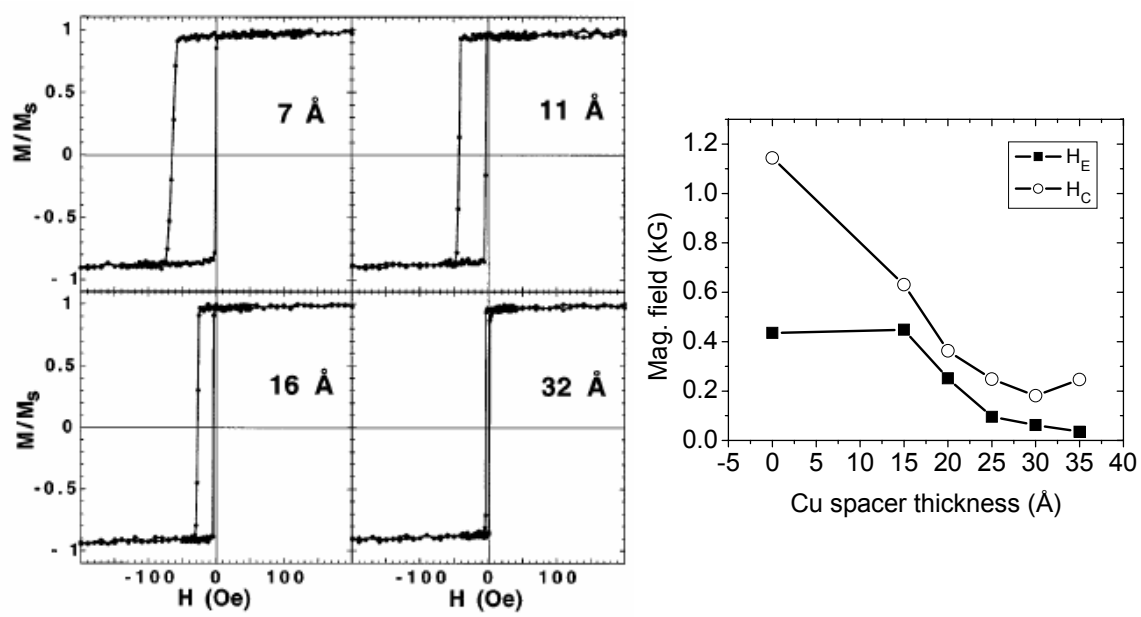


**Fig 2.7** a) Hysteresis loops for 30 nm Py/Au/30 nm CoO. The thickness of the Au spacer layer is indicated in each case (from Ref. 38). b) Our results showing the loop shift $H_E$ and coercivity $H_C$ as function of the Cu spacer layer thickness in Si(111)/Fe(6 nm)/Cu/CoO(2 nm)/Au(6 nm) wedge sample, measured with MSHG at temperature of 10K after field-cooling.

In a different kind of system, J. W. Cai et al. studied the exchange interaction between antiferromagnetic FeMn layers across a Cu spacer by employing the exchange bias as a probe in multilayers of "NiFe/thin FeMn/Cu/ thick FeMn." Interestingly, this group found that with variation of the Cu spacer thickness, the indirect exchange interaction, monitored through the response of the exchange bias, oscillated with a period of approximately 1.8–2.0 nm. This is about twice that for ferromagnetic films separated by a Cu spacer. From these results the authors deduced that the long-range oscillatory exchange interaction is a basic and universal feature in both metallic ferromagnetic layers separated by nonmagnetic metals and metallic antiferromagnetic layers separated by a nonmagnetic metal. It is expected to be due to the quantum interferences induced by the

spin-dependent interface reflection of Bloch waves with different oscillating periods originating from the difference in interface reflection conditions between ferromagnetic and antiferromagnetic spin ordering.[44] Although not directly addressing the long-range interaction between FM and AFM materials, the fact that the authors observe such interaction between AFM layers gives indirect evidence for the problem.

## 2.3 Theoretical models

Regarding exchange bias, it can be said that the experiments are well ahead of the theory. In the first model, proposed by Meiklejohn and Bean, assuming that $J_{FM} \geq J_{INT} \geq J_{AFM}$, the predicted $H_E$ values were orders of magnitude larger than the observed ones. Subsequent attempts at calculations were mainly focused on proposing a mechanism by which this number could be reduced. It is widely recognized that one of the most important reasons for the theoretical difficulties comes from the lack of experimental techniques able to probe the buried magnetic interfaces. As a consequence, all calculations, at one moment or another, make assumptions regarding these interfaces.

There are two "classical" theories for exchange bias although more have been developed.[45,46] Malozemoff was the first to propose a model based on random defects occurring at the FM/AFM interface.[47] The same year, Mauri et al. put forward an alternative explanation which main feature was a domain wall extending in the antiferromagnet.[48] Because of their importance, we will describe briefly these models below.

A domain wall mechanism but this time in the ferromagnet was also considered by Kiwi et al. in 1999. Our experiments, presented in Chapter six, address this hypothesis and because it has recently attracted significant attention we will discuss the FM domain wall model in more details.

### 2.3.1 Random interface model

In this model, the unidirectional anisotropy is the result of random interface roughness that gives rise to a random magnetic field acting on the interface spins (Fig. 2.8). This interface magnetic field pins the ferromagnetic spins at randomly located defect sites and the mechanism by which the magnetization reversal is affected is similar to that described in Fig. 2.1. The obtained loop shift is then:

$$H_E = \frac{2}{M_{FM} t_{FM}} \sqrt{\frac{J_{AFM} K_{AFM}}{a}}, \tag{2.4}$$

where a is the lattice parameter. This formula reduces the value obtained from Eq. 2.2 by two orders of magnitude and therefore is in better agreement with the experimental results. However, this theory relies heavily on a defect concentration at the interface which is not consistent with experiments.

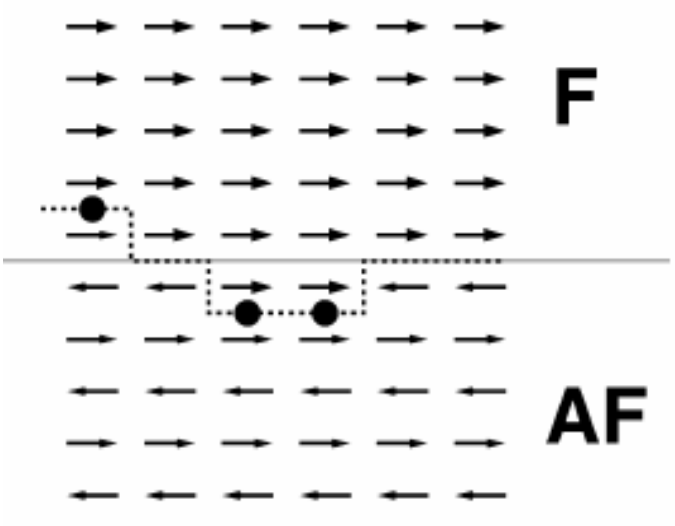


**Fig 2.8** Random defects at the ferromagnetic/antiferromagnetic interface (black dots) lead to the local pinning of the ferromagnetic interface spins.

### 2.3.2 Antiferromagnetic domain wall model

In order to lower the energy at the interface, Mauri et al. proposed the formation of a planar domain wall at the interface with the antiferromagnet when the magnetization rotates as it is shown in Fig. 2.9.

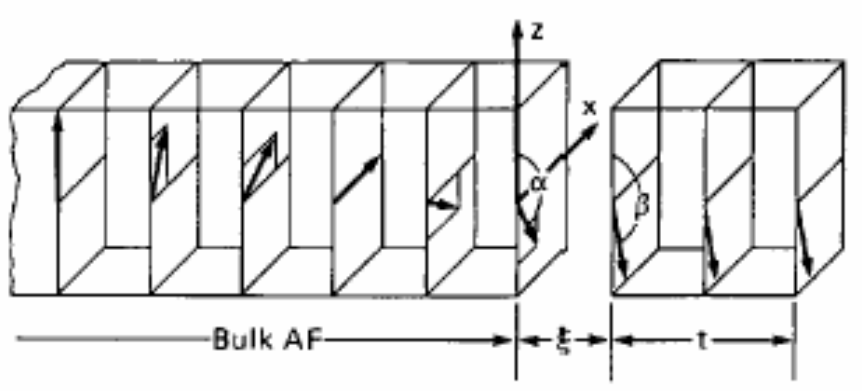


**Fig 2.9** Formation of a domain wall in the antiferromagnet at the interface with the ferromagnet material in the case of the Mauri model. The spins of only one sublattice of the antiferromagnet are shown. $\xi$ is the distance separating the two materials and t is the thickness of the ferromagnet.

The AFM was assumed to be infinitely thick and the spins were confined in the x-z planes. The AFM spins at the interface are strongly coupled to the FM layer and as the magnetization rotates under the influence of an external field, the interfacial AFM spins

follow the reversal while a domain wall develops in the AFM. The stiffness of the domain wall acts as the interfacial pinning described in Fig. 2.1: the first magnetization reversal is resisted by the domain wall, while the second reversal is facilitated as the domain wall springs back. Thus this mechanism also leads to a hysteresis loop shift.

With these assumptions, the exchange bias value is also in better agreement with the experimentally observed one than in the model of Meiklejohn and Bean. However, once again, the authors rely heavily upon an interface mechanism that one has not been able to verify experimentally.

### 2.3.3 Ferromagnetic domain wall model

While AFM domain walls have been featured prominently in both theoretical and experimental studies, FM domains have received much less attention. Because the *intra*ferromagnetic layer interaction is presumably much stronger than the *inter*facial interaction, most models neglect the FM spin structure perpendicular to the AFM/FM interface.[49]

Miller and Dahlberg were some of the first to propose the idea of a partial domain wall extending into the ferromagnet (see Fig 2.10).[50]

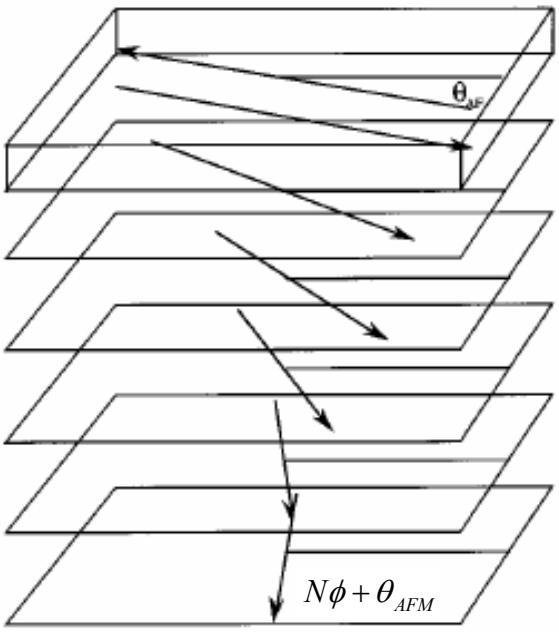


**Fig 2.10** A single ferromagnetic film N atoms thick covered with an antiferromagnetic layer. The angle between the spin orientation of each successive atomic layers is $\phi$. An external magnetic field is applied along a direction greater or equal to $N\phi + \theta_{AFM}$, where $\theta_{AFM} = 0$ is defined as the pinning direction of the antiferromagnet.

Three years later, Kiwi et al. proposed a theoretical model based on this idea.[51,52] The model was characterized by:

i) A compensated AFM interface.
ii) The first AFM interface layer is in a canted spin configuration with respect to the direction of the FM spins.
iii) The AFM interface freezes into a metastable state and as a consequence the EB energy is reversibly stored in a spring-like magnet or incomplete domain wall (IDW) in the FM.

An analytical solution of this model was proposed by Mejia-Lopez et al.[53] in which a dimensionless formula for $H_E$ was derived as a function of the effective interface coupling $k = J_{INT}/J_{FM}$ and the number of FM monolayers $N_{FM}$.[iii]

The formula reads:

$$H_E = -\frac{x\left[kx\left(2N_{FM}-1\right)\left(1-x^2\right)+24\right]}{N_{FM}\left[x^2\left(N_{FM}+1\right)+3\left(N_{FM}-1\right)\right]}, \tag{2.4}$$

where $x$ is the solution of a lengthy polynomial equation relating $k$ to $N_{FM}$. In the weak interfacial coupling limit, the expression becomes:

$$H_E = -\frac{k}{N_{FM}}, \tag{2.5}$$

which is very similar to Eq. 2.2.

This FM-IDW model has received significant attention from the scientific community and several interpretations of experimental results have been made in support of it.[54,55]

## 2.4 Conclusions

Already in the intuitive model that we first presented, we have seen that exchange bias is an interface effect. Next we have observed how this is reflected in the properties of the phenomenon such as the thickness of the antiferromagnetic layer or that of a nonmagnetic spacer inserted at the interface. Finally, we have shown how crucial the understanding of the interface is for the theoretical work on this subject and we have paid particular attention to the hypothesis of an incomplete domain wall forming in the ferromagnet.

In this Chapter, it has become evident that most experimental studies of exchange bias make use of the measurement of the hysteresis loop shift, which is presented as one of the main characteristics of the effect and has almost become synonymous with it. However, it is striking to realize that half a century of hysteresis loop shift measurements

[iii] In the formula for $k$, $J_{INT}$ is the same quantity as in Eq. 2.1 and $J_{FM}$ is the nearest neighbor exchange interaction for the ferromagnet.

have failed to solve the problem that this phenomenon represents. While studying the training effect, it is immediately obvious that repeated reversal of the magnetization dramatically affects the system. Furthermore, even in the case of a single hysteresis loop measurement, different consecutive reversal mechanisms can be observed[1]. Therefore, it becomes increasingly apparent that a complete understanding of exchange bias requires new alternative experimental approaches.

In the next Chapter, we will focus our attention on the interface sensitive technique of Magnetization-induced Second Harmonic Generation.

## References:

[1] J. Nogués, I. K. Schuller, J. Magn. Magn. Mater. **192**, 203 (1999).

[2] W. H. Meiklejohn and C. P. Bean, Phys. Rev. **102**, 1413 (1956).

[3] W. H. Meiklejohn and C. P. Bean, Phys. Rev. **105**, 904 (1957).

[4] W. H. Meiklejohn, J. Appl. Phys. **33**, 1328 (1962).

[5] J. S. Kouvel, J. Phys. Chem. Solids **21**, 57 (1961).

[6] J. S. Kouvel, J. Phys. Chem. Solids **24**, 795 (1963).

[7] H. Ohldag, A. Scholl, F. Nolting, E. Arenholz, S. Maat, A.T. Young, M. Carey, and J. Stöhr, Phys. Rev. Lett. **91**, 017203 (2003).

[8] C. Schlenker, Phys. Status Solidi **28**, 507 (1968).

[9] M. D. Stiles and R. D. McMichael, Phys. Rev. B **60**, 12950(1999).

[10] P. J. van der Zaag et al., J. Appl. Phys. **79**, 5103 (1996).

[11] T. Ambrose and C. L. Chien, J. Appl. Phys. **83**, 6822 (1998).

[12] A. J. Devasahayam and M. H. Kryder, J. Appl. Phys. **85**, 5519 (1999).

[13] D. Alders et al., Europhys. Lett. **32**, 259 (1995).

[14] T. Ambrose and C. L. Chien, Phys. Rev. Lett. **76**, 1743 (1996).

[15] D. Herrmann-Ronzaud, P. Burlet, and J. Rossat-Mignod, J. Phys. C **11**, 2123 (1978).

[16] M. Ali, C. H. Marrows, M. Al-Jawad, B. J. Hickey, A. Misra, U. Nowak, and K. D. Usadel, Phys. Rev. B **68**, 214420 (2003).

[17] H. Danan, H. Gengnagel, J. Steinert, A. Linzen, J. de Phys. (France) Coll. **32**, 1 (1971).

[18] E.V. Shipil, K.Y. Guslienko, B. Szymanski, IEEE Trans. Magn. **30**, 797 (1994).

[19] E. Pina, C. Prados, and A. Hernando, Phys. Rev. B **69**, 052402 (2004).

[20] C. Schlenker, S.S.P. Parkin, J.C. Scott, and K. Howard, J. Magn. Magn. Mater. **54**, 801 (1986).

[21] K. Zhang, T. Zhao, and M. Fujiwara, J. Appl. Phys. **89**, 6910 (2001).

[22] S.G. te Velthuis, A. Berger, and G.P. Felcher, J. Appl. Phys. **87**, 5046 (2001).

[23] T.J. Moran, J.M. Gallego, I.K. Schuller, J. Appl. Phys. **78**, 1887 (1995).

[24] T.J Moran, I.K. Schuller, J. Appl. Phys. **79**, 5109 (1996).

[25] T.J. Moran, J. Nogués, D. Lederman, I.K. Schuller, Appl. Phys. Lett. **72**, 617 (1998).

[26] A. Hochstrat, Ch. Binek, and W. Kleemann, Phys. Rev. B **66**, 092409 (2002).

[27] H. Hoffmann, Phys. Rev. Lett. **93**, 097203 (2004).

[28] C. Binek, Phys. Rev. B **70**, 014421 (2004).

[29] D. Niebieskikwiat and M. B. Salamon, Phys. Rev. B **72**, 174422 (2005).

[30] C. Binek, X. He, and S. Polisetty, Phys. Rev. B **72**, 054408 (2005).

[31] M. Takahashi, A. Yanai, S. Taguchi and T. Suzuki, Jpn. J. Appl. Phys. **19,** 1093 (1980).

[32] L. Smardz, U. Köbler, W. Zinn, Vacuum, **42**, 283 (1991).

[33] R. Jungblut, R. Coehoorn, M.T. Johnson, J. Aan De Stegge, A. Reinders, J. Appl. Phys. **75**, 6659 (1994).

[34] Z. Qian, J. M. Sivertsen, and J. H. Judy, J. Appl. Phys. **83**, 6825 (1998).

[35] T. C. Schulthess and W. H. Butler, Phys. Rev. Lett. **81**, 4516 (1998).

[36] H. Xi and R. M. White, Phys. Rev. B **61**, 80 (2000).

[37] M. D. Stiles and R. D. McMichael, Phys. Rev. B **63**, 064405 (2001).

[38] N.J. Gökemeijer, T. Ambrose and C.L. Chien, Phys. Rev. Lett. **79**, 4270 (1997).

[39] M. Gruyters, M. Gierlings, and D. Riegel, Phys. Rev. B **64**, 132401 (2001).

[40] L. Thomas, A. J. Kellock, and S. S. P. Parkin, J. Appl. Phys. **87**, 5061 (2000).

[41] T. Mewes, B. F. P. Roos, S. O. Demokritov, and B. Hillebrands, J. Appl. Phys. **87**, 5064 (2000).

[42] M.-T. Lin, C. H. Ho, C.-R. Chang, and Y. D. Yao, Phys. Rev. B **63**, 100404 (R) (2001).

[43] Y.-J. Lee, C.-R. Chang, T.-M. Hong, C. H. Ho and M.-T. Lin, J. Magn. Magn. Mater. **239**, 57 (2002).

[44] J. W. Cai, W. Y. Lai, J. Teng, F. Shen, Z. Zhang, and L. M. Mei, Rhys. Rev. B **70**, 214428, (2004).

[45] N.C. Koon, Phys. Rev. Lett. **78**, 4865 (1997).

[46] M.D. Styles, R.D. McMickael, Phys. Rev. B **59**, 3722 (1999).

[47] A.P. Malozemoff, Phys. Rev. B **35**, 3679 (1987).

[48] D. Mauri, H.C. Siegmann, P.S. Bagus, E. Kay, J. Appl. Phys **62**, 3047 (1987).

[49] W.A.A. Macedo, B. Sahoo, V. Kuncser, J. Eisenmenger, I. Felner, J. Nogues, K. Liu, W. Keune and I. K. Schuller, Phys. Rev. B **70**, 224414 (2004).

[50] B.H. Miller and E. Dan Dahlberg, Appl. Phys. Lett. **69**, 3932 (1996).

[51] M. Kiwi, J. Mejia-Lopez, R.D. Portugal and R. Ramirez, Europhys. Lett. **48**, 573 (1999).

[52] M. Kiwi, J. Mejia-Lopez, R.D. Portugal and R. Ramirez, Appl. Phys. Lett. **75**, 3995 (1999).

[53] J. Meija-Lopez, R. Ramirez and M. Kiwi, J. Magn. Magn. Mater. **241**, 364 (2002).

[54] Z.-P. Li, O. Petracic, R. Morales, J. Olamit, X. Batlle, K. Liu, and I.K. Schuller, Phys. Rev. Lett. **96**, 217205 (2006).

[55] S. Roy, M. R. Fitzsimmons, S. Park, M. Dorn, O. Petracic, I. V. Roshchin, Zhi-Pan Li, X. Batlle, R. Morales, A. Misra, X. Zhang, K. Chesnel, J. B. Kortright, S. K. Sinha, and I. K. Schuller, Phys. Rev. Lett. **95**, 047201 (2005).

# Chapter three

# Magneto-optical effects

When a light wave penetrates into a metal, the electrons of the material are brought into motion by the incoming electromagnetic field. Usually, they oscillate with the same frequency as that of the incident light; however, for more intense electromagnetic fields higher order harmonics appear.[1] This response of the material is called *induced polarization* and can be written as:[2]

$$P = P(0) + P(\omega) + P(2\omega) + P(3\omega) + \ldots \tag{3.1}$$

Each of the harmonics of the fundamental light wave thus radiates at the corresponding frequency resulting in linear responses, Second Harmonic Generation (SHG), third harmonic generation, etc. In this Chapter we will consider only the terms $P(\omega)$, corresponding to linear optics and in particular the Magneto-Optical Kerr Effect (MOKE), and $P(2\omega)$ corresponding to SHG and Magnetization-induced Second Harmonic Generation (MSHG).

MOKE was first observed in 1877 by J. Kerr and it appears in three principal configurations with respect to the direction of the magnetization in the material regarding the plane of optical incidence: polar, longitudinal and transverse. (see Fig. 3.1) In the first two cases, it is characterized by a change of the polarization and/or intensity of reflected light due to a component of the magnetization parallel to the k-vector of the incoming beam. It is a so called "bulk effect" as it occurs throughout the entire light penetration region of the material, as opposed to the surface and interface sensitive MSHG, which in the dipolar approximation and for centrosymmetric materials probes magnetization only in these regions.

In the following paragraphs, the Kerr effect will be briefly discussed. Then a description of SHG, MSHG and the tensor components of their susceptibilities will be given. Finally a formalism for calculating (M)SHG intensities will be provided.

## 3.1. Magneto-optical Kerr effect

MOKE is the result of a difference in the refraction indices for left and right circularly polarized light caused by the presence of a magnetization (this does not occur only in "magnetic" materials and has first been observed by Faraday in a glass tube). We can

calculate these refraction indices by solving in the Fourier domain the wave equation for the electric field vector **E** in a medium:

$$\nabla \times \left(\nabla \times \mathbf{E}(\mathbf{r},t)\right) + \frac{\vec{\varepsilon}(\mathbf{r},t)}{c^2}\frac{\partial^2}{\partial t^2}\mathbf{E}(\mathbf{r},t) = 0 \tag{3.2}$$

where $\vec{\varepsilon}$ is the dielectric tensor of the medium, which for arbitrary direction of the magnetization $\mathbf{M}(m_x, m_y, m_z)$ can be written as:

$$\vec{\varepsilon}(\omega) = \begin{pmatrix} \varepsilon_0(\omega) & \varepsilon_1(\omega)m_z & \varepsilon_1(\omega)m_y \\ -\varepsilon_1(\omega)m_z & \varepsilon_0(\omega) & \varepsilon_1(\omega)m_x \\ -\varepsilon_1(\omega)m_y & -\varepsilon_1(\omega)m_x & \varepsilon_0(\omega) \end{pmatrix} \tag{3.3}$$

The diagonal components of this tensor are nonmagnetic and the off-diagonal ones contain the magnetization contribution. Fig. 3.1 shows the schematic orientation of the experiment.

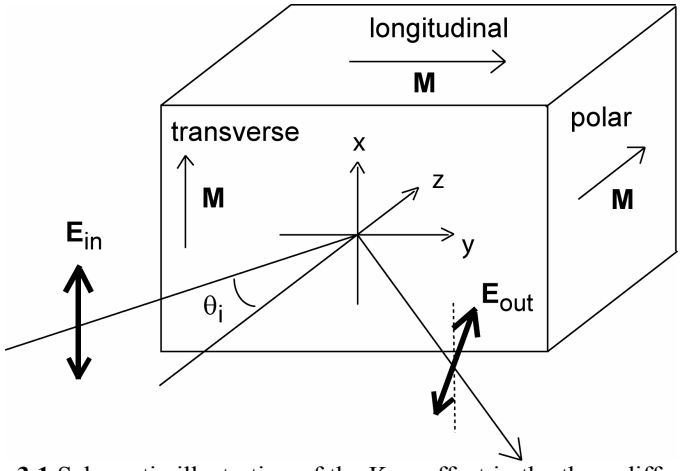


**Fig. 3.1** Schematic illustration of the Kerr effect in the three different configurations.

There are three different Kerr configurations with respect to the optical (y-z) plane: transverse with **M** along (1,0,0), longitudinal with **M** along (0,1,0) and polar with **M** along (0,0,1), see Fig. 3.1. In the longitudinal case, it can be said that the magnetization along the y direction results from electrical current loops in the x-z plane. Since the medium is isotropic, mirror reflection operations should not affect it. If we now perform a mirror reflection operation in the x-y plane, we can see that this will result in reversing the direction of the current loop producing the magnetization, i.e. the magnetization direction will be reversed. This operation reduces the symmetry and therefore all components of the dielectric tensor associated with it (namely $\pm\varepsilon_1 m_z$) should be zero. The same argument applies for the mirror reflection in the y-z plane, i.e. $\pm\varepsilon_1 m_x = 0$. Only the mirror operation in the x-z plane conserves the direction of **M** and therefore

$\pm\varepsilon_1 m_y \neq 0$. By following a similar reasoning the tensor components for the polar and transverse configuration can be found. This is important since we will encounter the same kind of symmetry conservation arguments for determining the tensor elements of the nonlinear susceptibility in the cases of SHG and MSHG.
For the three Kerr configurations, the expression of the right (+) and left (–) circularly polarized waves is of the form: $\mathbf{E}^{\pm}(\omega) = E^{\pm} e^{i\omega(t-\frac{1}{c}\mathbf{n}_{\pm}\cdot\mathbf{r})}$, with $\mathbf{n}_{\pm}$ respectively the refraction index vectors for the circular polarization. The solutions of Eq. 3.2 are then:

$$\text{longitudinal Kerr effect:} \quad n_{\pm}^2 = \varepsilon_0 \pm i\varepsilon_1 \sin\theta_t \tag{3.4}$$

$$\text{polar Kerr effect:} \quad n_{\pm}^2 = \varepsilon_0 \pm i\varepsilon_1 \cos\theta_t \tag{3.5}$$

$$\text{transverse Kerr effect :} \quad n_1^2 = \varepsilon_0 \text{ and } n_2^2 = \varepsilon_0 + \frac{\varepsilon_1^2}{\varepsilon_0} \tag{3.6}$$

where $\theta_t$ is the transmission angle.

It can be seen that for both the polar and the longitudinal cases the different refraction indices will result in different reflections for left and right circularly polarized light. As a consequence, the polarization of the incoming linearly polarized light will be rotated (Kerr rotation) and will become elliptical (Kerr ellipticity). However, no such effects are present for the transverse Kerr effect; only the amplitude and the phase of the reflected light will be affected by magnetism.

Note that a "Kerr rotation-like" effect can still be observed in the transverse configuration if the polarization of the incoming light is in an intermediate position between S and P. In that case, if there is a different amplitude and/or phase change for the S and P components, the net result will be a rotation and/or ellipticity variation

In our studies we used mainly the longitudinal Kerr effect.

## 3.2. Second Harmonic Generation

As it was introduced earlier, intense electromagnetic fields can affect the optical properties of matter leading to nonlinear optical effects.[3] Thus, the induced polarization in the material can contain higher-order terms; see Eq. 3.1, where the polarization at the second harmonic frequency is given by:

$$\mathbf{P}(2\omega) = \chi^D \mathbf{E}(\omega)\mathbf{E}(\omega) + \chi^Q \mathbf{E}(\omega)\nabla\mathbf{E}(\omega) \tag{3.7}$$

In this formula, $\mathbf{E}(\omega)$ represents the electric field at the fundamental frequency $\omega$, $\chi^D$ is a 3rd-rank susceptibility tensor representing the electric dipole contributions and $\chi^Q$ is a 4th-rank susceptibility tensor representing the quadrupolar contributions.

Dipolar contributions are forbidden in the bulk of centrosymmetric materials and only appear at places where the inversion symmetry is broken,[4] such as a surface or an

interface.[5,6] For that reason, $\chi^{D}$ is often referred to as "surface/interface contribution" to SHG.

The quadrupolar contributions $\chi^{Q}$ include the gradient of the electric field in the surface region of the sample (due to the electronic structure of the surface) and that of the fundamental light-induced electric field (due to absorption along the light penetration depth). Because this term is present in all materials it is often called "bulk contribution" to the SHG. In the limit of thin films, its value is usually much smaller[iv,7] than that of the dipolar "surface/interface contribution" and therefore it may be included into an effective nonlinear susceptibility $\chi^{eff}$, so that:

$$\mathbf{P}_i(2\omega) = \chi_{ijk}^{eff}\mathbf{E}_j(\omega)\mathbf{E}_k(\omega) \tag{3.8}$$

where the indices $i$, $j$ and $k$ refer to the Cartesian coordinates. For the sake of simplifying the notations, in the following, we will omit the superscript "*eff*". In principle, the 3rd rank tensor $\chi^{(2)}$ has 27 elements; however because $\mathbf{E}_j(\omega)$ and $\mathbf{E}_k(\omega)$ are equivalent for a single beam, the two last indices can be exchanged. This brings the number of independent tensor elements to 18 and those can be written in their general form as:

$$\begin{pmatrix} P_x \\ P_y \\ P_z \end{pmatrix} = \begin{pmatrix} \chi_{xxx} & \chi_{xyy} & \chi_{xzz} & \chi_{xyz} & \chi_{xzx} & \chi_{xyx} \\ \chi_{yxx} & \chi_{yyy} & \chi_{yzz} & \chi_{yzy} & \chi_{yzx} & \chi_{yxy} \\ \chi_{zxx} & \chi_{zyy} & \chi_{zzz} & \chi_{zyz} & \chi_{zxz} & \chi_{zyx} \end{pmatrix} \begin{pmatrix} E_x^2 \\ E_y^2 \\ E_z^2 \\ 2E_yE_z \\ 2E_zE_x \\ 2E_xE_y \end{pmatrix} \tag{3.9}$$

The number of components can be further reduced by considering symmetry operations, for instance in the case of second harmonic generated from an isotropic surface laying in the x-y plane (see Fig. 3.2).

Here we consider only the two mirror reflection operations in the planes y-z and x-z since it is clear that the sample is not invariant under a mirror operation in the x-y plane. Because **P** and **E** are vectors, changing x to –x (this is equivalent to a mirror operation in the y-z plane) changes $P_x$ to $-P_x$ as well as $E_x$ to $-E_x$. Therefore, $x \to -x \Rightarrow P_x \propto \chi_{xxx}\cdot E_xE_x \to -P_x \propto \chi_{xxx}\cdot(-E_x)(-E_x)$ which is only possible if $\chi_{xxx} = 0$. Similarly, $x \to -x \Rightarrow P_x \propto \chi_{xyy}\cdot E_yE_y \to -P_x \propto \chi_{xyy}\cdot E_yE_y$ which requires $\chi_{xyy} = 0$. On the other hand, $x \to -x \Rightarrow P_x \propto \chi_{xzx}\cdot E_zE_x \to -P_x \propto \chi_{xzx}\cdot E_z(-E_x)$ where

[iv] The quadrupole contribution can sometimes be significant. This has been observed for instance, in the case of a Fe/Au superlattice where the second-harmonic is produced by a top surface and many interfaces. In this case there is a strong cancellation expected of the interface dipole contribution between neighboring interfaces $I_n$ and $I_{n+1}$ due to their opposite orientation. However a small difference in the local optical fields, which are retarded and attenuated at the lower interface leads to a fully antisymmetric part of the interface susceptibilities that contributes to the quadrupole part together with a response from the interior of the layers.

$\chi_{xzx} \neq 0$. Henceforth, all tensor components with an odd number of indices x are eliminated. The same reasoning can be applied to the $y \to -y$ transformation (mirror operation in the x-z plane) and it is also found that tensor elements with an odd number of y indices are zero. Since obviously the inversion symmetry is not conserved under $z \to -z$, the last component $\chi_{zzz} \neq 0$.

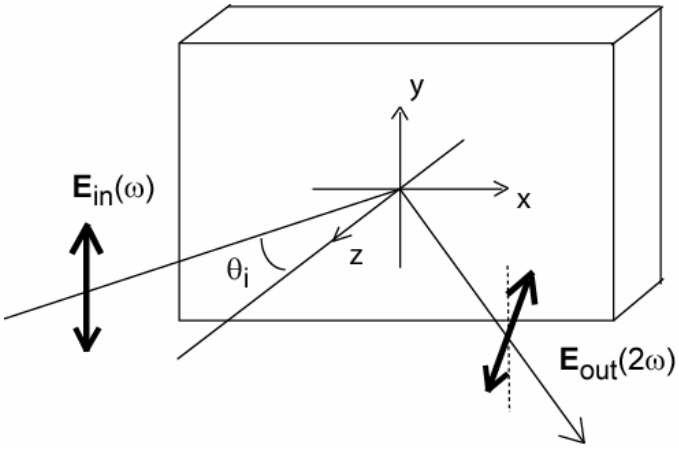


**Fig. 3.2** Schematic illustration of the second harmonic generation from an isotropic surface in the x-y plane.

Consequently, Eq. 3.9 becomes:

$$\begin{pmatrix} P_x \\ P_y \\ P_z \end{pmatrix} = \begin{pmatrix} 0 & 0 & 0 & 0 & \chi_{xzx} & 0 \\ 0 & 0 & 0 & \chi_{yzy} & 0 & 0 \\ \chi_{zxx} & \chi_{zyy} & \chi_{zzz} & 0 & 0 & 0 \end{pmatrix} \begin{pmatrix} E_x^2 \\ E_y^2 \\ E_z^2 \\ 2E_yE_z \\ 2E_zE_x \\ 2E_xE_y \end{pmatrix} \tag{3.10}$$

where $\chi_{yzy} = \chi_{xzx} \neq \chi_{zyy} = \chi_{zxx} \neq \chi_{zzz}$.

## 3.3. Magnetization-induced Second Harmonic Generation

In the presence of a magnetization in addition to the crystallographic term in Eq. 3.8, a magnetic contribution to the second harmonic polarization appears:

$$\mathbf{P}_i(2\omega) = \chi_{ijk}^{cr}\mathbf{E}_j(\omega)\mathbf{E}_k(\omega) + \chi_{ijkl}^{magn}\mathbf{E}_j(\omega)\mathbf{E}_k(\omega)\mathbf{M}_l \tag{3.11}$$

where $\chi_{ijkl}^{magn}$ is a 4[th]-rank axial tensor for the magnetization (**M**) induced part. This new term is the source of Magnetization-induced (or Magnetic) Second Harmonic Generation.[8,9]

Though MSHG from magnetic surfaces was first predicted by Ru-Pin Pan *et al.*,[10] a discussion of magnetism in the context of second harmonic generation can already be found in the papers of Pershan[11] and Adler,[12] whereas the corresponding magnetic point symmetry groups were given by two scientists in France.[13] In their paper entitled "Génération du second harmonique dans les substances magnétiques ordonnées" (*Generation of Second Harmonic in Magnetically Ordered Substances*, presented by Louis Néel), Joseph Lajzerowicz and Marcel Vallade clearly state that taking into account the magnetic symmetry groups one should expect the generation of second harmonic due to magnetic properties. Furthermore, to our best knowledge, the first expression for $\chi_{ijkl}^{magn}$ was derived by Borisov and Lyubchanskii in a paper published in the Soviet Union.[14]

Shortly after the paper of Ru-Pin Pan et al., MSHG was observed experimentally from an Fe surface[15] and from Co/Au interfaces.[16]

Similarly to MOKE, we can observe a change in the polarization and/or intensity of the second harmonic light due to the presence of magnetization in the sample. However, because of its extreme sensitivity to symmetry breaking, this technique has become an important tool for probing magnetism[17] at surfaces and especially at buried interfaces.[18-24] Additionally, since in this thesis we are interested in ferromagnetic/antiferromagnetic interfaces it should be noted that MSHG signals can also be generated by antiferromagnetic ordering in materials.[25,26]

Since **M** is an axial vector, by definition it is invariant under inversion symmetry. Therefore, just as it was discussed previously for SHG, in centrosymmetric media MSHG can only be generated at surfaces and interfaces.[27]

Although not affected by the inversion symmetry, magnetization does change sign upon time reversal symmetry.[28,29] Just as with linear MOKE and SHG we can find the particular components of $\chi_{ijkl}^{magn}$ by looking at its invariance under $\mathbf{r} \to -\mathbf{r}$ and $t \to -t$.

Fig. 3.3 shows the two main configurations for MSHG.

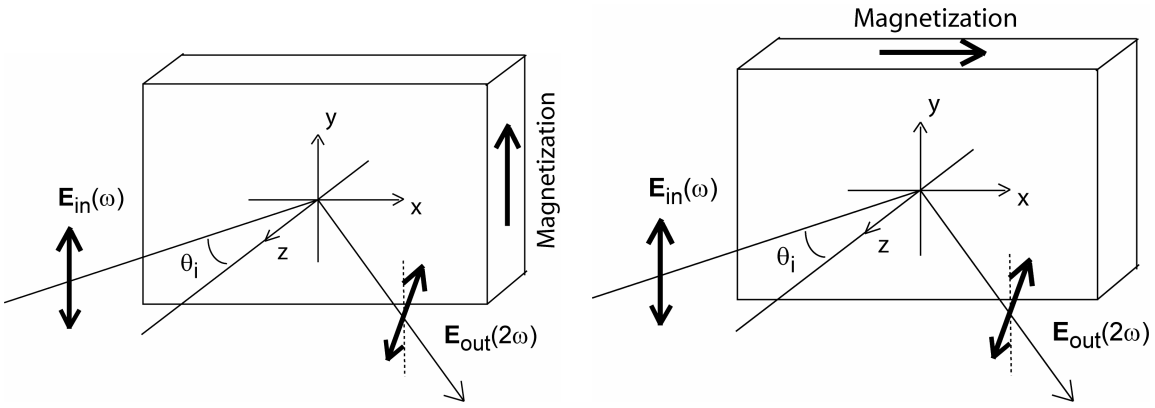


**Fig. 3.3** The two main geometries for MSHG. In the left panel the transverse configuration with the magnetization along the y-direction and in the right panel the longitudinal configuration with the magnetization along the x-direction.

In the longitudinal configuration **M** is along the x-axis and therefore the 4th-rank tensor $\chi_{ijkl}^{magn}$ can be considered as a 3rd-rank tensor for the particular case $l=1$. In the following we will discuss only this magnetic tensor and in order to simplify the notations we will omit the superscript. Applying a mirror reflection in the y-z plane does not affect the sign of $M_x$. Consequently, the symmetry operation $x \to -x$ leads to the following formula $P_x \propto \chi_{xxx}(M_x)\cdot E_x E_x \to -P_x \propto \chi_{xxx}(M_x)\cdot(-E_x)(-E_x)$ and therefore $\chi_{xxx}(M_x)=0$. In the same manner it can be found that all tensor components with an odd number of indices x are zero.

A mirror reflection in the x-z place however does change the sign of $M_x$ ($M_x$ can be regarded as resulting from electrical current loops in the y-z plane and a reflection in the x-z plane changes the direction of the current in the loops, effectively reversing the sign of $M_x$) .Therefore, when we apply $y \to -y$, this operation is accompanied by $M_x \to -M_x$. Henceforth $P_y \propto \chi_{yyy}(M_x)\cdot E_y E_y \to -P_y \propto \chi_{yyy}(-M_x)\cdot(-E_y)(-E_y)$. It follows that $\chi_{yyy}(-M_x)=-\chi_{yyy}(M_x)$, i.e. that $\chi_{yyy}$ is odd in the magnetization (it reverses sign when **M** reverses sign). On the other hand, if we now consider the component $\chi_{yzy}$ we see that $P_y \propto \chi_{yzy}(M_x)\cdot E_z E_y \to -P_y \propto \chi_{yyy}(-M_x)\cdot E_z(-E_y)$, i.e. $\chi_{yzy}(-M_x)=\chi_{yzy}(M_x)$ which means that this tensor component is even in the magnetization. Accordingly, all the nonzero tensor components can be found:

$$\chi_{ijk1}^{magn}=\begin{pmatrix} 0 & 0 & 0 & 0 & \chi_{xzx}^{even} & \chi_{xyx}^{odd} \\ \chi_{yxx}^{odd} & \chi_{yyy}^{odd} & \chi_{yzz}^{odd} & \chi_{yzy}^{even} & 0 & 0 \\ \chi_{zxx}^{even} & \chi_{zyy}^{even} & \chi_{zzz}^{even} & \chi_{zyz}^{odd} & 0 & 0 \end{pmatrix} \tag{3.12}$$

One can notice that the *even* components of this tensor are the same as those in Eq. 3.10. Therefore, the appearance of the *odd* tensor components can be seen as the result of introducing magnetization in the sample.[v]

Upon magnetization reversal, the second harmonic intensity changes, giving rise to a *magnetic contrast* according to:

$$I(2\omega) \propto \left|\chi^{even} \pm \chi^{odd}\right|^2 I^2(\omega), \tag{3.13}$$

where $\chi^{even}$ and $\chi^{odd}$ represent the total *even* and *odd* components including their relevant Fresnel factors respectively. One can then define the *asymmetry* (or relative magnetic contrast) as:

$$\mathcal{A}=\frac{I^{\uparrow}-I^{\downarrow}}{I^{\uparrow}+I^{\downarrow}}=\frac{2R}{1+R^2}\cos\phi \approx R\cos\phi \tag{3.14}$$

[v] Note however that the *even* components can depend on the magnetization via higher order terms, even in **M**.

where, $I^{\uparrow\downarrow}$ indicates the second-harmonic intensity for oppositely oriented magnetization, $R = \left|\chi^{odd}\right| / \left|\chi^{even}\right|$, and $\phi$ is the phase angle between $\left|\chi^{odd}\right|$ and $\left|\chi^{even}\right|$. It can be seen that for R<<1, the second harmonic asymmetry is linearly proportional to the magnetization.

However, it is important to notice that in order to have a magnetic contrast in the second harmonic intensity, we need a combination of *even* and *odd* components. If we consider the case of S-polarized fundamental light and a surface in the longitudinal configuration, the second harmonic generated along the P-direction will have the following polarization:

$$P^{S-P} = \chi^{even}_{zyy} \cdot \left|E_y\right|^2 \tag{3.15}$$

This term is even, therefore since $I(2\omega) \propto \left|P\right|^2 I^2(\omega)$ no magnetic contrast is to be observed. Similarly, if we examine the case of the second harmonic polarization along the S-direction, we find that:

$$P^{S-S} = \chi^{odd}_{yyy} \cdot \left|E_y\right|^2 \tag{3.16}$$

where the tensor component is odd and again since $I(2\omega) \propto \left|P\right|^2 I^2(\omega)$ there is no magnetic contrast.

However, if we consider the second harmonic polarization along a direction that is at 45° in between S and P we can combine equations 3.15 and 3.16 into:

$$I(2\omega) \propto \left( \left| \chi^{even}_{zyy} \cdot \left|E_y\right|^2 \right|^2 + \left| \chi^{odd}_{yyy} \cdot \left|E_y\right|^2 \right|^2 \pm 2 \cdot \left| \chi^{even}_{zyy} \cdot \left|E_y\right|^2 \right| \cdot \left| \chi^{odd}_{yyy} \cdot \left|E_y\right|^2 \right| \right) I^2(\omega) \tag{3.17}$$

giving rise to a magnetic contrast.

In a similar manner, it can be established that the tensor for the transverse configuration is[vi]:

$$\chi^{magn}_{ijk1} = \begin{pmatrix} \chi^{odd}_{xxx} & \chi^{odd}_{xyy} & \chi^{odd}_{xzz} & 0 & \chi^{even}_{xzx} & 0 \\ 0 & 0 & 0 & \chi^{even}_{yzy} & 0 & \chi^{odd}_{yxy} \\ \chi^{even}_{zxx} & \chi^{even}_{zyy} & \chi^{even}_{zzz} & 0 & \chi^{odd}_{zxx} & 0 \end{pmatrix} \tag{3.18}$$

By examining the associated second harmonic polarizations, the conditions for observing a magnetic contrast can be derived. (see also Ref. 30 and 31)

[vi] We can compare once again this tensor with the one in Eq. 3.10.

## 3.4. Calculating the MSHG intensity

The incoming electric field can be written as a sum of S and P polarization components, with unit vectors respectively $\hat{e}_S$ and $\hat{e}_P$ (see Fig. 3.4) :

$$\mathbf{E} = \hat{e}_S \cos(\psi) + \hat{e}_P \sin(\psi) \tag{3.19}$$

where $\psi$ is the angle between the incoming polarization and the S-direction of the polarizer.

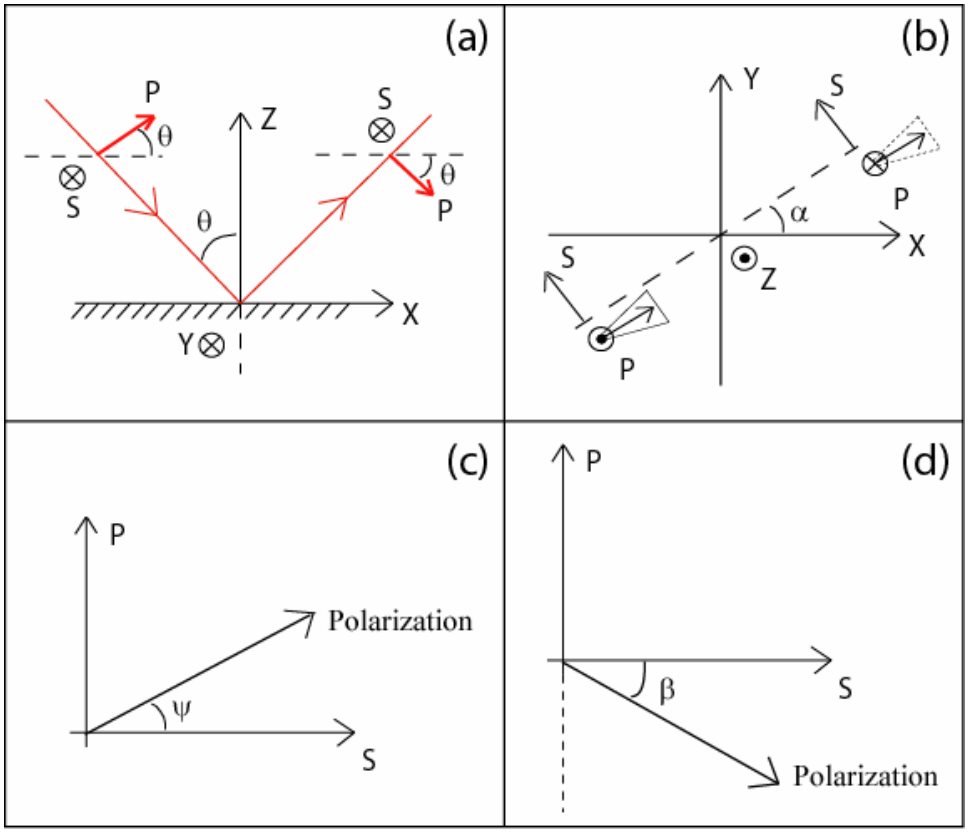


**Fig. 3.4** In (a), a schematic representation of the fundamental and the second harmonic beams relative to the sample as well as the incoming angle θ. In (b), α is the angle between the optical plane of incidence and the x-direction on the sample. In (c), ψ is the angle between the S-direction of the polarizer and the incoming polarization. In (d), β is the angle between the S-direction of the analyzer and the directions of outgoing second harmonic polarization.

These unit vectors can be expressed in terms of the Cartesian coordinates for a coordinate system that we chose on the sample:

$$\begin{aligned}\hat{e}_S &= -\sin(\alpha)\hat{x} + \cos(\alpha)\hat{y} \\ \hat{e}_P &= \cos(\theta)\cos(\alpha)\hat{x} + \cos(\theta)\sin(\alpha)\hat{y} \pm \sin(\theta)\hat{z}\end{aligned} \tag{3.20}$$

where $\theta$ is the angle of incidence and $\alpha$ is the angle between the plane of incidence and the x-direction.

Replacing the unit vectors in 3.19 with the expressions 3.20 we obtain the values of the local electric fields:

$$\begin{aligned}E_X^{IN} &= E_0\big(\cos(\theta)\cos(\alpha)\sin(\psi) - \sin(\alpha)\cos(\psi)\big)\hat{x} \\ E_Y^{IN} &= E_0\big(\cos(\theta)\sin(\alpha)\sin(\psi) + \cos(\alpha)\cos(\psi)\big)\hat{y} \\ E_Z^{IN} &= E_0\sin(\theta)\sin(\psi)\hat{z}\end{aligned} \tag{3.21}$$

The outgoing polarization can then be calculated by:

$$\begin{pmatrix} P_X^{OUT} \\ P_Y^{OUT} \\ P_Z^{OUT} \end{pmatrix} = \begin{pmatrix} \chi_{XXX} & \chi_{XYY} & \chi_{XZZ} & \chi_{XYZ} & \chi_{XXZ} & \chi_{XXY} \\ \chi_{YXX} & \chi_{YYY} & \chi_{YZZ} & \chi_{YYZ} & \chi_{YYZ} & \chi_{YXY} \\ \chi_{ZXX} & \chi_{ZYY} & \chi_{ZZZ} & \chi_{ZYZ} & \chi_{ZYZ} & \chi_{ZXY} \end{pmatrix} \cdot \begin{pmatrix} E_X^{IN\,2} \\ E_Y^{IN\,2} \\ E_Z^{IN\,2} \\ 2E_Y^{IN}E_Z^{IN} \\ 2E_X^{IN}E_Z^{IN} \\ 2E_X^{IN}E_Y^{IN} \end{pmatrix} \tag{3.22}$$

where the susceptibility tensor represents the properties of the sample. Note that for simplicity we have neglected the Fresnel coefficients, which could also be (partially) included in the effective tensor components. The outgoing polarization is expressed in terms of S and P as:

$$\begin{pmatrix} P_S^{OUT} \\ P_P^{OUT} \end{pmatrix} = \begin{pmatrix} -\sin(\alpha) & \cos(\alpha) & 0 \\ \cos(\theta)\cos(\alpha) & \cos(\theta)\sin(\alpha) & -\sin(\theta) \end{pmatrix} \cdot \begin{pmatrix} P_X^{OUT} \\ P_Y^{OUT} \\ P_Z^{OUT} \end{pmatrix} \tag{3.23}$$

The second harmonic polarization after the analyzer is then given by:

$$P_{Analyzer} = P_S^{OUT}\cos(\beta) - P_P^{OUT}\sin(\beta) \tag{3.24}$$

where $\beta$ is the angle between the analyzer and the S-direction.

Finally, the second harmonic intensity is calculated with:

$$I \propto \left|P_{Analyzer}\right|^2 \tag{3.25}$$

Fig 3.5 shows the calculated SHG intensity as function of the azimuthal rotation angle of two hypothetic cubic single crystalline samples with (001) and (111) surface orientations. The corresponding symmetry groups are 4m and 3m respectively.

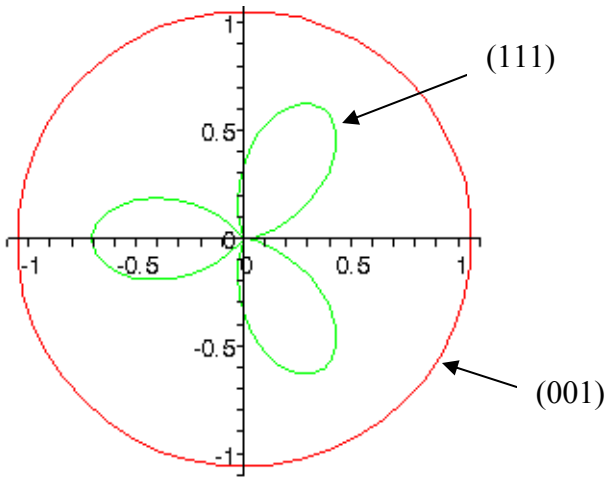


**Fig. 3.5** For the $P_{IN}$-$S_{OUT}$ configuration, the simulated SHG intensity as function of azimuthal rotation angle of the sample in the case of an isotropic tensor such that $\chi_{YZY} = \chi_{XZX} = 1 \neq \chi_{ZYY} = \chi_{ZXX} = 2 \neq \chi_{ZZZ} = 3$ and in the case of a three-fold (3m) tensor such that $\chi_{XXX} = -\chi_{XYY} = -\chi_{YXY} = 1 \neq \chi_{YZY} = \chi_{XZX} = \chi_{ZYY} = \chi_{ZXX} = 2 \neq \chi_{ZZZ} = 3$.

## References:

[1] A.C. Newell and J.V. Moloney, "Nonlinear Optics", ed. by Addison-Wesley Publishinng Company, 1992.

[2] "Nonlinear Optics in Metals", K.H. Benneman, Oxford Sci. Publ., 1999.

[3] J.F. McGilp, J. Phys. D Appl. Phys. **29** 1812 (1996).

[4] V. N. Gridnev, V. V. Pavlov, R. V. Pisarev, A. Kirilyuk, and Th. Rasing, Phys. Rev. B **63**, 184407 (2001).

[5] A. Kirilyuk, G. M. Knippels, A. F. van der Meer, S. Renard, Th. Rasing, I. R. Heskamp, and J. C. Lodder, Phys. Rev. B **62**, R783 (2000).

[6] K. J. Veenstra, A. V. Petukhov, E. Jurdik, and Th. Rasing, Phys. Rev. Lett. **84**, 2002 (2000).

[7] K. Sato, A. Kodama, M. Miyamoto, A. V. Petukhov, K. Takanashi, S. Mitani, H. Fujimori, A. Kirilyuk, and Th. Rasing, Phys. Rev. B **64**, 184427 (2001).

[8] A. Kirilyuk J. Phys. D: Appl. Phys. **35** R189 (2002).

[9] M. Fiebig, D. Fröhlich, K. Kohn, St. Leute, Th. Lottermoser, V. V. Pavlov, and R. V. Pisarev, Phys. Rev. Lett. **84**, 5620 (2000).

[10] R.-P. Pan, H.D. Wei and Y.R. Shen, Phys. Rev. B **39**, 1229 (1989).

[11] P. S. Pershan, Phys. Rev. **130**, 919 (1963).

[12] E. Adler, Phys. Rev. **134**, A728 (1964).

[13] J. Lajzerowicz and M. Vallade, C.R. Acad. Sci. Paris **264**, 1819 (1967).

[14] S.B. Borisov and I.L. Lyubchanskii, Opt. Spektrosk. **61**, 1274 (1986) [Opt. Spectrosc. (USSR) **61**, 801 (1986)].

[15] J. Reif, J.C. Zink, C.M. Shneider and J. Kirschner, Phys. Rev. Lett. **67**, 2878 (1991).

[16] H.A. Wierenga, M. W. J. Prins, D. Abraham and Th. Rasing, Phys. Rev. B **50**, 1282 (1994).

[17] A. V. Petukhov, I. L. Lyubchanskii, and Th. Rasing, Phys. Rev. B **56**, 2680 (1997).

[18] A. Kirilyuk and Th. Rasing, J. Opt. Soc. Am. B **22**, 148 (2005).

[19] P. van Gelderen, S. Crampin, Th. Rasing, and J. E. Inglesfield, Phys. Rev. B **54**, R2343 (1996).

[20] H. A. Wierenga, W. de Jong, M. W. J. Prins, Th. Rasing, R. Vollmer, A. Kirilyuk, H. Schwabe, and J. Kirschner, Phys. Rev. Lett. **74**, 1462 (1995).

[21] M. Straub, R. Vollmer, and J. Kirschner, Phys. Rev. Lett. **77**, 743 (1996).

[22] B. Koopmans, M. Groot Koerkamp, Th. Rasing, and H. van den Berg, Phys. Rev. Lett. **74**, 3692 (1995).

[23] T. M. Crawford, C. T. Rogers, T. J. Silva, and Y. K. Kim, Appl. Phys. Lett. **68**, 1573 (1996).

[24] A. Kirilyuk, Th. Rasing, R. Mégy, and P. Beauvillain, Phys. Rev. Lett. **77**, 4608 (1996).

[25] M. Fiebig, D. Fröhlich, B. B. Krichevtsov, and R. V. Pisarev, Phys. Rev. Lett. **73**, 2127 (1994).

[26] M. Fiebig, D. Fröhlich, G. Sluyterman, and R. V. Pisarev, Appl. Phys. Lett. **22**, 2906 (1995).

[27] W. Hübner and K. H. Bennemann, Phys. Rev. B **52**, 13411 (1995).

[28] M. Trzeciecki and W. Hübner, Phys. Rev. B **62**, 13888 (2000).

[29] R. Stolle, K. J. Veenstra, F. Manders, Th. Rasing, H. van den Berg, and N. Persat, Phys. Rev. B **55**, R4925 (1997).

[30] K. J. Veenstra, *Phase Sensitive Nonlinear Magneto-Optical Spectroscopy*, Ph.D. thesis, Radboud University Nijmegen, the Netherlands (2000).

[31] H. Wierenga, *Magnetization induced optical Second Harmonic Generation on magnetic multilayers*, Ph.D. thesis, Radboud University Nijmegen, the Netherlands (1995).

# Chapter four

# Experimental framework

We have seen that Magnetization-induced Second Harmonic Generation (MSHG) is sensitive to surface and interface magnetization, while the linear magneto-optical Kerr effect (MOKE) can provide us with information on the bulk magnetization. Although both techniques can be used separately, applying them simultaneously presents many advantages because they are complementary.

First of all, simultaneously measuring MSHG and MOKE implies that there is no "time dependence". It is always possible that in between two separate measurements the sample changes due to oxidation, chemical intermixing at the interfaces etc. Furthermore, the synchronization of the two techniques insures that the magnetization properties of the sample are probed at exactly the same spot for both techniques and hence spot size and location dependence is also avoided in the results. Additionally, from a purely experimental point of view, measuring MSHG and MOKE simultaneously allows one to use the results of one technique as a valuable tool to troubleshoot the other.[vii]

On the other hand, such simultaneous measurements require compromises to be made. For instance, the best configuration for MSHG is often that with P-polarized incident light in a transverse magnetization. However, as we saw in the previous Chapter, in this geometry there is neither Kerr rotation nor Kerr ellipticity for linear MOKE. Additionally, for MOKE it is preferable to use a Faraday cell or a photo-elastic modulator as a source of modulation for the lock-in amplifier, while for MSHG a chopper is necessary in order to improve the signal-to-noise ratio with the gated mode counting on the photon counter.

Moreover, there are specific necessities for each technique. For example MSHG requires low average laser power and high peak power in order to avoid heating the sample, while laser power damage on the detector is rarely an issue. On the other hand, reflected laser power has to be handled very carefully with respect to the MOKE photo-detectors and consequently the lock-in amplifier sensitivity.

In this Chapter we will first present the combined MSHG and MOKE setup and then the Ultra High Vacuum (UHV) equipment that was used for preparing clean sample surfaces and interfaces in some of our experiments.

[vii] One should note, however, that even in such a scheme artifacts are possible due to the different profile of the linear and second order polarization created with a focused laser beam. (see Ref. 1)

## 4.1. Combined MSHG and MOKE setup

In Fig. 4.1, the laser source was an Argon-pumped, mode-locked, Ti-Sapphire laser at 800 nm with a Gaussian profile, a pulse width duration ~100 fs and a repetition rate of 82 MHz. The incoming laser power was attenuated using a chopper (C) that additionally provided a reference source for the lock-in amplifier (which was used in the detection of MOKE). A Glan-Taylor polarizer (GT) was used to select the incoming polarization. Subsequently, a lens (L) focused the light onto a spot with diameter of ~100 μm on the sample. Immediately after the lens a color filter RG630 (CF) ensured that no SHG coming from the optical components or the laser was reaching the sample. After reflection from the sample, the laser beam encountered another lens (L') that made it collinear again. Next, a dichroic mirror (DM) separated the fundamental from the generated second harmonic and after passing the appropriate color filters (RG630 and BG39 respectively) each beam followed its own detection line. For MSHG a Glan-Thompson (GTh) analyzer selected the relevant tensor components in the nonlinear susceptibility and a photo-multiplier tube (PMT) was employed for the detection of the photons. For MOKE, a split diode detector consisting of a Wollaston prism (WP) and two photodiodes was used.

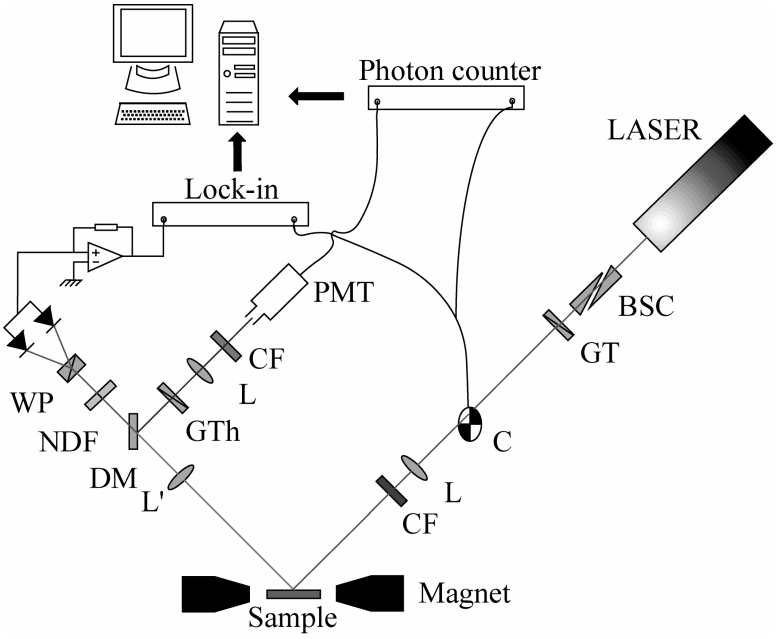


**Fig. 4.1** Schematic representation of the simultaneous MSHG and MOKE setup as described above. The Babinet-Soleil compensator (BSC) rotated the incoming light polarization. The neutral density filter (NDF) was used to attenuate the laser light intensity on the photo-diodes.

After pre-amplification (Stanford Research SR445) the signal from the PMT reached a photon counter (Stanford Research SR400) and the results were stored on a computer as function of the applied magnetic field. Simultaneously, the signal from the lock-in

amplifier (Stanford Research SR530) was stored. The magnetic field was applied in the longitudinal configuration.

## 4.2. Ultra High Vacuum system

In our studies, a single crystal of nickel was cleaned and oxidized in an Ultra High Vacuum system (UHV).[2] Fig. 4.2 shows the UHV chamber which can reach a pressure of $1x10^{-11}$ mbar. It is pumped first with a Turbomolecular pump (Balzers, TPU 270), then at lower pressure with an ion pump (Varian, picotorr 350) having a built-in Titanium Sublimation Cartridge. To lower further the pressure, Cryopumping with liquid nitrogen can be used. The chemical composition of the substances inside the chamber was monitored by a mass spectrometer (MS).

The cleaning was done by argon ion sputtering with a mini beam ion gun (IG) (MinibeamI, Kratos Analytical).[3] The Ar was dosed with a leak valve (LV). After sputtering, the sample was annealed at 600º by means of electron bombardment from a tungsten filament that was built in the sample holder, behind the sample. For the purpose of this bombardment, the filament was set at -600 V relative to the sample. The temperature was measured with a K-type thermo-couple fixed on the sample surface.

Structural and chemical analyses of the surface were conducted with Low Energy Electron Diffraction (LEED) and Auger Electron Spectroscopy (AES), combined in the Spectaleed LEED/AES-system (SL) from Omicron.

In a LEED experiment,[4,5] the normally incident low energy (30-150 eV) electron beam is regarded as a succession of electron waves. These waves are scattered by regions of high localized electron densities – the surface atoms. Only the elastically scattered electrons contribute to the diffraction pattern that can be observed on a spherical fluorescent screen behind the electron gun. Secondary electrons are removed by an energy filtering grid that precedes the fluorescent screen. The analysis of the spot positions in the diffraction pattern provides information on the symmetry and rotational alignment of the unit cell of the crystal.[6] The existence of a sharp spot pattern implies the existence of a well ordered surface[7] (see Fig. 4.3a).

AES is commonly used to determine the composition of the surface layers of the sample.[8,9] As for LEED, an electron gun is directed normally to the sample and the combination of grids and the fluorescent screen serve as detector. The incident electrons, having energy ~3 keV, eject core electrons from the atoms at the surface, thus producing core holes in the energy levels of these atoms. Such an atom is then in a highly excited state and in order to lower its energy, an electron from a higher energy level drops to the level of the core hole. In this decay process, the energy liberated is simultaneously transferred in the form of kinetic energy to a second electron situated in the higher energy level. The latter is then ejected from the atom in the direction of the detection apparatus. The fluorescent screen is electronically connected to spectrometer electronics (SE). Since the initial ionization is non-selective, the core hole may occur in different shells and there may be various Auger transitions for any given chemical element.[10,11] Since each chemical element in the sample will give a characteristic spectrum of kinetic energy peaks (see Fig. 4.3b), AES can be used to determine the composition of the surface layer. In particular, it is used to check whether the surface studied is really clean.

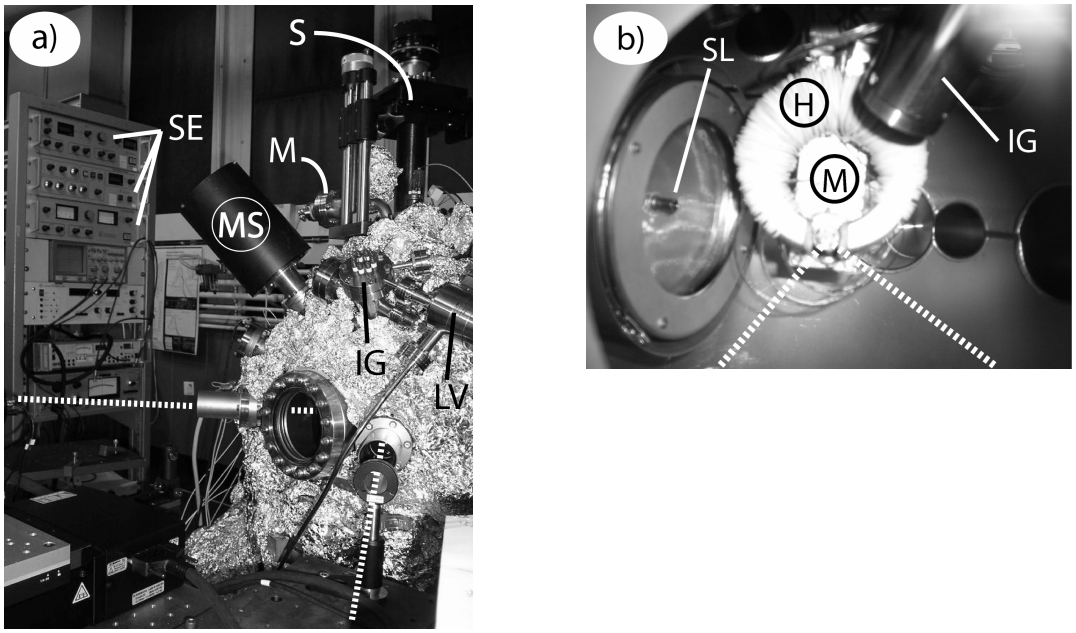


**Fig. 4.2** Photographs of the exterior (a) and the interior (b) of the UHV setup. The letters designate visible parts or leads for different components described in this section. The dashed line represents the laser beam, entering the UHV chamber from the left side of the picture.

The system is equipped with an in situ electromagnet constituting of a UHV compatible kapton isolated copper wire that is winded around a soft iron yoke (H). The magnet has a remanence of less than 15 Oe and saturates above 1400 Oe. In the ultra high vacuum pressure range, the magnet can only be operated at low currents and/or for a short time as the heating of the coils leads to severe outgassing.

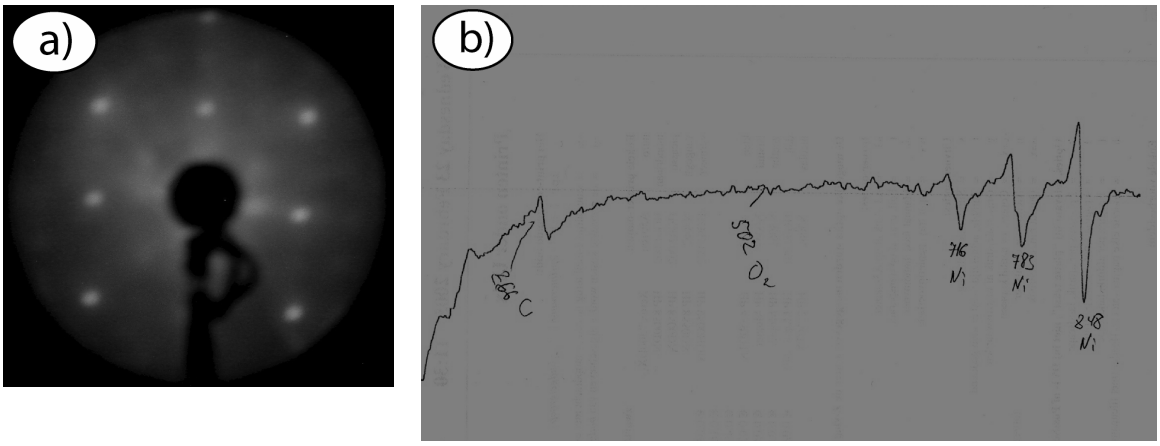


**Fig. 4.3** A non-oxidized Ni(001) surface. In (a), the LEED image shows the characteristic pattern of a (001) surface. In (b), the three most pronounced characteristic peaks on Ni can be seen in the AES spectrum (EP=3 keV). There is no peak at 502 eV which demonstrates the absence of O2. A small peak can be seen at 266 eV signifying the segregation of carbon.

The sample holder (S) is made of aluminum oxide and the clamps that hold the sample in position are produced from molybdenum.

A dual stepper motor drive (M) model SMD2, from AML (Arun Microelectronics LTD.) specifically designed for operation in ultra high vacuum was used in order to rotate the sample inside the chamber.

## References:

[1] A. Kirilyuk and Th. Rasing, J. Opt. Soc. Am. B **22**, 148 (2005).

[2] K. J. Veenstra, *Phase Sensitive Nonlinear Magneto-Optical Spectroscopy*, Ph.D. thesis, Radboud University Nijmegen, the Netherlands (2000).

[3] S. Hofmann, Surface and Interface Analysis, **2**, 148 (2004).

[4] M. G. Lagally, Appl. Surface Sci. **13**, 260 (1982).

[5] F. Jona, Surface Sci. **68**, 204 (1977).

[6] H. Ohtani, C. -T. Kao, M. A. Van Hove and G. A. Somorjai, Prog, Surface Sci. **23**, 155 (1986).

[7] A. Zangwill, *Physics at surfaces*, ed. by Cambridge university press, 1996.

[8] Frank Settle, *Handbook of instrumental techniques for analytical chemistry*, Chapter 42, Prentice-Hall, Inc. (2000).

[9] T. E. Gallon and J. A. D. Matthew, Rev. Phys. Technol. **3**, 31 (1972).

[10] J. J. Lander, Phys. Rev. **91**, 1382 (1953).

[11] J. P. Coad and J. C. Rivière, Z. Phys. **244**, 19 (1971).

# Chapter five

## Quadratic contributions to MSHG during magnetization reversal[viii]

Previously, we have seen that exchange bias is a magnetic phenomenon that occurs at the interface between ferromagnetic and antiferromagnetic materials, the understanding of which appears to be a challenge. We have also introduced the MSHG experimental technique as a very good probe for studying surface and interface magnetism.

In the exchange bias effect, one can expect a different magnetic behavior from the interface and the bulk, for instance, due to the possible formation of domain walls in the antiferromagnet[1,2] or the ferromagnet.[3-6] Therefore this problem is particularly suitable for a simultaneous investigation with MSHG and MOKE. However, when comparing the results from these techniques, it is of great importance to understand that MSHG is not always linearly proportional to the magnetization whereas MOKE usually is.

In this chapter we will focus our attention on the magnetization-induced quadratic contributions to MSHG during magnetization reversal. Our results revealed a clear difference in the magnetization hysteresis loop, depending on whether it was measured with MSHG or MOKE. Furthermore, this difference was found to be in good qualitative agreement with the expected magnetic behavior at the interface and in the bulk in the case of exchange bias effect. However we show that the observed difference is due to a quadratic dependence on the magnetization in the MSHG intensity[7] and most likely is not of magnetic origin.

## 5.1. Sample preparation[ix]

The composition of our thin-film samples was Si(111)/Fe/CoO/Au. Initially, 6nm Fe was deposited by molecular beam epitaxy (MBE) on hydrogen-passivated Si(111). After the preparation of 2 nm CoO,[8,9] the sample was covered by a 6 nm Au cap layer to prevent contamination from the atmosphere. Exchange bias was induced by cooling the sample from a temperature of 300 K (for CoO $T_N$=291 K), in the presence of an external magnetic field of 2.5 kOe.

[viii] Based on Phys. Stat. Sol. (B) **242**, 3027 (2005)

[ix] Samples were grown by Dr. M. Gruyters in Humboldt-Universität zu Berlin, Institut für Physik, Berlin, Germany.

## 5.2. Results and discussion

Fig. 5.1a shows the magnetization reversal observed by MOKE and MSHG. We can see a clear difference between the two curves. First, the exchange bias value is different – it is larger for the MSHG. Second, the shape of the hysteresis curves differs – while the magnetic reversal observed with MOKE is symmetrical, the MSHG curve presents a sharp first reversal and then a more gradual second reversal.

Since the MOKE signal is related to the "bulk" magnetization, while the MSHG is supposed to be more sensitive to interface effects, the difference between the two curves can be related to their different origin. Indeed, as the exchange bias results from the AFM pinning at the interface, it is reasonable to say that its value is higher at the interface and hence the larger value of loop shift observed with MSHG.

Furthermore, we know that the AFM pins the FM at the interface.[10] When the "bulk" of the FM starts to reverse, the interface spins remain pinned in the direction of the bias. At some point though, the external field overcomes the exchange interaction and then the interfacial spins reverse sharply. This can give rise to the square behavior during the first reversal with MSHG. While completing the hysteresis, the interfacial spins start their reversal sooner, since the exchange interaction and the external field act together, and this produces a more gradual second reversal as seen again with MSHG.

These results were reproducible on several samples with different composition and seemed to provide evidence that our observation was of general character, i.e. intrinsically related to the exchange bias effect.

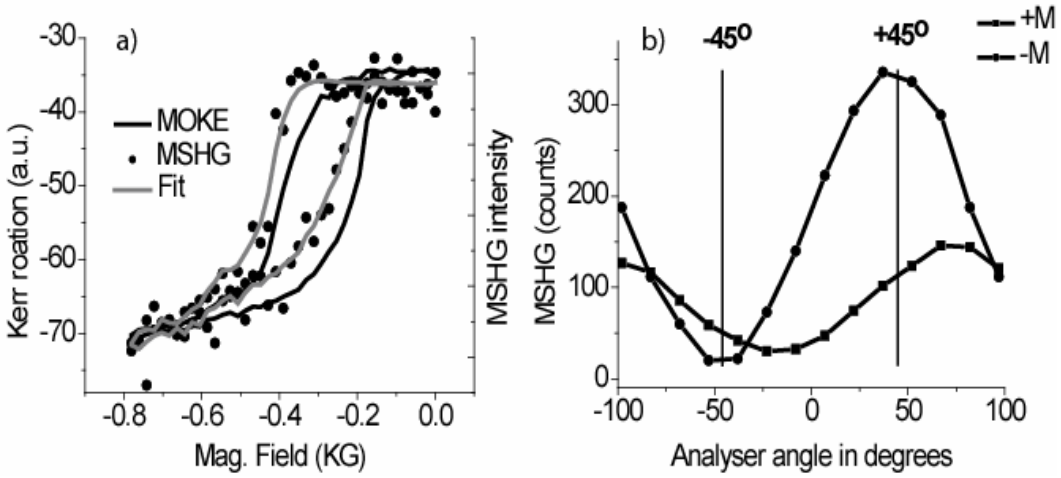


**Fig. 5.1** (a), simultaneous MOKE (black line) and MSHG (dots) measurements of the exchange biased samples at temperature 50 K. The grey line is a numerical fit for the MSHG intensity data. (b), the MSHG intensity as function of analyzer rotation for +M and –M.

The explanation given above assumes that the MSHG signal is a direct (linear) measure of the magnetization at the interface. As we saw in Eq. 3.13, in the presence of a magnetization, the second harmonic intensity is given by:[11]

$$I(2\omega,\mathbf{M}) \propto \left( \left|\chi^{even}\right|^2 + \left|\chi^{odd}(\mathbf{M})\right|^2 \pm 2\left|\chi^{even}\right|\left|\chi^{odd}(\mathbf{M})\right| \right) \cdot I^2(\omega), \quad (5.1)$$

which is indeed linearly dependent on the magnetization for $\left|\chi^{odd}(\mathbf{M})\right| / \left(2\left|\chi^{even}\right|\right) << 1$. This relationship ensures that we can use MSHG as tool for probing the AFM/FM interface.

However, an alternative explanation could be that the bulk and the interface behave in the same manner but that there is a quadratic component in the MSHG signal that distorts the hysteresis loop, making it asymmetrical. Indeed, it follows directly from Eq. 5.1, that if the condition $\left|\chi^{odd}(\mathbf{M})\right| / \left(2\left|\chi^{even}\right|\right) << 1$ is not fulfilled, the quadratic terms in the intensity dependence become important.

Fig. 5.1a shows a numerical fit for the MSHG intensity data based on Eq. 5.1 assuming a quadratic dependence on **M**. The magnetization behavior was given by the results observed with MOKE[x] and we chose $\chi^{odd}/\chi^{even} = 1.42$. It is clear that the fit accounts very well for the MSHG results, supporting the possibility of an alternative explanation for our results. In order to demonstrate which explanation is the real one, we performed two more measurements.

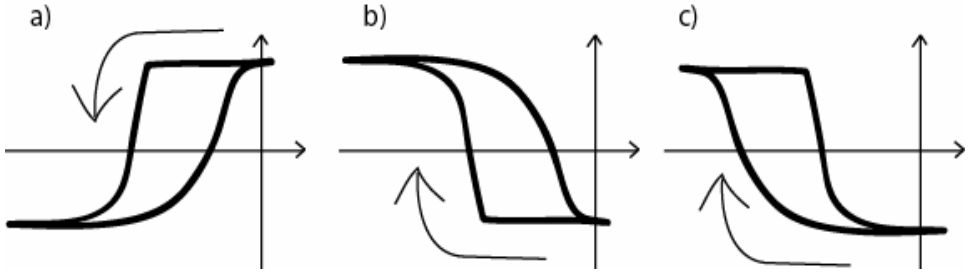


**Fig. 5.2** Schematic representation of the MSHG hysteresis loop asymmetry for analyzer at +45° (a) and at –45° : for a magnetic origin of the asymmetry (b) and for an optical origin (c).

In the first measurement, we modified the optical part of the experiment, while keeping the magnetic part unchanged. This was done by rotating the analyzer from the +45º to the –45º position.

In Fig. 5.1b, the MSHG intensity dependence on the analyzer rotation is plotted and we can see that between +45º and –45º the magnetic contrast is reversed. Fig. 5.2a gives a schematic representation of the MSHG hysteresis loop in Fig. 5.1a emphasizing the asymmetry. Therefore, if the asymmetry in the hysteresis loop has a magnetic origin, we can expect the first reversal to be sharp, because of the action of the pinned AFM spins (see Fig. 5.2b). On the other hand, if the origin is of optical nature, the reversal will reproduce the magnetic behavior of the curve in Fig. 5.2a, with only a symmetry change that accounts for reversing the MSHG intensity levels, as in Fig. 5.2c.

[x] The values of a MOKE hysteresis curve were used for $\chi^{odd}(\mathbf{M})$.

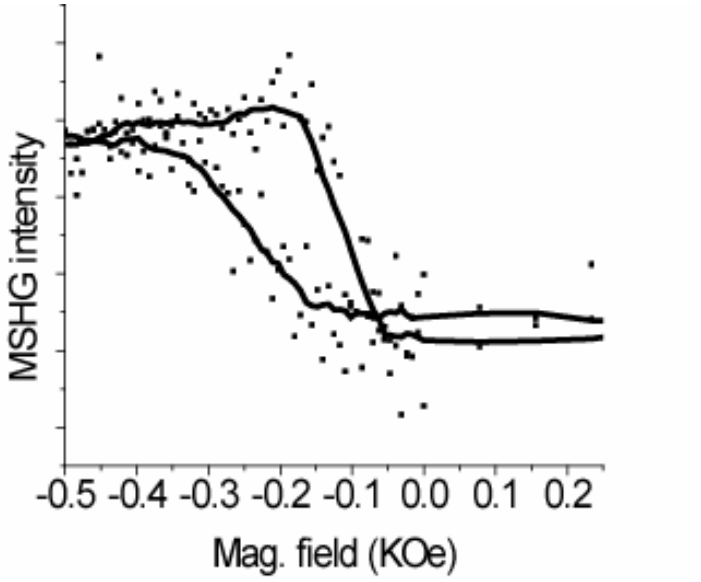


**Fig. 5.3** MSHG intensity as function of magnetic field for temperature 50 K with analyzer at –45°.

The obtained experimental result is plotted in Fig. 5.3. There is a clear similarity between this curve and the one in Fig. 5.2c. This is in agreement with the assumption of a quadratic contribution distorting the signal.

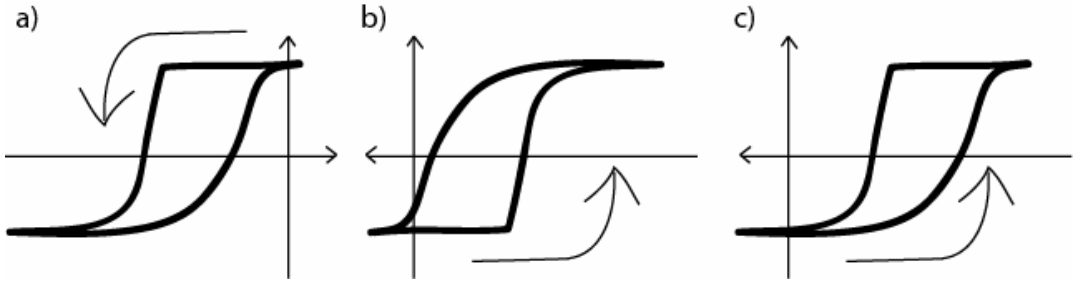


**Fig. 5.4** Schematic of the hysteresis loop shape after positive field-cooling (a). After negative field-cooling, in the case of real magnetic effect (b), and in case of an optical origin (c).

In our second measurement, we modified the magnetic part of the experiment while keeping the optical one unchanged. For this purpose, we field-cooled the sample in an opposite field. The first consequence of this manipulation will be a positive loop shift, as represented on Fig. 5.4b and 5.4c. Fig. 5.4a gives again a schematic representation of our initial hysteresis loop. And again, if the reason for the asymmetry is magnetic, we expect the first reversal to be sharp, as in Fig. 5.4b, while an optical cause of the asymmetry will reproduce the initial curve, as shown in Fig. 5.4c.

The obtained results are shown in Fig. 5.5, where it is clearly visible that the shape of the two hysteresis curves is similar, in the same manner as Fig 5.4a resembles Fig 5.4c.

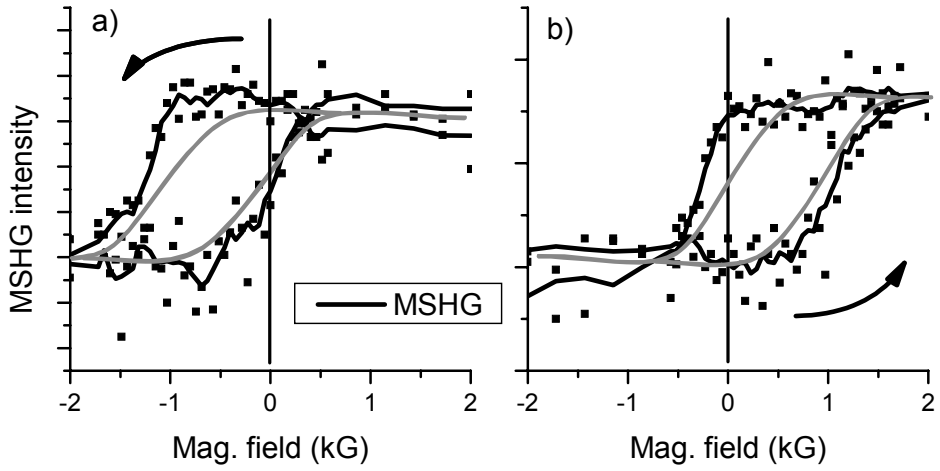


**Fig. 5.5** MSHG intensity as function of applied magnetic field, at a temperature of 10 K for positive (a) and negative (b) field-cooling. The hysteresis grey lines are guides to the eye representing a symmetrical reversal.

## 5.3. Conclusions

We have demonstrated that the asymmetry of the MSHG hysteresis curve from a CoO/Fe system is due to a quadratic dependence of the MSHG intensity on **M** and is not directly (linearly) representative of the magnetic behavior at the exchange-biased AFM/FM interface. Thus, although our data seemed initially in excellent agreement with the intuitively appealing model of the magnetic phenomenon that we were trying to investigate, they turned out to be produced by a magneto-optical nonlinearity.

It is quite clear that the solution of this problem should be addressed at its source, namely the condition $\left|\chi^{odd}(\mathbf{M})\right| / \left(2\left|\chi^{even}\right|\right) << 1$ in Eq. 5.1. In order to ensure that this ratio is conserved, we need to enhance the even term in the MSHG signal. This can be done for instance with the help of a nonlinear crystal or thin film placed immediately after the sample. One should keep in mind however that the fundamental and the second harmonic propagate with different speeds and therefore particular attention should be directed towards the phase of MSHG.

In conclusion, although the technique of magnetization-induced second harmonic generation shows great potential for the simultaneous studies of surface/interface and bulk effects, the results above show that it should be employed carefully.

## References:

[1] D. Mauri, H.C. Siegmann, P.S. Bagus, E. Kay, J. Appl. Phys **62**, 3047 (1987).

[2] M. D. Stiles and R. D. McMichael, Phys. Rev. B **60**, 12950(1999).

[3] B.H. Miller and E. Dan Dahlberg, Appl. Phys. Lett. **69**, 3932 (1996).

[4] M. Kiwi, J. Mejia-Lopez, R.D. Portugal and R. Ramirez, Europhys. Lett. **48**, 573 (1999).

[5] M. Kiwi, J. Mejia-Lopez, R.D. Portugal and R. Ramirez, Appl. Phys. Lett. **75**, 3995 (1999).

[6] J. Meija-Lopez, R. Ramirez and M. Kiwi, J. Magn. Magn. Mater. **241**, 364 (2002).

[7] K. J. Veenstra, *Phase Sensitive Nonlinear Magneto-Optical Spectroscopy*, Ph.D. thesis, Radboud University Nijmegen, the Netherlands (2000).

[8] G. S. Higashi, Y. J. Chabal, G. W. Trucks and K. Raghavachari, Appl. Phys. Lett. **56,** 656 (1990).

[9] M. Gruyters and D. Riegel, Phys. Rev. B **63**, 052401 (2001).

[10] H. Ohldag, A. Scholl, F. Nolting, E.Arenholz, S. Maat, A. T. Young, M. Carey and J. Stöhr, Phys. Rev. Lett. **91**, 017203 (2003).

[11] A. Kirilyuk and Th. Rasing, J. Opt. Soc. Am. B **22**, 148 (2005).

# Chapter six

# Uncompensated spins at the CoO/Cu interface[xi]

In the previous chapters we have discussed the fact that exchange bias is an interface effect that has remained without a complete explanation for almost 50 years. The main reason for this lack of understanding appears to be the lack of experimental data relevant to the buried ferromagnetic/antiferromagnetic interface. Indeed, only a few techniques allow the study of buried magnetic interfaces such as neutron diffraction,[1] magnetic dichroism[2] (or in conjunction with photoemission electron microscopy[3]), and conversion electron Mössbauer spectroscopy,[4] and the studies of exchange bias interfaces using these techniques are often challenging.[5]

Additionally, researchers have started questioning the measurements of hysteresis loops, on which the investigation of exchange bias has been mainly focused. Thus, new ways of examining the effect are desirable.

We have also seen that MSHG is an experimental technique capable of probing interface magnetism with a high sensitivity, though care should be taken in the interpretation of its data (see Chapter five). Until now it has been mainly used for studies of magnetism at ferromagnetic interfaces. In the following, we will show that it can also be applied to the investigation of antiferromagnetic/nonmagnetic interfaces.

In this Chapter, we will demonstrate how MSHG can be employed to study the exchange bias. We will see that the appearance of exchange bias, which essentially causes the appearance of a mirror plane magnetic symmetry in the sample, can be monitored not only by means of the loop shift, but also by the MSHG relative magnetic contrast (or asymmetry) and the second harmonic Kerr rotation. In the case of rotating incoming polarization, we will see that the contribution to the MSHG signal by the pinned uncompensated spins in the antiferromagnet actually *dominates* the contribution from the ferromagnetic interfaces, thereby allowing a *direct observation* of these spins. Finally, we will show that the use of MSHG gives us the possibility to see pinned uncompensated spins in the antiferromagnet beyond the range of what the loop shift can probe.

## 6.1. Introduction

Recent research suggests that a small number of uncompensated AFM spins at the interface might be the origin of the loop shift.[6] Interestingly, the authors show that the

[xi] Based on Phys. Rev. Lett. **96**, 67206 (2006) and Phys. Rev. B **73**, 233101 (2006)

intuitive model for exchange bias is in principle correct although one should not assume an ideal AFM/FM interface as did Meiklejohn and Bean. On the other hand, it has also been suggested that the main part of those uncompensated spins will couple to the ferromagnet and rotate with it,[7,8] thus contributing to the coercivity enlargement. These explanations present exchange bias as essentially an interfacial effect, having a next-neighbor range.

However, other studies revealed a long-range nature of exchange bias: upon insertion of a nonmagnetic spacer layer between the FM and the AFM, some authors observed an exponential[9] or even sharper[10] decrease of the effect, while others have reported an oscillatory behavior;[11] in some cases oscillations were shown to occur only at certain temperatures.[12]

In order to elucidate the role of the interfaces and to understand the interplay between the short and long range aspects of exchange bias, we have applied the interface-sensitive technique of magnetization-induced second harmonic generation MSHG in combination with the "bulk"-sensitive linear magneto-optical Kerr effect (MOKE) to investigate both the temperature dependence of exchange bias and its value as function of the distance(X) separating the FM from the AFM across a Cu spacer. We show that the appearance of exchange bias at the temperature $T_B$ is accompanied by the formation of pinned uncompensated spins at the AFM/spacer interface, in agreement with observations made by other techniques.[6-8,13] Those spins are aligned under the influence of the FM interface and are directly responsible for exchange bias. To our surprise, we find that while the hysteresis loops measurement indicates an almost complete disappearance of exchange bias above X = 3.5 nm, MSHG reveals that, even at this thickness, there is still a good alignment of pinned uncompensated spins at the AFM/spacer interface below $T_B$.

Our results indicate that the range upon which the FM influences the magnetic order at the AFM interface extends even further than the distance determined from the hysteresis loop shift. In addition, we demonstrate the excellent sensitivity of the MSHG technique to probe these very important but buried interfaces as we observe that for large exchange bias values, the nonlinear magneto-optical susceptibility of the sample is dominated by the tensor elements associated with the CoO/Cu interface rather than by those associated with the ferromagnetic Fe interfaces. This indicates that MSHG offers the possibility of a *direct observation* of the spins responsible for exchange bias.

Some work on detecting uncompensated spins in exchange biased systems with MSHG has been done previously[14] on a different type of multilayers (without spacer), however the authors concentrated on a single aspect of the MSHG dependence (the polarization rotation) and the observed effects were very subtle.

## 6.2. Experimental details[xii]

The basic structure of our layered samples was Si(111)/Fe/Cu/CoO/Au. Initially, 6nm Fe was deposited by molecular beam epitaxy (MBE) on hydrogen-passivated Si(111),[15] followed by a Cu layer with varying thickness. After the preparation of 2 nm CoO,[16] the

[xii] Samples were grown by Dr. M. Gruyters in Humboldt-Universität zu Berlin, Institut für Physik, Berlin, Germany.

sample was covered by a 6 nm Au cap layer to prevent contamination from the atmosphere. The Cu thickness was varied both on a single sample, in the form of a stepped wedge, and as a series of separate samples. The Fe film possesses a single crystalline bcc(110) surface orientation[17] while the CoO consists of densely packed roundly shaped particles.[16] Transmission electron microscopy showed sharp interfaces for all the discussed Cu thicknesses (see Fig 6.1). Because the CoO does not reveal any X-ray diffraction peaks, it is assumed to be amorphous.

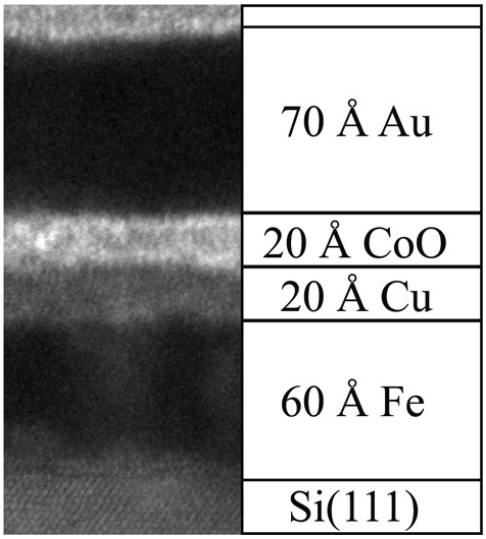


**Fig. 6.1** Transmission electron microscopy micrograph of the samples show sharp interfaces and no interdiffusion.

Exchange bias was induced by cooling the sample from a temperature of 300 K, in the presence of an external magnetic field of 2.5 kOe. Hysteresis loops extended from -4.5 kOe to +4.5 kOe. In all experiments, the light polarization was linear.

## 6.3. Results

For intense electromagnetic fields, such as those generated by a pulsed laser beam $\mathbf{E}(\omega)$ incident on a thin multilayer film, the polarization at the harmonic frequency $2\omega$ is given by Eq. 3.8, which we can rewrite in the form of:

$$\mathbf{P}_i^{(l)}(2\omega) = \chi_{ijk}^{(l)} \mathbf{E}_j^l(\omega) \mathbf{E}_k^l(\omega) \tag{6.1}$$

where $\chi_{ijk}$ is a third order polar tensor describing the second order non-linear optical (NLO) susceptibility at the symmetry breaking interface between the centrosymmetric films and *l* numbers the interfaces in our sample.[18]

In this Chapter we use the model based on the work of Sipe[19] and applied among others by Wu et al.[20] which does not include the contribution of quadrupolar terms from

the bulk. Therefore the tensor elements that we use are "effective" and may contain a contribution from these terms.

### 6.3.1. The relative magnetic contrast

We can separate two types of contributions to the susceptibility: the "magnetic"( $\chi_{odd}$ ) and "non-magnetic"( $\chi_{even}$ ), depending on whether the tensor elements associated with them change sign upon reversal of the magnetic moment, see inset in Fig. 6.2. Note that the non-magnetic part also includes defects or microstructure effects. It should be understood here that any such effects do not have a magnetic orientation, and in particular, that they will not reverse after field-cooling in an opposite external magnetic field.

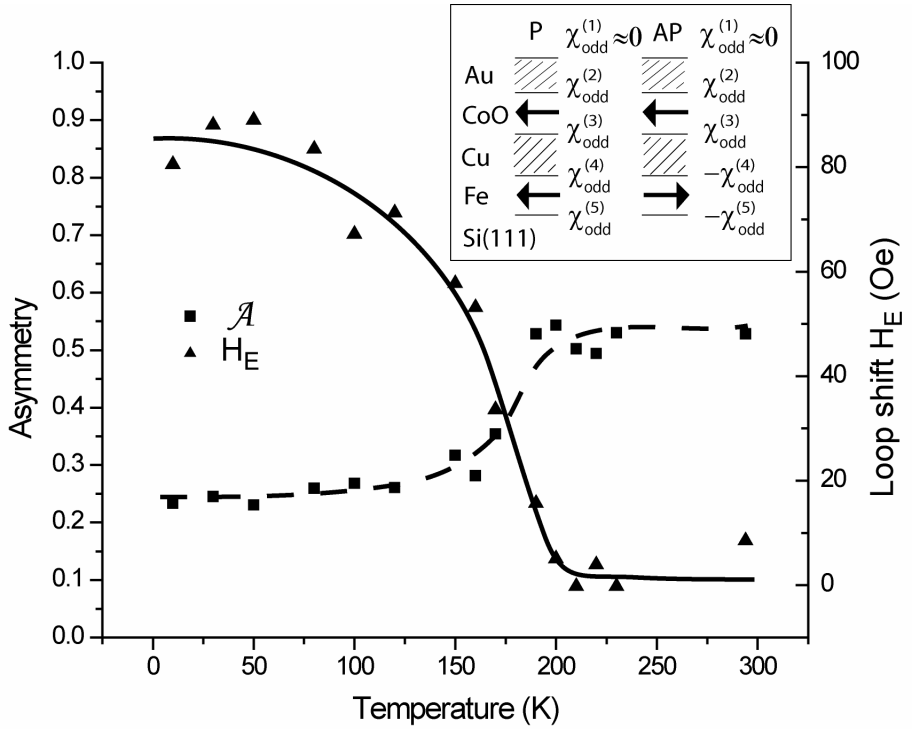


**Fig. 6.2** Temperature dependence of the asymmetry $\mathcal{A}$ (squares) and of the loop shift $H_E$ (triangles) measured with MSHG from a sample with Cu thickness 2.5 nm. The lines are guides to the eye. Inset: effective second-order susceptibilities from different interfaces of the sample, in the case of negative exchange bias, below $T_B$. $\mathcal{A}$ is determined by reversing the Fe layer magnetization with an applied external field. The arrow in the CoO symbolizes the pinned uncompensated spins in the AFM.

The non-zero net magnetic moment at the CoO interfaces is related to the exchange bias and its sign can be reversed if the sample is field-cooled in an opposite magnetic field. We can distinguish two types of configurations: parallel (P) and antiparallel (AP), that are

related to the relative orientation of the FM layer, see insert in Fig. 6.2. In the case of the AP configuration, the sample was field-cooled down to the temperature of measurement and then the orientation of the FM layer was reversed by reversing the external magnetic field.

For a fixed polarizer-analyzer combination, the second-order susceptibility $\chi$ at any given interface can be described by a single number. In the limit of ultra-thin films we can combine those susceptibilities:

$$\chi_{odd}^{P} = \left(\chi_{odd}^{(2)} + \chi_{odd}^{(3)}\right) + \left(\chi_{odd}^{(4)} + \chi_{odd}^{(5)}\right) \tag{6.2a}$$

$$\chi_{odd}^{AP} = \left(\chi_{odd}^{(2)} + \chi_{odd}^{(3)}\right) - \left(\chi_{odd}^{(4)} + \chi_{odd}^{(5)}\right) \tag{6.2b}$$

$$\chi_{even} = \chi_{even}^{(1)} + \chi_{even}^{(2)} + \chi_{even}^{(3)} + \chi_{even}^{(4)} + \chi_{even}^{(5)} \tag{6.2c}$$

Note that here we have included a possible contribution of the Au/CoO interface $\chi_{odd}^{(2)}$.

A potential contribution from the AFM ordering in CoO is incorporated in the nonmagnetic part as it should be symmetrical with respect to the direction of the field cooling.[21]

The second harmonic intensity for the parallel and antiparallel configurations is then given by:

$$I^{P/AP} = \left|\chi_{even} + \chi_{odd}^{P/AP}\right|^2 I^2 \tag{6.3}$$

where $I$ is the intensity of the incoming fundamental light. For observing an MSHG contrast, only the sign change of $\chi_{odd}$ relative to $\chi_{even}$ is relevant. In nonabsorbing materials, the relative phase between these susceptibilities is 90° and therefore they do not interfere. However, in the case of our samples interference is allowed and the relative phase can be considered to be temperature independent as the optical properties of the sample do not change noticeably in the temperature range that we consider.[22]

Further, we can define the asymmetry $\mathcal{A}$ (or relative magnetic contrast) as:

$$\mathcal{A} = \frac{I^{P} - I^{AP}}{I^{P} + I^{AP}} = \frac{2R}{1+R^2}\cos\phi \tag{6.4}$$

where $R = \left|\chi_{odd}^{(4)} + \chi_{odd}^{(5)}\right| / \left|\chi_{even} + \chi_{odd}^{(2)} + \chi_{odd}^{(3)}\right|$ and $\phi$ is the phase angle between numerator and denominator. For $R^2 << 1$ $\mathcal{A}$ is proportional to R, whereas for $R^2 >> 1$, it is proportional to 1/R. For the intermediate case, $R \approx 1$, $\mathcal{A}$ is constant and equal to $\cos\phi$.

Above $T_B$, exchange bias and thus the possible magnetic contributions of the CoO interfaces disappear, i.e. $\chi_{odd}^{(2)} = \chi_{odd}^{(3)} = 0$. In that case, R can be written simply as the ratio between the magnetic and nonmagnetic tensor elements:

$$R = \left|\chi_{odd}^{(4)} + \chi_{odd}^{(5)}\right| / \left|\chi_{even}\right| \tag{6.5}$$

Below $T_B$ the presence of pinned uncompensated spins at the CoO interfaces may lead to $\chi_{odd}^{(2)}$ and $\chi_{odd}^{(3)} \neq 0$, resulting in a decrease in R and consequently, for $R^2<<1$, a decrease in $\mathcal{A}$. This is illustrated in Fig. 6.2, which shows the temperature dependence of both $\mathcal{A}$ and the exchange bias value measured with MSHG for a sample with X = 2.5 nm. These results clearly demonstrate the appearance of $\chi_{odd}^{(2)}$ and/or $\chi_{odd}^{(3)} \neq 0$.

## 6.3.2. The Au/CoO interface

In order to check the presence of a contribution of the Au/CoO interface, i.e. $\chi_{odd}^{(2)}$, we studied the MSHG intensity as function of the analyzer rotation at different temperatures for all Cu spacer thicknesses. Fig. 6.3b shows that for X = 3.5 nm, below $T_B$, the curves demonstrate a polarization rotation due to the appearance of new tensor components – those responsible for the pinned AFM spins at the interface(s). However, for X = 0 nm, (Fig. 6.3a) there is no such rotation.

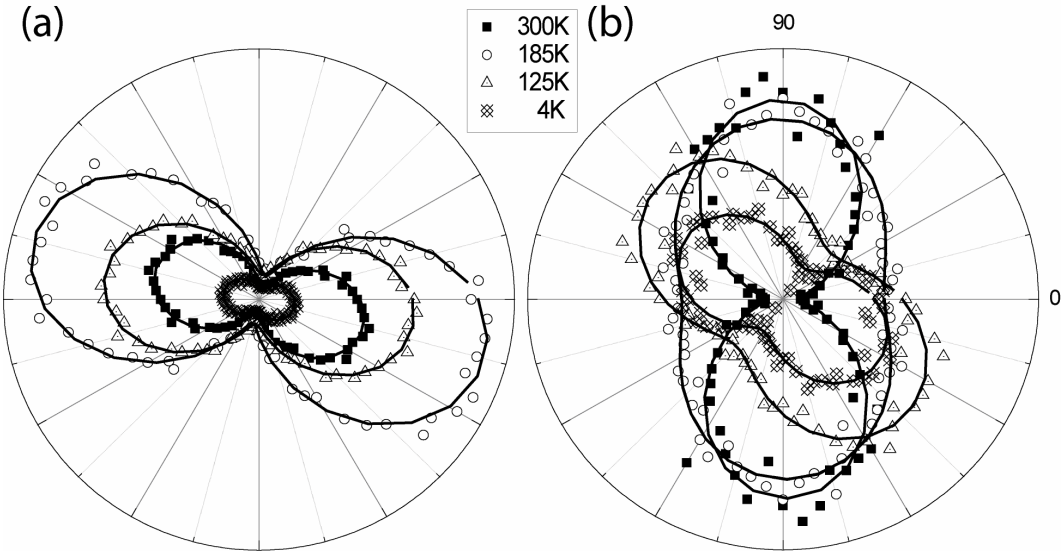


**Fig. 6.3** MSHG intensity from a sample with Cu thickness 0 nm (a) and 3.5 nm (b) as function of analyzer rotation angle.

Therefore, since the Au/CoO interface is common for these two cases, while the CoO/Cu appears only for X>0 nm, we can conclude that $\chi_{odd}^{(2)} \approx 0$ and that the observed spin order is located at the CoO/Cu interface.

## 6.3.3. The CoO/Cu interface dominates the MSHG signal

We have just established that the spin polarization of the CoO/Cu interface has a contribution to the MSHG signal. It is well known (especially in ferromagnets) that reversing the interface magnetization gives rise to a magnetic contrast. Therefore, we

expect that reversing the spin polarization at the CoO/Cu interface will lead to observable effects in the MSHG signal.

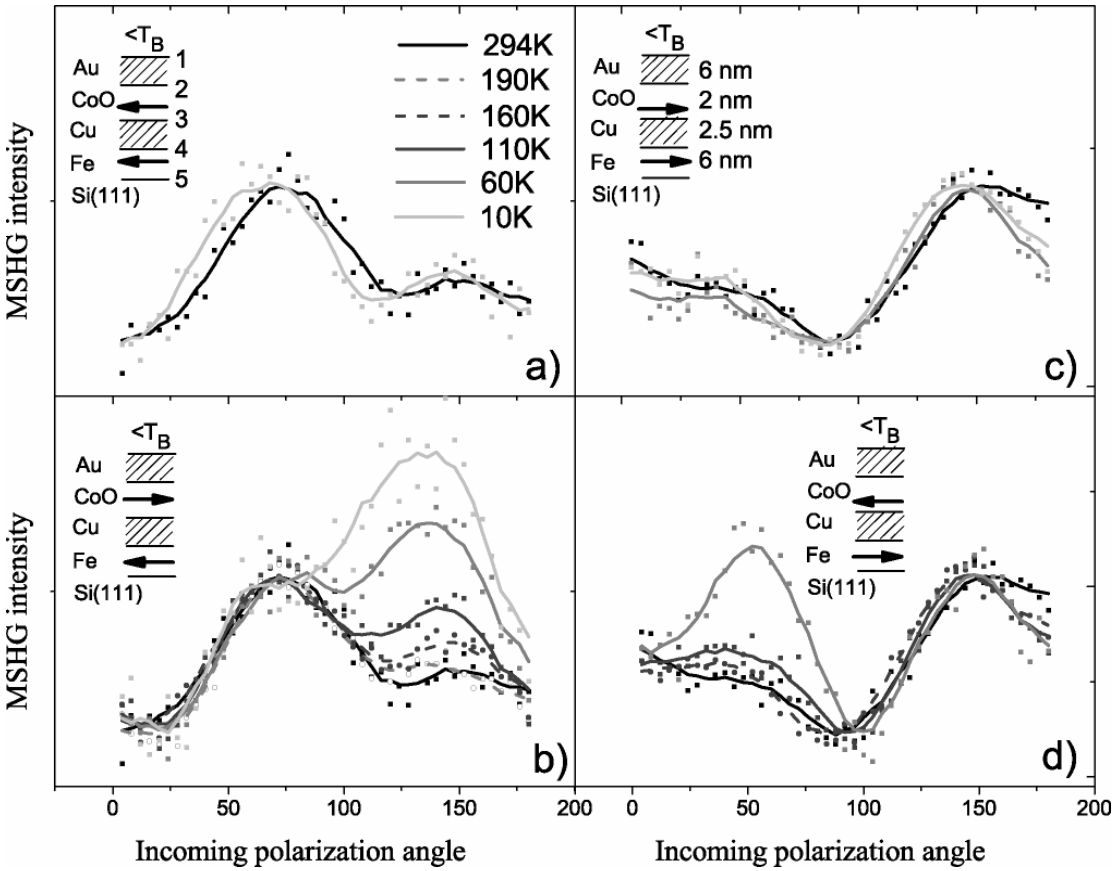


**Fig. 6.4** MSHG intensity as function of the rotation of the fundamental light polarization from the $P_{in}$ direction at different temperatures, after negative field cooling (a) and after positive field cooling (b) for $M_{Fe}<0$ and after positive (c) and negative (d) field cooling for $M_{Fe}>0$. The analyzer was fixed along the $S_{out}$ direction. The signal was normalized to the room temperature response. In the inset, the magnetization at the sample interfaces above and below $T_B$ is represented, indicating the parallel (a & c) and antiparallel (b & d) configurations.

Fig. 6.4 shows the MSHG intensity as function of the rotation of the fundamental light polarization at different temperatures. During the measurements, the applied external field ($\mathbf{H_0}$) and therefore the magnetization at the Fe interfaces ($\mathbf{M_{Fe}}$) was along the negative direction (i.e. $\mathbf{H_0}$, $\mathbf{M_{Fe}}<0$). In Fig. 6.4a, the MSHG signal in the parallel configuration can be seen above $T_B$ ($T_B$ ~185 K, see Fig. 6.2) and after field cooling to 10 K. The curves exhibit two peaks: a large one at ~70° and a smaller one at ~145°. We observe that the two curves are very similar. On the other hand, Fig. 6.4b shows the MSHG response in the antiparallel configuration above $T_B$ and after field cooling. Again, we see that above $T_B$ (T = 294 K and T = 190 K), the curves are similar, however below $T_B$ the signal starts changing with decreasing temperature, indicating a polarization

rotation due to the appearance of new tensor components – $\chi_{odd}^{(3)}$. The latter are related to the appearance of a new magnetic symmetry at the interface, due to the pinned uncompensated spins at the CoO/Cu interface.

The nature of this change can be better understood when we look at Fig. 6.4c. Here, we plotted again the MSHG intensity as function of the rotation of the fundamental polarization at different temperatures, but this time $\mathbf{H_0}$, $\mathbf{M_{Fe}}$>0. We can see that above $T_B$, the curves exhibit two peaks close to the angles in Fig. 6.4a but having an inverse relationship: there is a large one at ~145° and a smaller one at ~60°. Therefore, the temperature dependence of the SHG polarization in Fig 6.4b corresponds to a transition from the magnetization state of Fig. 6.4a to the magnetization state in Fig. 6.4c. In other words, we can conclude that the change in the MSHG response in Fig. 6.4b at $T<T_B$ is due to a reversal of the sign of the total magnetic part of the NLO susceptibility in the sample. The same can be seen in Fig. 6.4d. Thus, the MSHG technique allows us not only to detect $\chi_{odd}^{(3)}$, which originates from the pinned uncompensated spins at the CoO/Cu interface, but also shows that its absolute value becomes larger than those from $\chi_{odd}^{(4)}$ and $\chi_{odd}^{(5)}$, which are associated with the Fe interfaces.

### 6.3.4. The second harmonic Kerr rotation

Another way of examining the $\chi_{odd}^{(3)}$ tensor components is by studying the nonlinear optical Kerr rotation $\theta_K^{(2)}$. This is done by performing the following experiment: the fundamental polarization was fixed while the analyzer was rotated. Fig. 6.5 shows the thus obtained MSHG Kerr rotation angle at different temperatures (during the measurements, $\mathbf{H_0}$, $\mathbf{M_{Fe}}$<0). We can see that for positive field cooling (antiparallel configuration) there is a clear change in $\theta_K^{(2)}$ from 0° to 50°, which exactly follows the variations of the exchange bias loop shift $H_E$. On the other hand, for negative field cooling (parallel configuration) there is no change in $\theta_K^{(2)}$ with temperature.

Note that 50° is the direction of the MSHG polarization for $\mathbf{H_0}$, $\mathbf{M_{Fe}}$>0 after positive field cooling. This is a parallel configuration, and since we have established that for parallel configurations there is no or little change occurring with temperature, we can conclude that again the change of the second harmonic Kerr rotation angle from 0° to 50° must be attributed to a sign change in $\chi_{odd}$!

This sign reversal can be explained in the following way. Above $T_B$, the sign of $\chi_{odd}$ is solely determined by $\chi_{odd}^{(4)}$ and $\chi_{odd}^{(5)}$. When the sample is field cooled in the direction in which the measurement is performed, (i.e. parallel configuration), the appearance of $\chi_{odd}^{(3)}$ does not affect this sign (see Eq. 6.2a). There is only a change in the absolute value of $\chi_{odd}^{P}$ and it does not have a very pronounced influence on the MSHG signal since the magnetization of the sample is saturated. However, when the sample is field cooled in one direction after which the external field is reversed, (i.e. antiparallel configuration, see Eq. 6.2b), the sign of $\chi_{odd}$ changes for $\left|\chi_{odd}^{(3)}\right| > \left|\chi_{odd}^{(4)} + \chi_{odd}^{(5)}\right|$ and hence

the large MSHG response that is observed. The fact that we see an effect in the antiparallel configuration and not in the parallel one may also indicate that MSHG is particularly sensitive to $\chi_{odd}^{(3)}$ through the frustrations between the AFM pinned uncompensated spins and the FM ones.

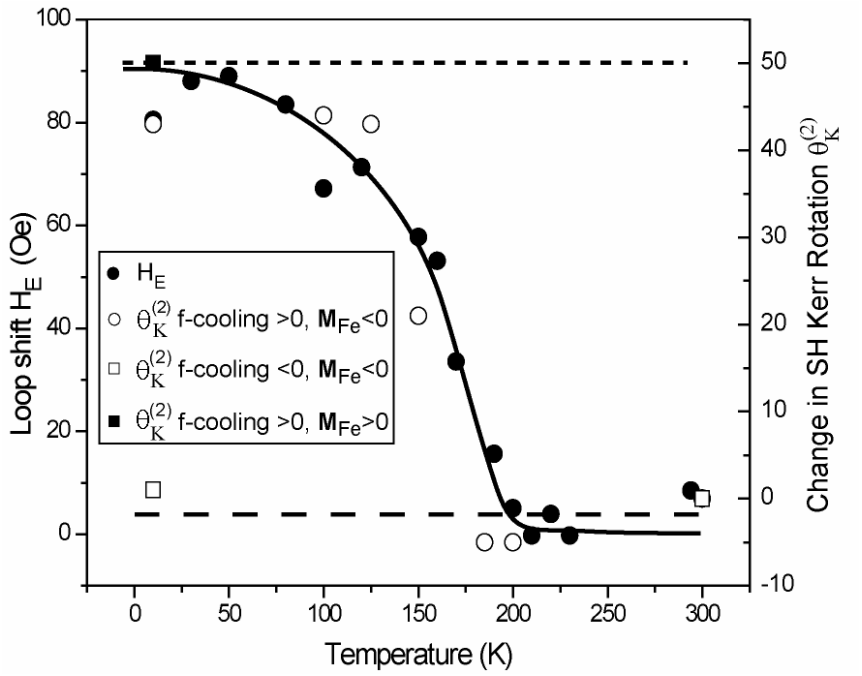


**Fig. 6.5** The exchange bias loop shift $H_E$ and the change in the second harmonic Kerr rotation as function of temperature. $H_0$ and $M_{Fe}$<0, after positive (empty circles) and negative (empty squares) field cooling. The polarizer was fixed along the $S_{in}$ direction while –10° corresponds to the $P_{out}$ direction of the analyzer.

The consequences of this finding are quite general. The fact that the signal generated by $\chi_{odd}^{(3)}$, i.e. originating from the pinned uncompensated spins at the CoO/Cu interface, dominates over the contribution from the Fe interfaces suggests that MSHG can be used for *direct observation* of the exchange bias related spins in a large variety of samples. Indeed, depending on the fundamental wavelength, the angle of incidence and the refraction indices of the materials, it is in principle possible to optically "quench" the contributions to the MSHG signal from the FM interfaces while at the same time enhancing the response from the relevant AFM interface.

Understanding that there is a clear difference in the MSHG response between the parallel and antiparallel configurations gives us additional insight into the sensitivity of the MSHG asymmetry $\mathcal{A} = \left(I^P - I^{AP}\right)/\left(I^P + I^{AP}\right)$ to the temperature variations of exchange bias that we have found previously. Clearly, it is the variations of $I^{AP}$ that give rise to this sensitivity, i.e. the changes of the value of $\chi_{odd}$, including its sign reversal.

### 6.3.5. Spin polarized interface beyond the range of $H_E$

To investigate the decrease of exchange bias as function of the distance separating the AFM and FM layers, we used a "wedge" sample with six different thicknesses of Cu spacer. In Fig. 6.6a and 6.6b the loop shift $H_E$ and the asymmetry $\mathcal{A}$ of this sample are plotted as a function of temperature showing an almost opposite behavior of these two quantities: while $H_E$ decreases strongly with thickness, the temperature dependence of $\mathcal{A}$ increases. Note that in Fig. 6.6b the thickness dependence is visible only below $T_B$; from this we can conclude that the observed effect is of magnetic and not optical nature. Despite some scattering in the data, the trends are absolutely clear: for X = 1.5 nm, there is no pronounced change in the asymmetry with decreasing temperature, whereas for larger thickness the asymmetry diminishes gradually and clearly with decreasing temperature.

The asymmetry for X = 0 nm is given as a reference. Note that for the absence of a spacer the optical response is very different since the number of layers and interfaces is smaller. Though the loop shift values are almost the same as those for X = 1.5 nm, this was not found to be the case for the coercivity with X = 0 nm exhibiting twice the coercivity values of X = 1.5 nm.

The inset in Fig. 6.6 shows that the $H_E$ dependence on spacer thickness shows a sign of oscillation around X = 2 nm for T>100 K. This interesting feature, which is possibly due to a RKKY-like coupling between the FM and the AFM, has been observed previously by M-T Lin et al.[12]

For $T<T_B$, Fig. 6.6 shows that at X = 1.5 nm, the exchange bias is relatively large and increases strongly with decreasing temperature from $T_B$, while the MSHG asymmetry remains constant. On the other hand, for X = 3.5 nm, the exchange bias is almost zero, and does not change much with temperature, while the asymmetry decreases strongly below $T_B$.

Here we observe the dependence of $\mathcal{A}$ on the Fe interfaces: for X = 1.5 nm, $\mathcal{A}$ remains constant, indicating that here $R \approx 1$ (see discussion above). For X>1.5 nm, the contribution of the Fe interfaces ($\chi_{odd}^{(4)}$ and $\chi_{odd}^{(5)}$) decreases, leading to R<<1 and thus $\mathcal{A} \approx R$.

A calculation based on Fresnel coefficients and the refractive index of Cu gives indeed a diminishing of the SHG contribution from the Cu/Fe interface by almost 50% with increasing thickness of the Cu spacer from 1.5 nm to 3.5 nm (see Table 6-I).

| Cu-X | 1.5 nm | 2 nm | 2.5 nm | 3 nm | 3. 5 nm |
|---|---|---|---|---|---|
| SHG | 0.767 | 0.686 | 0.608 | 0.534 | 0.464 |

**TABLE 6-I**. Calculation of SHG intensity reflected from the lower interface of a VOID/Cu/VOID thin film for different thicknesses of Cu, normalized to the upper interface.

To further investigate the MSHG sensitivity to the pinned uncompensated spins at the CoO/Cu interface as a function of the Cu spacer thickness, Fig 6.7 shows the observed loop shift $H_E$ and $\theta_K^{(2)}$ as function of temperature for various Cu spacers. We can see that

for a Cu thickness of 3.5 nm, the loop-shift in Fig. 6.7a is zero, while the second harmonic Kerr rotation in Fig. 6.7b still indicates the presence of pinned uncompensated spins. This result is consistent with our previous experiment that monitored the MSHG asymmetry derived from hysteresis loop measurements (Fig. 6.6). It is important to notice that the data in Fig. 6.7 were obtained from a different experiment. Although the conditions for the two measurements are different, both are sensitive to $\chi_{odd}^{(3)}$.

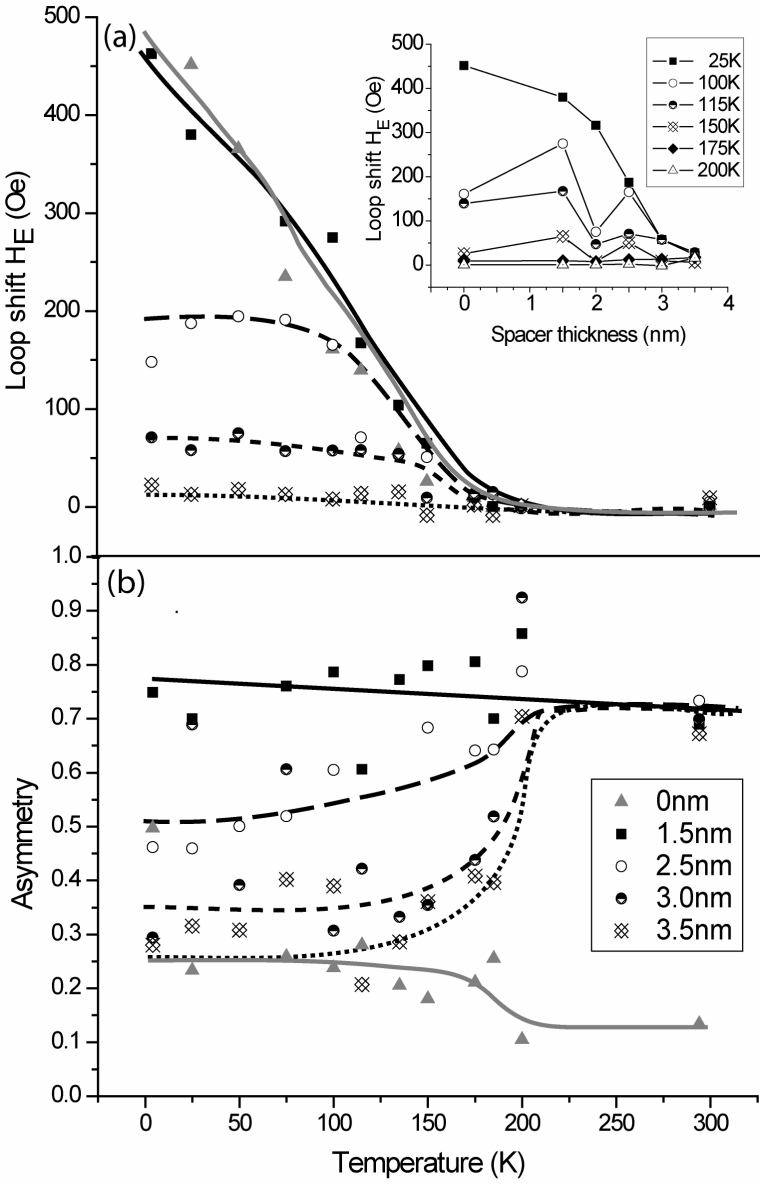


**Fig. 6.6** Temperature dependence of the exchange bias loop shift measured with MOKE (a) and of the asymmetry measured with MSHG (b). The lines are guides to the eye.

It appears that for a thickness of Cu = 3.5 nm, the magnetic order of CoO is influenced by the Fe although the effect is not strong enough to induce measurable exchange bias effects in return. One should realize that for small spacer thickness, the FM layer plays a

double role: it induces pinned AFM spins, but also diminishes the number of uncompensated spins available for pinning by strongly coupling to them and forcing them to reverse with the magnetization. On the other hand, for thicker spacer layers, the FM coupling to the uncompensated spins becomes weaker and therefore these are less affected by the magnetization reversal, i.e. they remain pinned in the direction of exchange bias.

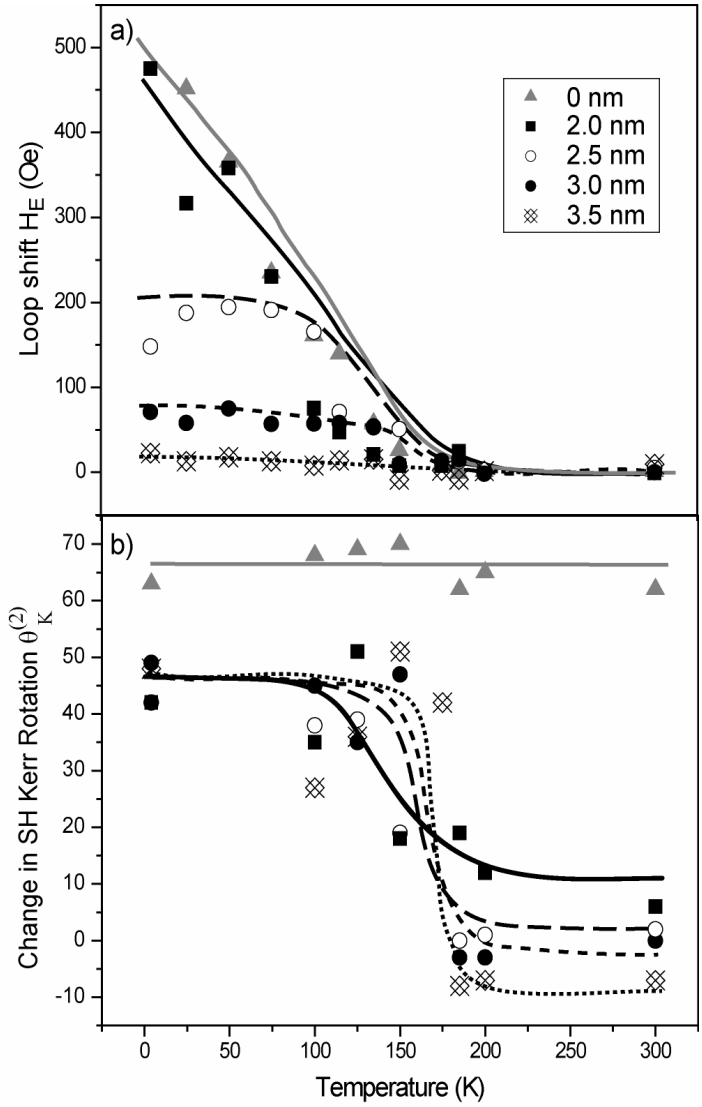


**Fig. 6.7** Temperature dependence of the exchange bias loop shift measured with MOKE (a) and of the SH Kerr rotation measured with MSHG (b). The lines are guides to the eye.

In other words, the coupling between the AFM uncompensated spins and the FM spins is in competition with the coupling between the former and the AFM lattice. As the temperature diminishes and the AFM order appears, for pinned uncompensated spins to occur at the interface, the AFM/FM interaction should be just strong enough for some spins to overcome the AFM ordering. This could occur at defect sites, for instance due to

atomic scale roughness. Once the AFM order is established the newly formed pinned uncompensated spins are locked to the AFM lattice and remain pinned. However, if the AFM/FM interaction is very strong, while reversing the FM layer causes some of the AFM spins to "unpin" from the AFM lattice and to follow the direction of the FM reversal. The two processes coexist in equilibrium in the case of a direct AFM/FM interface and it is quite likely that parameters such as the interface roughness play an important regulatory role. Upon the insertion of an increasingly thicker spacer layer we are able to "tip the balance" in favor or the first process.

The distance across which the pinning process occurs extends until a limit that remains to be determined experimentally. In our case we can conclude that this limit is larger than 3.5 nm.

## 6.4. Conclusion

In this Chapter we have demonstrated that the presence of ferromagnetically ordered AFM spins at the CoO/Cu interface can be clearly observed in the MSHG asymmetry (relative magnetic contrast), the second harmonic Kerr rotation and in the temperature dependence of the rotated incoming polarization angle. It has been also shown that MSHG signal coming from this spin polarized interface can equal and even dominate the signal from the ferromagnetic interfaces, therefore providing us with an opportunity for direct observation of the interface magnetic order. We have thus demonstrated the potential of MSHG to study the exchange bias effect.

This new possibility allows us to study the limits upon which the FM layer affects the AFM magnetic ordering at the interface in exchange biased multilayers. We have provided evidence that the range of this phenomenon is relatively large and that it extends beyond distances where effects in the hysteresis loop shift are observed.

The difficulty to fully understand the exchange bias effect has often been attributed to the lack of interface-specific results. Our data, presented in this Chapter, show that the intuitive model of interface spin-pinning is in principle correct. This is in agreement with the results of Ohldag et al. which were measured with another interface-specific technique.[6]

We have also suggested the potential importance of atomic scale roughness as a regulatory mechanism between the processes of creating pinned AFM uncompensated spins (responsible for the loop shift) and AFM uncompensated spins that follow the FM magnetization reversal (responsible for the increased coercivity). In the next Chapter we will focus our attention on the role of atomic scale roughness.

## References:

[1] H. Zabel, R. Siebrecht and A. Schreyer, Physics B **276**, 17 (2000).

[2] J.B. Kortright, D.D. Awschalom, J. Stöhr, S.D. Bader, Y.U. Idzerda, S.S.P. Parkin, I.K. Schuller and H.C. Siegmann, J. Magn. Magn. Mater. **207**, 7 (1999).

[3] B.P. Tonner, D. Dunham, T. Droubay, J. Kikuma and J. Denlinger, J. Electron Spectrosc. Relat. Phenom. **78**, 13 (1996).

[4] T. Shinjo and W. Keune, J. MAgn. Magn. Mater. **200**, 598 (1999).

[5] W.A.A. Macedo, B. Sahoo, V. Kuncser, J. Eisenmenger, I. Felner, J. Nogues, K. Liu, W. Keune and I. K. Schuller, Phys. Rev. B **70**, 224414 (2004).

[6] H. Ohldag, A. Scholl, F. Nolting, E.Arenholz, S. Maat, A. T. Young, M. Carey and J. Stöhr, Phys. Rev. Lett. **91**, 017203 (2003).

[7] H. Ohldag, T.J. Regan, J. Stöhr, A. Scholl, F. Nolting, J. Lüning, C. Stamm, S. Anders and R.L. White, Phys. Rev. Lett. **87**, 247201 (2001).

[8] W. J. Antel, Jr., F. Perjeru and G. R. Harp, Phys. Rev. Lett. **83**, 1439 (1999).

[9] N.J. Gökemeijer, T. Ambrose and C.L. Chien, Phys. Rev. Lett. **79**, 4270 (1997).

[10] M. Gruyters, M. Gierlings, and D. Riegel, Phys. Rev. B **64**, 132401 (2001).

[11] T. Mewes, B.F.P. Roos, S.O. Demokritov and B. Hillebrands, J. Appl. Phys. **87**, 5064 (2000).

[12] M.-T. Lin, C.H. Ho, C.-R. Chang and Y.D. Yao, Phys. Rev. B **63**, 100404(R) (2001).

[13] K. Takano, R.H. Kodama and A.E. Berkowitz, W. Cao and G. Thomas, Phys. Rev. Lett. **79**, 1130 (1997).

[14] L. C. Sampaio, A. Mougin, J. Ferre, P. Georges, A. Brun, H. Bernas, S. Poppe, T. Mewes, J. Fassbender and G. Hillebrands, Europhys. Lett. **63**, 819 (2003).

[15] G. S. Higashi, Y. J. Chabal, G. W. Trucks and K. Raghavachari, Appl. Phys. Lett. **56**, 656 (1990).

[16] M. Gruyters and D. Riegel, Phys. Rev. B **63**, 052401 (2001).

[17] M. Gruyters, Surf. Sci. **515**, 53 (2002).

[18] A. Kirilyuk and Th. Rasing, J. Opt. Soc. Am. B **22**, 148 (2005).

[19] J.E. Sipe, J. Opt. Soc. Am. B **4**, 481 (1987).

[20] Y. Z. Wu, R. Vollmer, H. Regensburger, X.-F. Jin and J. Kirschner, Phys. Rev. B **63**, 054401 (2000).

[21] M. Fiebig, Th. Lottermoser, V. V. Pavlov and R. V. Pisarev, J. Appl. Phys. **93**, 6900 (2003).

[22] V. V. Pavlov, R. V. Pisarev, A. Kirilyuk, and Th. Rasing, Phys. Rev. Lett. **78**, 2004 (1997).

# Chapter seven

# Magnetic properties at the Co surface and the Mn/Co interface[xiii]

In the previous chapters, we have presented the phenomenon and experimental investigation of exchange bias. As pointed out previously, the need for investigation methods other than the hysteresis loop shift and the lack of experimental data directly from the AFM/FM interface are among the most important reasons for our failing to achieve a complete understanding of the phenomenon.

So far we have seen how MSHG can provide us with new ways to study this problem. Both the MSHG asymmetry and the second harmonic Kerr rotation have been discussed as alternative and complementary probes for the AFM/FM interface magnetic properties. Although handling the MSHG technique can sometimes be difficult, as for instance when a quadratic dependence on the magnetization appears in the signal, we have demonstrated that this experimental approach has the potential for direct observation of the magnetic order at the exchange biased interface.

Concerning the necessity for new information originating directly from the relevant but buried AFM/FM interface, we have proved the usefulness of MSHG as it allowed us to observe the presence of pinned uncompensated spins at the CoO/Cu interface at a Cu spacer thickness where the loop shift indicated no exchange bias. We have also seen that our interface-specific data confirm the validity of the interface spin-pinning principles of the intuitive model, presented in Chapter two.

In this Chapter, we will take our study a step further, examining the structural and magnetic properties on the interface between a layer-by-layer grown Co on a Cu(001) single crystal and a subsequently deposited Mn film. We will focus our attention on the preservation of interface roughness after capping with Mn, and then we will investigate the relationship between the roughness and the net magnetic moment at the exchange biased Mn/Co interface. Furthermore, the magnetization reversal properties of the interface with respect to the Co bulk will be studied and a comparison with previous work on a clean Co surface will then be made.

[xiii] Based on V.K. Valev, A. Kirilyuk, Th. Rasing, F. Dela Longa, J.T. Kohlhepp, B. Koopmans, "Oscillations of the net magnetic moment and magnetization reversal properties of the Mn/Co interface", *submitted.*

# 7.1. Introduction

With decreasing material thicknesses, the structural properties of surfaces and interfaces play an increasingly important role in magnetism. Step sites, island sizes or roughness can have a strong influence upon the magnetic moment, the magnetization reversal behavior or the magnetic anisotropies, including exchange bias.[1,2]

The latter is a striking example of how dramatically the magnetic characteristics of a bilayer can be influenced by the properties at the AFM/FM interface.

In another clear example of structural properties affecting magnetism, during the layer-by-layer growth of Co films on Cu(001), it has been found that the surface magnetic moment is enhanced at half filled layers due to the larger magnetic moment of step atoms as compared to atoms within the flat surface.[3] On the other hand, upon deposition of one monolayer of oxygen on a similarly grown Fe(001) surface, magnetic moment oscillations with opposite phase were observed, indicating that the strain/stress conditions in the O/Fe monolayer controlled the magnetization while the step edges played a minor role.[4] However, to our knowledge no such oscillations were ever observed at a buried interface. Although investigation of surfaces is in principle readily undertaken down to the atomic scale with techniques such as scanning probe microscopy, buried interfaces, being out of reach for direct probes, remain a challenge.

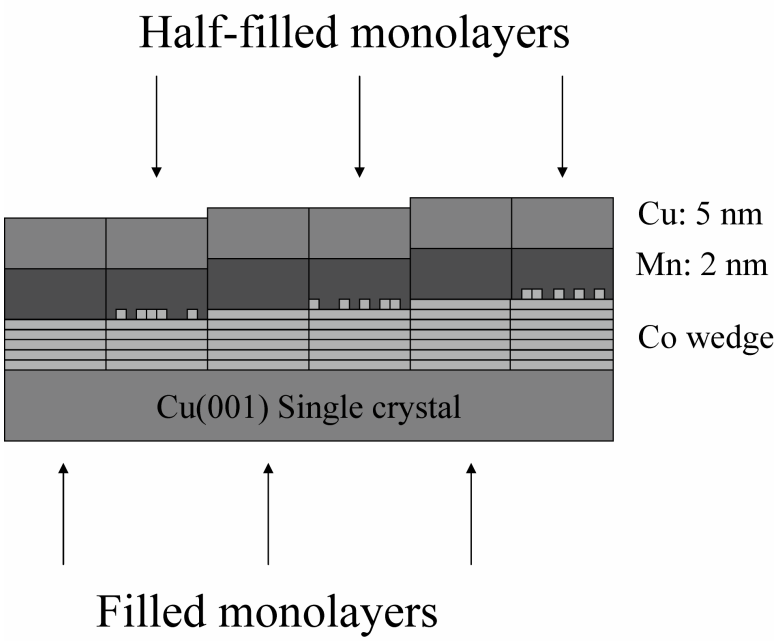


**Fig. 7.1** The sample structure: in the layer-by-layer growth mode of Co deposited on Cu(001) single crystal, each new monolayer starts by forming islands that (almost) completely fill the surface before the next monolayer starts growing.

We have applied the interface-sensitive technique of Magnetization-induced Second Harmonic Generation (MSHG) in combination with the Magneto-Optical Kerr Effect (MOKE) to the study of Mn/Co bilayers, where the Co was a layer-by-layer grown

wedge on a Cu(001) single crystal and the Mn was deposited as a thin film on top. Each new Co layer starts by forming islands that (almost) completely fill the surface before the next monolayer starts growing. Thus, the wedge passes through alternating phases of being atomically flat (filled layer) and rough (half-filled layer) as can be observed with scanning tunneling microscopy[5] (see Fig. 7.1 and 7.2).

This system allows us to explore the role of atomic scale roughness at the AFM/FM interface in a well-controlled way. However, upon deposition of Mn, several mechanisms, such as strong interdiffusion or annealing, could provoke the smoothing of the rough interface regions.

Our data provide unambiguous evidence that the roughness at the interface remains after capping. These results are obtained from the direct observation of the MSHG intensity produced by dominantly non-magnetic tensor elements. Furthermore, we find an indication of magnetic moment oscillations at the exchange biased interface between the layer-by-layer grown Co on Cu(001) and the antiferromagnetic Mn. After showing how information on the magnetic moment can be extracted from the oscillations of the MSHG signal, we conclude that the former is maximal at filled monolayers. The origin of these oscillations is then discussed in terms of several possible mechanisms.

Additionally, it has been previously found that magnetization reversal at the surface of a Co/Cu(001) system may differ from the bulk one.[6] It is therefore of great interest to know whether a similar behavior occurs at an interface, especially in the context of exchange bias where the question of the development of a domain wall in the Co might arise (see section 2.3.3. of Chapter two).

We find no difference in magnetization reversal between the interface and the Co bulk. Both MSHG and MOKE hysteresis loops exhibit the same loop shift and coercivity dependence as function of Co thickness. Furthermore, the two techniques present a similar hysteresis loop shape.

## 7.2. Experimental details

The Co(001)/Mn(001) bilayers were epitaxially grown on atomically clean and flat Cu(001) singe crystals (miscut<0.1°) at 330 K in a multichamber molecular beam epitaxy (MBE) system (VG-Semicon V80M) with a base pressure better than $1x10^{-11}$ mbar. The Co layers were deposited in a wedge structure (roughly 9-13 ML thick) using an e-gun evaporator with feedback control of the flux whereas the 25 ML thick Mn films were prepared using a temperature stabilized and extensively degassed Knudsen cell. All nominal thicknesses were controlled by calibrated quartz-crystal monitors, with an accuracy of roughly 3%. During the growth, the pressure never rose above $5x10^{-11}$ mbar and the growth rates were 1-2 monolayers (ML)/min. Under these conditions, it was shown that the Mn adopts a face-centered-tetragonal (fct) structure with a c/a ratio of roughly 1.05, before it transforms around 50-60 ML to the thermodynamically stable complex $\alpha$-Mn structure.[7] The fct-Mn(001) is antiferromagnetic even at room temperature and is able to induce a sizable exchange anisotropy in the Co layers[7] (see Fig. 7.2) To avoid oxidation of the layer during the ex-situ experiments, the bilayers were covered with a 5 nm thick Cu capping layer.

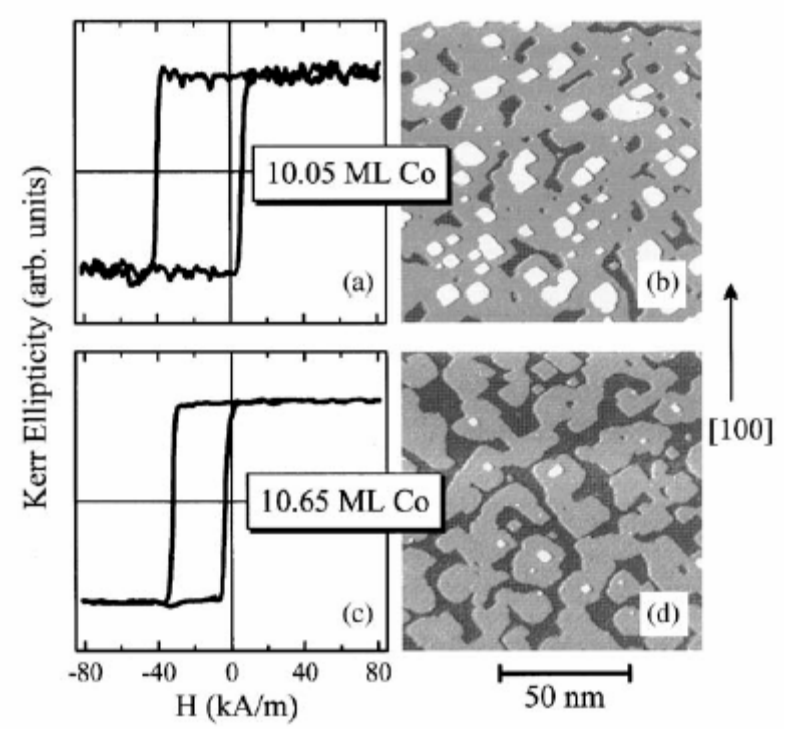


**Fig. 7.2** In (a), sizable exchange anisotropy can be observed for the flat Mn/Co interface. In (b), the STM micrograph of the corresponding filled monolayer Co surface. In (c), the loop shift presented for a rough Mn/Co interface. In (d), the STM micrograph of the corresponding half-filled monolayer Co surface.

MSHG measurements were performed using laser power between 20 and 40 mW and the light was focused to a spot with diameter of around 100 μm. The angle of incidence $\theta$ was 45° and the magnetic field was applied in the longitudinal and the transverse configurations (see Fig. 7.3). All our measurements presented in this Chapter were done at room temperature.

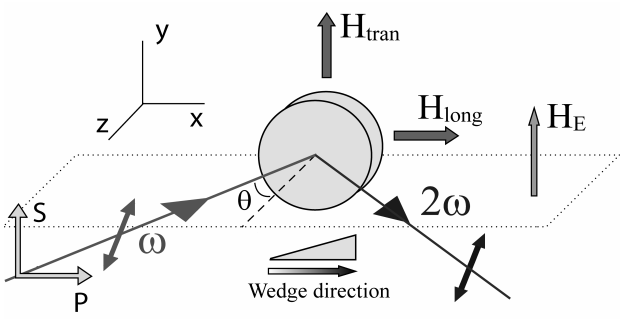


**Fig. 7.3** Experimental configuration. $\mathbf{H}_{tran}$ and $\mathbf{H}_{long}$ represent the directions of applied field for the transverse and the longitudinal configurations respectively. $\mathbf{H}_E$ indicates the direction of the unidirectional anisotropy. The sample was oriented along the Cartesian directions.

Following Eq. 3.13 and the conventions therein, for the P-P polarizer-analyzer combination, in the transverse magnetic field geometry (see Fig. 3.3), we can define the average MSHG intensity and asymmetry as:[8]

$$I^{PP}(2\omega) = \frac{I^{\uparrow} + I^{\downarrow}}{2} \propto \left|\chi_{eff}^{even}\right|^2 + \left|\chi_{eff}^{odd}\right|^2 \approx \left|\chi_{eff}^{even}\right|^2 \tag{7.2}$$

$$\mathcal{A} = \frac{I^{\uparrow} - I^{\downarrow}}{I^{\uparrow} + I^{\downarrow}} \propto \frac{\left|\chi_{eff}^{odd}\right|\left|\chi_{eff}^{even}\right|}{\left|\chi_{eff}^{odd}\right|^2 + \left|\chi_{eff}^{even}\right|^2}\cos\varphi \approx \frac{\left|\chi_{eff}^{odd}\right|}{\left|\chi_{eff}^{even}\right|}\cos\varphi \tag{7.3}$$

where $\varphi$ is the phase difference between $\chi_{eff}^{odd}$ and $\chi_{eff}^{even}$, and the quantities $I^{\uparrow}$ and $I^{\downarrow}$ are the MSHG intensities for opposite directions of the magnetization. From Eq. 7.2, it follows that for $\left|\chi_{eff}^{even}\right| >> \left|\chi_{eff}^{odd}\right|$, the MSHG intensity in the P-P configuration measures the structural properties of the interface.

## 7.3. Results

In Fig. 7.4, the MSHG intensity is plotted as function of increasing Co thickness. It is clear that the oscillations of $I^{PP}$ present maxima at half-filled monolayers, and therefore appear to be related to the interface roughness. This is consistent with a signal that is dominantly originating from the top Co interface since in systems with inversion symmetry the MSHG is generated in regions where this symmetry is broken, i.e. the regions with higher roughness.[9,10] The amplitude of the oscillations is approximately 20%; however one should take into account that there is a contribution to the observed signal by the second Co interface, but of opposite phase. Therefore it is difficult to extract quantitative information from this amplitude since the detected MSHG is affected by interference between these interfaces. The increase of the total $I^{PP}$ in Fig. 7.4 results from the fact that due to the increasing Co thickness the signal generated at the second Co interface diminishes, although very slightly.

A further confirmation that the oscillations in $I^{PP}$ should be attributed to the interface roughness comes from examining the magnetization contribution to the odd tensor components. For the P-S polarizer-analyzer combination, in the longitudinal magnetic field geometry, the MSHG intensity for the effective values of the susceptibilities is given by $I_{long}^{PS}(2\omega) \propto \left|\chi_{yxx}^{odd} + \chi_{yzz}^{odd}\right|^2$. Consequently, $\sqrt{I_{long}^{PS}(2\omega)}$ is proportional to $\chi_{eff}^{odd}$. However, note that although $\chi_{eff}^{odd}$ is directly proportional to the magnetization,[4] it can and most likely will also be affected by the local electromagnetic fields (LEF) and local electronic structure (LES)[11] as we can see from the following equation (see Ref. 12):

$$\chi_{ijk}^{odd}(\mathbf{M}) = \frac{e^3}{\hbar^2}\sum_{\mathbf{k},\sigma}\sum_{\nu,c,c'}\left(\sum_m \pm b_{\nu m}^* \frac{\langle r_i\rangle_{\nu c}\langle r_j\rangle_{cc'}\langle r_k\rangle_{c'\nu}}{(2\omega-\omega_{c\nu})(\omega-\omega_{c'\nu})} + 35 \quad similar \quad terms\right) f_\nu(\mathbf{k},\sigma) \quad (7.4)$$

where $\sigma$ is a spin index, the $\pm$ signs correspond to spin up and down, respectively; $\mathbf{k}$ denotes the electron wave vectors; $\nu,c,c'$ are band indices for the valance and conduction bands; $f_\nu(\mathbf{k})$ is the Fermi distribution function for the spin state $|\nu,\mathbf{k}\rangle$; $\langle r_i\rangle_{\nu c}$ is a matrix element for the $i$th component of the electronic displacement vector for the transition $c \leftrightarrow \nu$; $\omega_{c\nu} = (E_c - E\nu)/\hbar$ and $b_{\nu m}$ is a material specific constant.

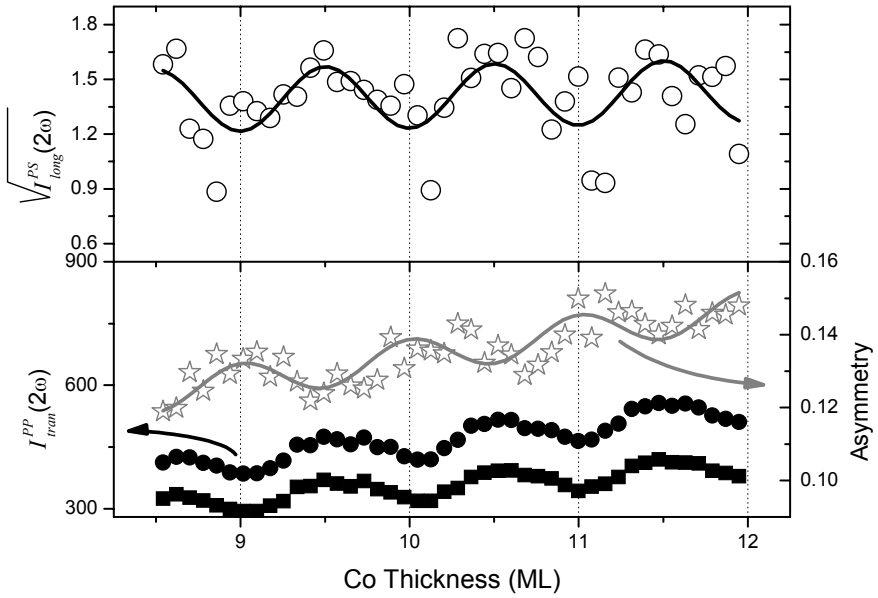


**Fig. 7.4** MSHG intensity as function of Co thickness. Empty circles: the square root of the MSHG intensity for the P-S polarizer-analyzer combination in the longitudinal magnetic field geometry. The MSHG intensity for the P-P polarizer-analyzer combination in the transverse magnetic field geometry for positive (full circles) and negative (full squares) magnetic field. The MSHG asymmetry as function of Co thickness is represented by the empty stars.

It is clear that $f_\nu(\mathbf{k})$ or $\langle r_i\rangle_{\nu c}$ are different at island edges and thereby can contribute to the oscillations of $\chi_{eff}^{odd}$. Henceforth, we believe that extracting purely magnetic information from the variations of the "odd" components alone is impossible as both the LEF and the LES on the one hand and the magnetic moment on the other hand could be oscillating.

In Fig. 7.4, we observe that the monolayer oscillations of $\sqrt{I_{long}^{PS}(2\omega)}$ are in phase with those of the roughness, i.e. maxima occur at half-filled monolayers. In order to make

sure that the measurement had no "contamination" from "even" tensor components, the magnetic contrast was measured and found to be zero. From this we can conclude that either the LEF and the LES contributions to $\chi_{eff}^{odd}$ dominate or that both these contributions and the magnetic moment oscillate in phase with the roughness.

In order to lift this ambiguity, we examined the magnetic asymmetry. From Eq. 7.3, it follows that for $\left|\chi_{eff}^{even}\right| >> \left|\chi_{eff}^{odd}\right|$, $\mathcal{A}$ is proportional to the ratio of "odd" tensor elements divided by the "even" ones. Assuming that the nonvanishing "even" and "odd" components are similarly affected by the LEF and LES, this quantity is to a first approximation only proportional to the magnetic moment.

Thus, in Ref. 11, Eq 19 reads:

$$\mathcal{A} \approx \frac{\chi_{\alpha,\beta,\gamma}^{odd}}{\chi_{i,j,k}^{even}} \approx \frac{\lambda_{LS}}{E_{\mathbf{k}\mu}} \left( \frac{F_{0;\mu}}{F_{\mu;\mu'}} \right)^{1/2} \tag{7.5}$$

where $\lambda_{LS}$ is the spin-orbit interaction constant, **k** is the wave vector of the electromagnetic wave, $E_{\mathbf{k}\mu}$ is the magnetic excitation energy for the state $\mu$ at wave vector **k** and $F_{0;\mu}$ is the oscillator strength of the transition between the ground state and the excited state $\mu$.

Similarly, with the notations of Eq. 7.4 we find in Ref. 12:

$$\mathcal{A} \approx \frac{\chi_{\alpha,\beta,\gamma}^{odd}}{\chi_{i,j,k}^{even}} \approx u_b \sum_m 6 b_{vm} \tag{7.6}$$

where $u_b$ is the number of Bohr magnetons per surface atom and $b_{vm}$ is the same quantity as in Eq. 7.4.

In Fig. 7.4, we can see that the asymmetry exhibits clear monolayer oscillations but with opposite phase with respect to the interface roughness. Consequently, we can conclude that the interface net magnetic moment is maximal at the flat regions of the interface. Furthermore, since the magnetic moment does not oscillate in phase with the LEF and the LES, to a first approximation, we can attribute the oscillations of $\chi_{eff}^{odd}$ to these two quantities.

The oscillations of the interface net magnetic moment could be due to inhomogeneities across the Co thin film. For instance, it is conceivable that under the influence of roughness the magnetization reversal at the interface is incomplete or differs from that of the bulk.

To compare the bulk magnetic properties with those of the interface, we measured the MSHG and MOKE hysteresis loops at filled and half-filled monolayers. In Fig. 7.5 we can see that both hysteresis loops exhibit the same loop shape indicating similar magnetization reversal behavior.

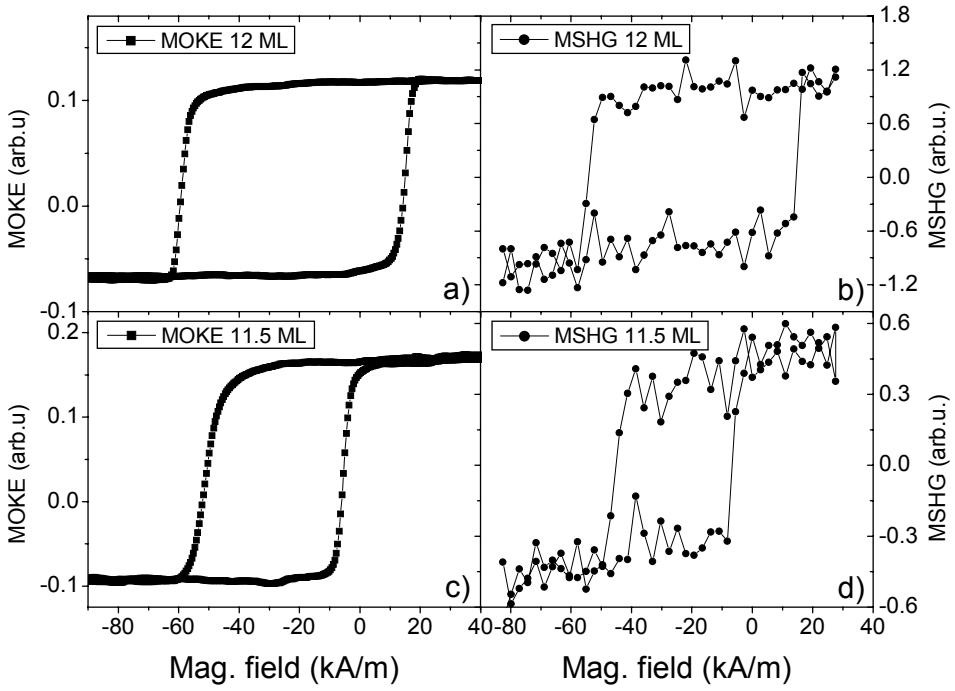


**Fig. 7.5** Hysteresis loops from MOKE (left panels) and MSHG (right panels) taken at thicknesses of 12 ML and 11.5 ML of Co.

This is further confirmed when we examine the values of the coercivity $H_C$ and the loop shift $H_E$ as function of the Co thickness (see Fig. 7.6).

Indeed both techniques reveal the same characteristic behavior and the small differences observed are likely due to slightly different calibrations of the MSHG and MOKE setups or to a small temperature increase from the higher laser power necessary for MSHG. Since we have demonstrated that the MSHG signal originates from the interface (monolayer-period oscillations are in phase with interface roughness), we can conclude that the bulk and the interface Co spins behave in the same way, i.e. that there is no difference in magnetization reversal between the bulk and the interface. Previously, a difference was found by Gruyters et al. between the surface and the bulk magnetization of Co/Cu(001) which was attributed by the authors to free surface states.[6] However these do not exist in the case of a Mn/Co interface.

To our knowledge, the fact that the magnetization at the interface and in the bulk of these systems behave in a similar way was never observed before. Our results are of importance for the understanding of exchange bias, since they exclude the possibility of a partial[13] or incomplete domain wall (IDW)[14,15] formation in the ferromagnet under the influence of the pinning of the antiferromagnet, as it has been proposed in the IDW-FM model,[16] (see Chapter two, section 2.3.3). Please note that our samples correspond very well to the conditions outlined for testing this model: a compensated AFM interface, where the AFM spins are in a spin-flop state with respect to the direction of the FM magnetization.

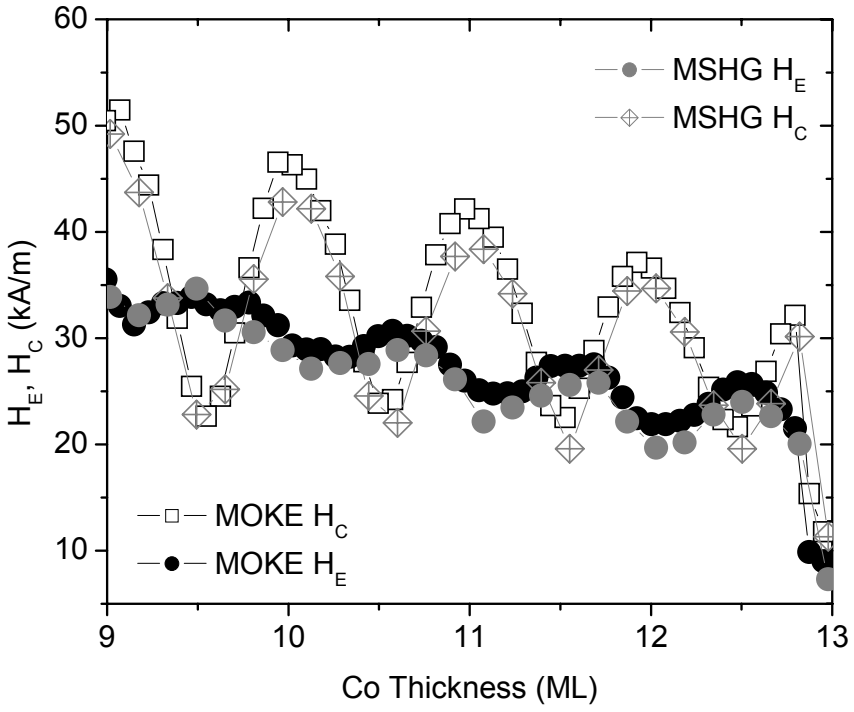


**Fig. 7.6** Coercivity and loop shift of the hysteresis curves from MSHG (in gray) and MOKE (in black) as function of the Co thickness.

Explaining the enhancement of the net magnetic moment in the case of an interface is significantly more difficult than in the case of a surface. Indeed, while it has been shown that there is an increased magnetic moment on the island edges of the Co surface,[3] we believe that this explanation cannot be retained for the interface because of the presence of Mn atoms. On the other hand, variations in the strain/stress conditions between flat and rough regions of the Mn/Co interface should be considered as a possible mechanism,[4] for instance, considering the possibility that Mn-Co bonds could cause an outward relaxation of the top-most layer of Co atoms. It appears to us that there is no theoretical work that has addressed this problem in the case of a Mn/Co bilayer. A precise description will certainly have to take into account several interface-specific factors, such as interdiffusion and interfacial alloying.[17] In this particular case, it is clear that the analysis also has to include the exchange bias interaction.

A relationship between an enhancement of the interfacial net magnetic moment and the presence of AFM pinned uncompensated spins should not be excluded. Indeed, we have demonstrated previously that the presence of such spins can affect strongly the MSHG signal.[18] Nevertheless the experiments that we describe in this Chapter are not sensitive to *pinned* uncompensated spins, since in the MSHG asymmetry the magnetic moment is a quantity that changes sign upon magnetization reversal. This is confirmed by the fact that the oscillations of the exchange bias and those of the net magnetic moment have opposite phases.

Instead, our experiment could reveal AFM uncompensated spins that are strongly coupled to the FM ones and that reverse with them, thereby contributing to an enhancement of the interfacial net magnetic moment. It has been found that this type of AFM uncompensated spins is responsible for the enlargement of the coercivity in exchange biased systems.[19] We would therefore expect a similar behavior between the coercivity and the net magnetic moment, and this would lead to maxima in the MSHG oscillations at the flat regions of the interface, in accordance with our observations. The simultaneous enhancement in net magnetic moment and coercivity is therefore consistent with the presence of Mn uncompensated spins at the exchange-biased interface.

Please note that at the end of the previous Chapter, we have suggested the potential importance of atomic scale roughness as a regulatory mechanism between the processes of creating pinned AFM uncompensated spins (responsible for the loop shift) and AFM uncompensated spins that follow the FM magnetization reversal (responsible for the increased coercivity). In Fig. 7.6, the observed out of phase oscillations between $H_E$ and $H_C$ fully support this hypotheses!

However, although one should not exclude the presence of such unpaired uncompensated Mn spins, it has been suggested that, at the interface, the AFM favors an orthogonal alignment with respect to the direction of the FM order (see Fig. 7.7).[5]

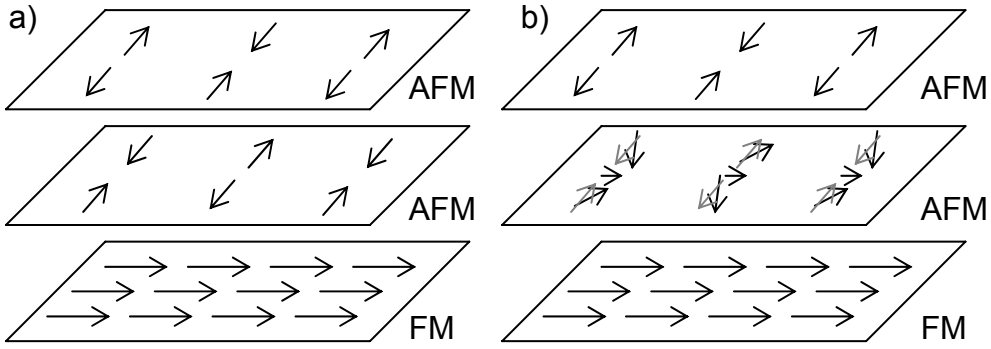


**Fig. 7.7** In a), a schematic representation of an orthogonal alignment between the spins of the ferromagnet and of the antiferromagnet. In b), a canting of the antiferromagnetic spins at the interface leads to the appearance of a magnetization component along the direction of the ferromagnetic magnetization and therefore to an enhancement of the interface net magnetic moment.

Consequently, a canting of the AFM spins at the interface could be responsible for an enhancement of the interface net magnetic moment. Reversing the magnetization is then accompanied by an inversion of the canting angle and thereby this process can contribute to the MSHG asymmetry. This is further supported by the fact that within the bi-quadratic coupling model, the canting has been suggested to cause an enhancement of coercivity,[20,21] which is again consistent with our observation that the oscillations of the MSHG asymmetry and the coercivity are in phase.

## 7.4. Conclusions

In conclusion, using the nonlinear optical technique of MSHG, we have provided unambiguous evidence that the roughness at the topmost monolayer of Co from a layer-by-layer grown Co/Cu(001) is preserved after capping with Mn. The effect of this roughness on the net magnetic moment of the exchange biased Mn/Co interface is directly observed with MSHG and the results are carefully analyzed. Within the limits of our assumptions we can conclude that the interfacial net magnetic moment is maximal at the flat interface regions. Most likely, this is the consequence of a canting of the AFM spins at the interface; however the nature of the exact mechanisms involved remains an open question.

Furthermore, previous work has reported a difference in the magnetization reversal behavior between the Co/Cu(001) surface and bulk. In the case of a Mn/Co interface, a similar difference is expected within the IDM-FM model. However, although our samples correspond very well to the conditions outlined for testing this model, we have demonstrated that the magnetization reversal behavior between the Co bulk and the Mn/Co exchange biased interface is collinear.

## References:

[1] W. H. Meiklejohn and C. P. Bean, Phys. Rev. **102**, 1413 (1956).

[2] J. Nogués, I. K. Schuller, J. Magn. Magn. Mater. **192**, 203 (1998).

[3] Q.Y. Jin, H. Regensburger, R. Vollmer, and J. Kirschner, Phys. Rev. Lett. **80**, 4056 (1998).

[4] M. Nyvlt, F. Bisio, J. Franta, C.L. Gao, H. Petek, and J.Kirschner, Phys. Rev. Lett. **95**, 127201 (2005).

[5] J.T. Kohlhepp, O. Kurnosikov and W.J.M. de Jonge, J. Magn. Magn. Magn. **286**, 220 (2005).

[6] M.Gruyters, T.Bernhard, and H.Winter, Phys. Rev. Lett. **94**, 227205 (2005).

[7] J.T. Kohlhepp and W.J.M. de Jonge, Phys. Rev. Lett. (in press).

[8] A. Kirilyuk and Th. Rasing, J. Opt. Soc. Am. B **22**, 148 (2005).

[9] A. Kirilyuk, Th. Rasing, M. Haast and J.C. Lodder. Appl. Phys. Lett. **72**, 2331 (1998).

[10] G. Tessier and P. Beauvillain Appl. Surf. Sci. **164**, 175 (2000).

[11] S.B. Borisov and I.L. Lyubchanskii, Opt. Spektrosk. **61**, 1274 (1986) [Opt. Spectrosc. (USSR) **61**, 801 (1986)].

[12] Ru-Pin Pan, H.D. Wei, Y.R. Shen, Phys. Rev. B, **39** 1229 (1989).

[13] B.H. Miller and E. Dan Dahlberg, Appl. Phys. Lett. **69**, 3932 (1996).

[14] M. Kiwi, J. Mejia-Lopez, R.D. Portugal and R. Ramirez, Europhys. Lett. **48**, 573 (1999).

[15] M. Kiwi, J. Mejia-Lopez, R.D. Portugal and R. Ramirez, Appl. Phys. Lett. **75**, 3995 (1999).

[16] J. Meija-Lopez, R. Ramirez and M. Kiwi, J. Magn. Magn. Mater. **241**, 364 (2002).

[17] M. Freyss, D. Stoeffler, and H. Dreyssé, Phys. Rev. B, **56**, 6047 (1997).

[18] V. K. Valev, M. Gruyters, A. Kirilyuk and Th. Rasing, Phys. Rev. Lett. **96**, 067206 (2006).

[19] H. Ohldag, T.J. Regan, J. Stöhr, A. Scholl, F. Nolting, J. Lüning, C. Stamm, S. Anders and R.L. White, Phys. Rev. Lett., **87**, 247201 (2001).

[20] N.C. Koon, Phys. Rev. Lett. **78**, 4865 (1997).

[21] T. C. Schulthess and W. H. Butler, Phys. Rev. Lett. **81**, 4516 (1998).

# Chapter eight

# NiO(111) growth on a Ni(001) surface

In the previous chapters, we demonstrated how the MSHG technique can be applied to the study of AFM/FM interfaces, in the case of the exchange bias effect. We saw that this experimental approach provides alternative and complementary ways of probing the magnetic order. We also demonstrated the capabilities of the technique to give information of important structural properties at the interface, such as atomic scale roughness. The samples studied so far were prepared outside our laboratory. In order to further investigate the AFM/FM interface, we performed an atomic scale oxidation of the surface of a 1 mm thick Ni (001) single crystal, as NiO is antiferromagnetic.

NiO has been the subject of many studies[1] and is often used in exchange bias devices.[2] In particular, NiO/Ni systems have been investigated as nanostructures[3,4] and in the form of thin films.[5,6] Yet despite their potential applications in magnetic multilayers[7] such as spin-valves,[8] so far, very little is known of their interfaces.[9]

Clearly, we do not expect to observe any exchange bias in our oxidized Ni single crystal. The ferromagnetic thickness is much too large (see chapter two, section 2.2.4.1) while the antiferromagnetic one is too small (see chapter two, section 2.2.4.2). However, the single crystalline system offers a well defined FM surface and the possibility for a well controlled AFM growth. Since MSHG is a symmetry sensitive technique (see Chapter three), it appears as the designated tool for investigating the interface crystallographic order, which, similarly to the interface roughness, is another structural characteristic that can have a dramatic influence on the physical properties of exchange bias systems.

In this Chapter we will investigate the NiO/Ni interface, where the NiO has been obtained after a clean Ni(001) single crystal surface has been exposed to oxygen. The, albeit preliminary, results show a dramatic symmetry change at the interface upon oxidation.

## 8.1. Introduction

Nickel oxide forms quite readily whenever a nickel surface is exposed to oxygen (see Fig 8.1).[10,11] It has been established that at room temperature, the rock salt NiO naturally grows as a well ordered oxide film.

The interaction of oxygen with atomically clean nickel surfaces undoubtedly establishes one of the most studied surface reactions.[12] A comprehensive review about

the oxygen-nickel reaction was given by Holloway,[13] and most relevant references can be found there. Virtually no surface sensitive technique has forgone to contribute to the understanding of this reaction, which, in fact, is a representative model system for the oxidation behavior of metal surfaces in general. In this sense, SHG is no exception and a detailed study of the nickel oxidation can be found in Ref. 14.

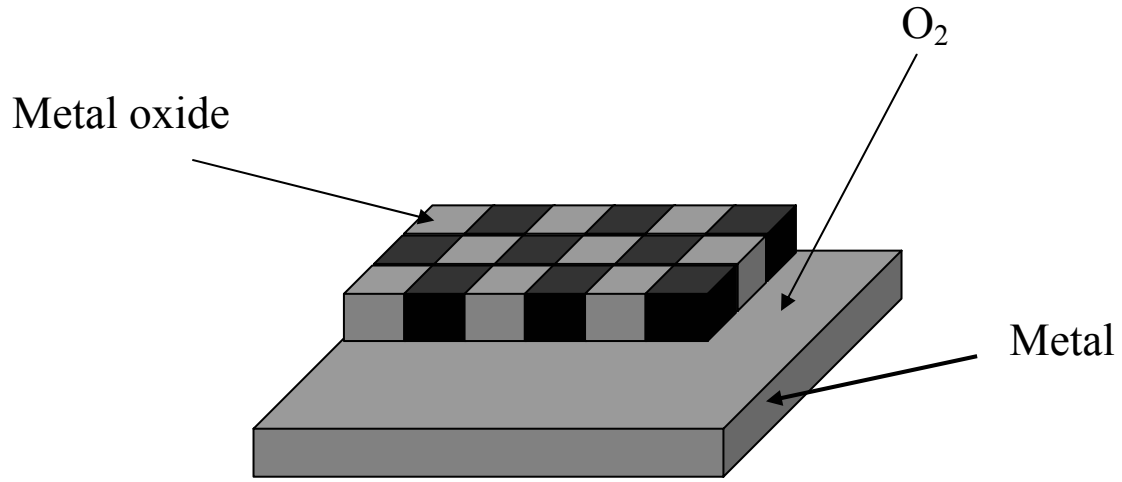


**Fig. 8.1** Schematic representation of the preparation of a nickel oxide layer on a nickel single crystal.

The reaction proceeds in three stages as a function of coverage. The first step is chemisorption. At room temperature, the oxygen forms ordered overlayers on the planes of nickel. In this chemisorption stage the oxygen atoms reside *above* favorable surface sites. Only the Ni(110) face shows a tendency to oxygen-induced surface reconstruction.[15]

The second stage is oxide nucleation to a depth of 2-3 atomic layers. A nucleation and growth model as proposed by Holloway and Hudson[16] has generally been accepted and has been verified with many techniques.[10] Various studies give deviating coverages at which nucleation first begins.[10] The nucleation rate is also temperature dependent,[12,17,18] and usually, the final thin NiO film is epitaxially related to the respective Ni face.

The third stage finally is a lateral growth to coalescence. Afterwards, a slow thickening process has been reported with different rate laws for different reaction temperatures.[10]

Of particular interest for this Chapter is that the epitaxial orientation of NiO on Ni(001) has been reported to follow not only (001) but also (111) and (7x7) patterns.[19-21]

Following Eq. 3.11, the MSHG intensity is proportional to the sum:

$$I(2\omega) \propto \left|(\sum \chi^{(2)}(\alpha))\right|^2 I^2(\omega), \tag{8.1}$$

where $\alpha$ is the angle of azimuthal rotation between the x symmetry axis on the sample and the plane of incidence and the Fresnel coefficients have been included in the effective

susceptibilities $\chi$. Additionally, we can include a possible contribution to the second harmonic signal by the NiO in the crystallographic part.[22,23]

## 8.2. Experimental details

The sample was a Ni(001) single crystal cleaned by Ar-sputtering in a UHV chamber and subsequently oxidized (for details see Chapter four, section 4.3). SHG measurements of the clean Ni surface were performed *in situ* while those of the NiO were done *in air*.

For the measurements *in situ*, because of the restrictions imposed by the design of the UHV chamber, the magnetic field was applied in the longitudinal configuration and the $S_{in}$-45°$_{out}$ polarization configuration was used so that the MSHG signal was sensitive to the longitudinal magnetization component. The sample holder was mounted on a UHV rotating motor (see Chapter four, section 4.3).

For the measurements *in air*, the magnetic field was applied in the transverse configuration and the $P_{in}$-$P_{out}$ and $S_{in}$-$P_{out}$ polarization configurations were used so that the MSHG signal was sensitive to the transverse magnetization components only. For these experiments, the sample holder was mounted on a motorized and computer controlled rotational stage.

## 8.3. Results

In the absence of magnetism, the (001) surface of a cubic crystal lattice is described by a second-order susceptibility tensor such as that in Eq. 3.10, which we can write as:

$$\chi^{cryst}_{4-fold} = \begin{pmatrix} 0 & 0 & 0 & 0 & cr1 & 0 \\ 0 & 0 & 0 & cr1 & 0 & 0 \\ cr2 & cr2 & cr3 & 0 & 0 & 0 \end{pmatrix}, \tag{8.2}$$

where $c1 \neq c2 \neq c3$. The SHG signal is then isotropic (see for example Fig. 3.5 in Chapter three).

For a magnetic surface however, new tensor elements appear, which are *odd* in the magnetization, i.e. they change sign when the magnetization is reversed. If we chose to indicate these components with an "*a*", for a magnetic field applied in the direction of the optical plane of incidence, the second-order susceptibility tensor is:

$$\chi^{magn}_{4-fold} = \begin{pmatrix} 0 & 0 & 0 & 0 & cr1 & a2 \\ a2 & a1 & a3 & cr1 & 0 & 0 \\ cr2 & cr2 & cr3 & a3 & 0 & 0 \end{pmatrix}, \tag{8.3}$$

where the "*cr*" components are *even* in the magnetization, i.e. they do not change sign upon magnetization reversal (note that those are the same components as the crystallographic ones in Eq. 8.2).

For a magnetic field applied perpendicular to the optical plane of incidence, the corresponding tensor is:

$$\chi^{magn}_{4-fold} = \begin{pmatrix} a1 & a2 & a3 & 0 & cr1 & 0 \\ 0 & 0 & 0 & cr1 & 0 & a2 \\ cr2 & cr2 & cr3 & 0 & a3 & 0 \end{pmatrix}. \tag{8.4}$$

We then see that for a magnetic field rotating around the sample, the tensor becomes:

$$\chi^{magn}_{4-fold} = \begin{pmatrix} a1\cos(\alpha) & a2\cos(\alpha) & a3\cos(\alpha) & 0 & cr1 & a2\sin(\alpha) \\ a2\sin(\alpha) & a1\sin(\alpha) & a3\sin(\alpha) & cr1 & 0 & a2\cos(\alpha) \\ cr2 & cr2 & cr3 & a3\sin(\alpha) & a3\cos(\alpha) & 0 \end{pmatrix} \tag{8.5}$$

where $\alpha$ is the angle between the x-axis of the crystallographic frame and the plane of incidence as described in Chapter three. Here we chose that the direction corresponding to 0º is that for the transverse magnetic field geometry and at 90º is that for the longitudinal magnetic field geometry. In our experiments, while the sample is rotating the external magnetic field remains constant in the frame of the laboratory. Therefore, from the point of view of the sample, it is the field that is rotating (as well as the optical plane of incidence, the polarization vectors, etc.). Henceforth Eq. 8.5 applies again.

Manipulating the sample in a UHV chamber can be challenging since the various wires (such as the thermocouple or the sample heater) wind up during the rotation and might break. For this reason, we had to limit ourselves to a $\pm 90°$ rotation only, which is not a major setback since the studied surface is symmetric and therefore the complete rotation data can be extrapolated.

Significantly more problematic was the positioning of the sample surface perpendicularly to the optical plane of incidence. Under the combined weight of the magnet and the UHV motor, the sample holder mounting presented a small tilt and, as a consequence, during rotation the laser spot probed different regions of the sample. Small defects on the surface (such as scratches) could then constitute a source of noise in the signal. However, this problem could be reduced by measuring the magnetic asymmetry (or relative magnetic contrast) of the surface, which was discussed in section 3.3 of Chapter three.

Fig. 8.2 shows the MSHG asymmetry curve obtained *in situ* from the clean Ni(001) surface. As expected, a 4-fold-like star is revealed with an angle of 90° between the peaks. The difference between the amplitude of the peaks can be explained by the sample surface tilt angle which introduces a slight additional 2-fold symmetry. In the inset a LEED picture shows the characteristic pattern of a cubic (001) lattice. The absence of oxygen on the surface was further confirmed by Auger Electron Spectroscopy (see for example Fig. 4.3b).

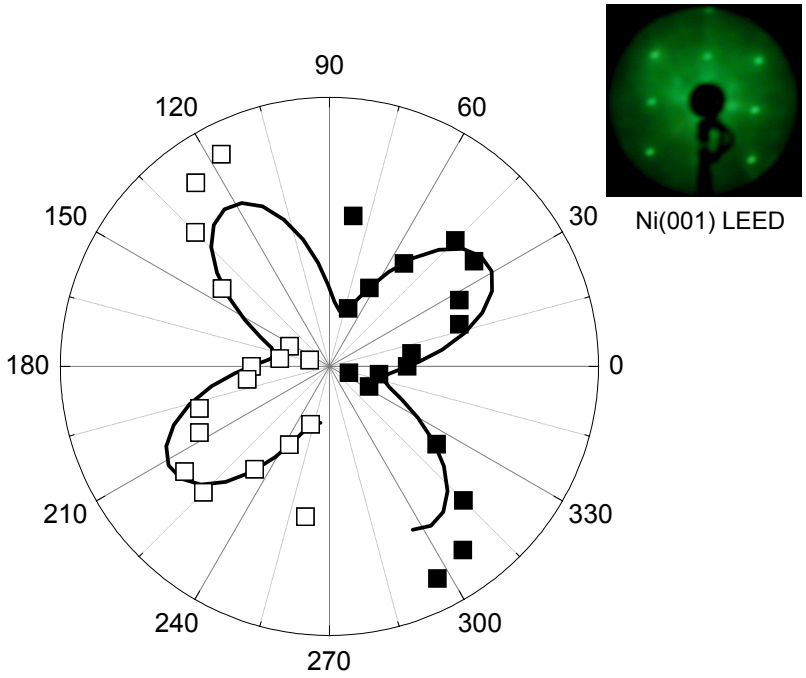


**Fig. 8.2** MSHG asymmetry of the clean Ni(001) as function of the azimuthal rotation of the sample in the UHV system for S-45º longitudinal geometry. The open squares on the graph were obtained by symmetry from the measured data (black squares). In inset, a LEED picture of the Ni(001) surface.

The 4-fold fit was obtained according to the method described in Chapter three, section 3.4. We substituted the susceptibility tensor of Eq. 8.5 into Eq. 3.22 and we obtained the MSHG intensity from Eq. 3.25. The magnetic asymmetry was then calculated by Eq. 3.14. The parameters of the tensor components are presented in Table 8-I. Note that for this calculation, we set our frame of reference on the sample.

| Ni(001) curve | cr1 | cr2 | cr3 | a1 | a2 | a3 | zero level |
|---|---|---|---|---|---|---|---|
| $\mathbf{S_{IN}\text{-}45°_{OUT}}$ | 0.8 | 1.94 | 2.94 | 1.6 | 0.6 | 2.4 | -0.51 |

**Table 8-I** Values of the tensor elements and the corrected zero signal level, for the fit in Fig. 8.2.

Initially, the angle between the x-direction of the crystal lattice of the sample and the plane of incidence was -17.7º ($\varphi$ = 17.7). For an incoming beam polarized along the S-direction, the MSHG asymmetry can be equal to zero when, at a certain angle of the sample, the MSHG intensities proportional to the $\chi_{xyy}^{odd}$ and $\chi_{yyy}^{odd}$ components cancel each other. This angle of cancellation can be influenced by the presence of additional symmetries in the signal. In the fit, the zero signal level had to be corrected by subtracting 0.51 which can be partially explained by the presence of quadrupole

contributions to the magnetization and the additional 2-fold anisotropy induced by the tilt angle between the sample surface and the optical plane of incidence.

It is clear that the fit in Fig. 8.2, although it reproduces the essential features of the Ni(001) 4-fold surface, is not perfect. Manipulating the sample inside the UHV presents difficulties that are in turn reflected in the observed results. In order to avoid these experimental limitations, we have oxidized the clean and single crystalline Ni surface in the UHV chamber. Oxidation of the Ni(001) surface was performed *in situ* at room temperature until the oxide formation was complete (more that 10 000 L). Subsequently the MSHG anisotropy measurements were done *in air*, on a standard optical table.

Fig. 8.3 shows the MSHG intensity measured as a function of the azimuthal rotation for both magnetization directions and for P-P and S-P polarizer-analyzer configurations. The data show a strong magnetic contrast and an unexpected 3-fold symmetry. Between P-P and S-P the 3-fold stars exhibit opposite phase, therefore the maxima in intensity are not due to artifacts such as scratches on the surface. Another difference between these two configurations is the opposite magnetic contrast.

As the Ni(001) surface is isotropic, as far as the crystallographic contribution to the SHG is concerned, this 3-fold signal can only be induced by the presence of NiO. Assuming NiO(111) growth on the Ni(001) single crystal leads to an additional anisotropic nonlinear susceptibility component (see Eq. 8.6). All the above mentioned features are reproduced by the fits (solid curves in Fig. 8.3) corresponding to the presence of tensor elements from a 3-fold crystallographic for NiO(111) and a 4-fold magnetic symmetry group for Ni(001).

It is important to note that all four fits were calculated simultaneously with a single formula, which was again obtained according to the method described in Chapter three. Furthermore, the parameters of the 4-fold magnetic tensor in Table 8-II were constrained to those of the clean Ni(001) surface in Table 8-I and are therefore identical to them.

The details are as follows: $\psi$ is the angle between the polarizer and the S-direction of polarization, it is along P for the blue and green curves ($\psi = \pi/2$ rad) and along S for the black and red curves ($\psi = 0$ rad). The noise level of the fit is set at 200 which is the minimum for the curves. The initial angle between the x-direction of the crystal lattice of the sample and the plane of incidence is 80º ($\varphi = 80$). The 3-fold crystallographic $\chi^{\mathrm{cr}}$ tensor is:

$$\chi^{cryst}_{3-fold} = \begin{pmatrix} c1 & -c1 & 0 & 0 & c2 & 0 \\ 0 & 0 & 0 & c2 & 0 & -c1 \\ c2 & c2 & c3 & 0 & 0 & 0 \end{pmatrix} \tag{8.6}$$

The entire fitting formula was multiplied by the amplitude constant “amp” which gives a correspondence between the units of the simulation and those of the experiment. It is 425 for both P-P curves and 38 for the S-P curves. The difference could partially be explained by the Fresnel coefficients which we did not take into account in our simulation. The 4-fold magnetic tensor components are again given by Eq. 8.5 with the same conventions.

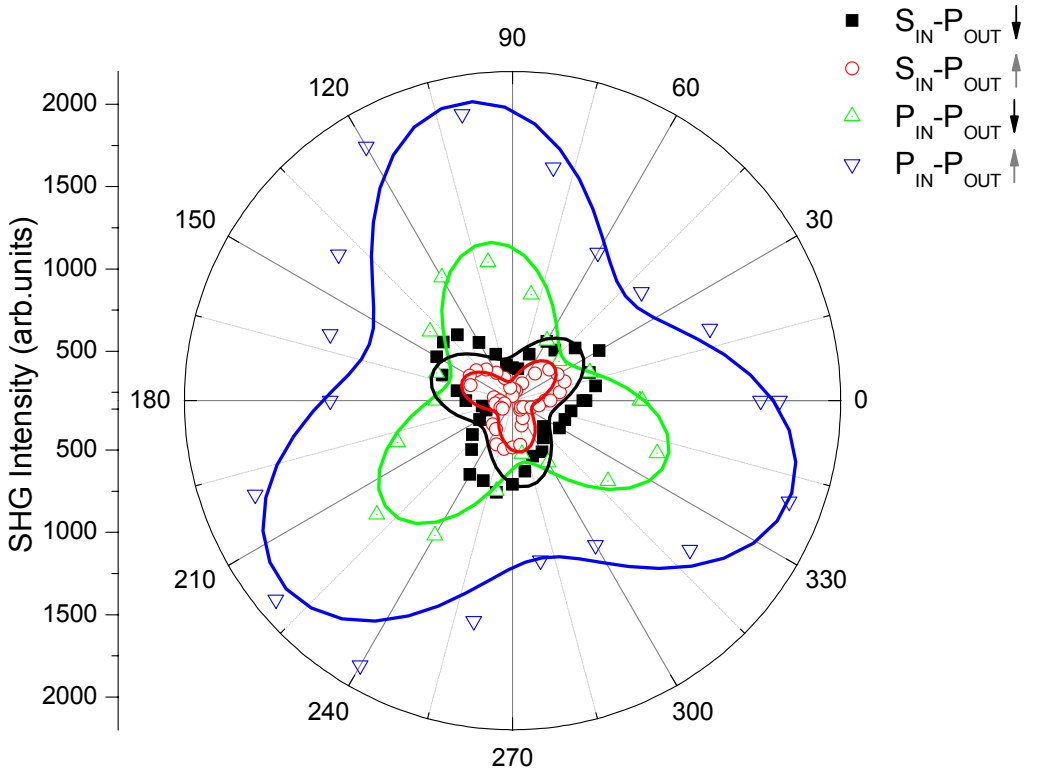


**Fig. 8.3** MSHG intensity as function of the azimuthal rotation of the sample for polarizer-analyzer configurations P-P and S-P for both directions of the magnetic field.

In Table 8-II, it can be seen that the absolute values of the magnetic tensor elements a1, a2 and a3 are the same for all four fits, while their sign changes according to the changes of magnetic field. Furthermore, all the crystallographic tensor components and the experimental constants are the same.

| Curve | cr1 | cr2 | cr3 | a1 | a2 | a3 | c1 | c2 | c3 | amp |
|---|---|---|---|---|---|---|---|---|---|---|
| **$S_{IN}$-$P_{OUT}$ (down)** | 0.8 | 1.94 | 2.94 | **–1.6** | **–0.6** | **–2.4** | 0.8 | 1.94 | 2.94 | 425 |
| **$S_{IN}$-$P_{OUT}$ (up)** | 0.8 | 1.94 | 2.94 | **+1.6** | **+0.6** | **+2.4** | 0.8 | 1.94 | 2.94 | 425 |
| **$P_{IN}$-$P_{OUT}$ (down)** | 0.8 | 1.94 | 2.94 | **–1.6** | **–0.6** | **–2.4** | 0.8 | 1.94 | 2.94 | 38 |
| **$P_{IN}$-$P_{OUT}$ (up)** | 0.8 | 1.94 | 2.94 | **+1.6** | **+0.6** | **+2.4** | 0.8 | 1.94 | 2.94 | 38 |

**Table 8-II** Values of the tensor elements and the signal amplitude, noise and phase constants for all the fits in Fig. 8.3.

## 8.4. Conclusion

We have seen that the clean surface of Ni(001) single crystal has a 4-fold symmetry as revealed by LEED and the MSHG asymmetry. On the other hand, upon oxidation, we have observed a 3-fold MSHG pattern for different polarizer-analyzer combinations. These data can be very well fitted with calculations of the MSHG intensity including a 3-fold symmetry tensor. Using different experimental techniques, NiO(111) growing on Ni(001) has already been reported in the literature.[16-18] Therefore, we can conclude that we have observed NiO(111) growth on Ni(001) surface by means of MSHG for the first time.

The consequences of such an AFM/FM interface can be dramatic for exchange bias. Indeed, while a NiO(001)/Ni(001) is a compensated interface, NiO(111)/Ni(001) is uncompensated and this difference in interface spin order will very likely result in a different exchange interaction.

These intriguing preliminary results are part of an ongoing experimental project, which at the moment has been discontinued due to technical problems with the equipment. Particularly, the precise conditions for this growth mode, such as temperature dependence and the amount of oxygen exposure remain to be elucidated.

## References:

[1] J. Nogués, I. K. Schuller, J. Magn. Magn. Mater. **192**, 203 (1999).

[2] Y. Hamakawa, H. Hoshiya,T. Kawabe, Y. Suzuki, R. Arai, K. Nakamoto, M. Fuyama, Y. Sugita, IEEE Transactions on Magnetics, **32**, 149 (1996).

[3] J. van Lierop, L.H. Lewis, K.E. Williams and R.J. Gambino, J. Appl. Phys. **91**, 7233 (2002).

[4] M. Fraune, U. Rüdiger, G. Güntherodt, S. Cardoso and P. Freitas, Appl. Phys. Lett. **77**, 3815 (2000).

[5] R. A. Lukaszew, M. Mitra, Z. Zhang and M. Yeadon, Eur. Phys. J. B **45**, 181 (2005).

[6] A.E.Berkowitz, J.H.Greiner, *J. Appl. Phys.* **35**, 925 (1964).

[7] M. Finazzi, M. Portalupi, A. Brambilla, L. Duò, G. Ghiringhelli, F. Parmigiani, M. Zacchigna, M. Zangrando, and F. Ciccacci, Phys. Rev. B **69**, 014410 (2004).

[8] C. H. Shang, G. P. Berera, and J. S. Moodera, Appl. Phys. Lett. **72**, 605 (1998).

[9] A.E. Berkowitz, K. Takano, J. Magn. Magn. Mater. **200**, 552 (1999).

[10] H.-J. Freundt, H. Kuhlenbeck and V. Staemmler, Rep. Prog. Phys. **59**, 283 (1996).

[11] Dalmai-Imelik G, Bertolini J C and Rousseau J Surf. Sci. **63**, 67 (1977).

[12] K. Wandelt, Surf. Sci. Rep. **2**, 1 (1982).

[13] P.H. Holloway J. Vacuum Sci. Technol. **18**, 653 (1981).

[14] K. J. Veenstra, *Phase Sensitive Nonlinear Magneto-Optical Spectroscopy*, Ph.D. thesis, Radboud University Nijmegen, the Netherlands (2000).

[15] J.F. van der Veen, R.G. Smeenk, R.M. Tromp and F.W. Saris Surface Sci. **79**, 212. (1979).

[16] P.H. Holloway and J.B. Hudson Surface Sci. **43**, 123 (1974).

[17] P.H. Holloway and J.B. Hudson Surface Sci. **43**, 141 (1974).

[18] D.F. Mitchell, P.B. Sewell and M. Cohen Surface Sci. **61**, 355 (1976).

[19] W. -D. Wang, N. J. Wu and P. A. Thiel, J. Chem. Phys. **92** (3), 2025 (1989).

[20] O. L. Warren and P. A. Thiel, J. Chem. Phys. **100** (1), 659 (1993).

[21] E. Kopatzki and R. J. Behm, Phys. Rev. Lett. **74**, 1399 (1995).

[22] M. Fiebig, D. Fröhlich, Th. Lottermoser, V.V. Pavlov, R. V. Pisarev and H.-J. Weber, Phys. Rev. Lett. **87**, 137201 (2001).

[23] M. Fiebig, Th. Lottermoser V.V. Pavlov and R. V. Pisarev, J.Appl. Phys. **93**, 6900 (2003).

# Summary

Exchange bias is an intellectually challenging problem with numerous present day and likely future applications, which for half a century has remained without a complete theoretical explanation despite the intense research interest that it has attracted. This thesis presents the interface specific technique of Magnetization-induced Second Harmonic Generation (MSHG) as a very promising alternative and/or complementary approach to the problem.

Exchange bias appears when a ferromagnet(FM)/antiferromagnet(AFM) system is cooled from above the Néel temperature but below the Curie temperature, in the presence of an external magnetic field. Its main characteristics are: a shift of the hysteresis loop away from the zero field position and an increase of the coercivity. The precise temperature at which the effect appears is called the blocking temperature ($T_B$).

Since Meiklejohn and Bean's first attempts at formulating a theoretical solution for the exchange bias problem, several other models have been proposed. Among them, is a recent and influential theory based on the idea that an incomplete domain wall (IDW) forms in the ferromagnet. It is important to notice that all theoretical efforts for understanding exchange bias are required, at one stage or another, to make a crucial assumption about the AFM/FM interface. This necessity highlights the need for experimental data resulting from direct probes of the interface.

The vast majority of the existing experimental investigations rely on measurements of the hysteresis loop shift – a quantity that has become almost synonymous with exchange bias. Yet fifty years of hysteresis loop shift measurements have failed to solve the problem. It is therefore necessary to devise new alternative ways of probing the unidirectional anisotropy characteristic of the exchange bias.

The nonlinear optical technique of Magnetization-induced Second Harmonic Generation (MSHG) is an interface-sensitive tool which has the potential to make a valuable contribution to the study of magnetic phenomena at buried interfaces, such as exchange bias. This is particular true when MSHG is used in combination with the linear Magneto-Optical Kerr Effect (MOKE). Indeed, while MSHG is surface/interface and bulk sensitive, MOKE is only bulk-sensitive and therefore, by comparing the two, we can isolate the purely interface-related information.

In order to demonstrate the usefulness of the MSHG technique as a valuable approach to the problem of exchange bias, we describe two alternatives to hysteresis loop shift measurements, namely the MSHG asymmetry and the nonlinear Kerr rotation. We prove that those quantities are able to provide information on the interface magnetic order in situations where the hysteresis loop shift cannot: such as when a CoO layer is

separated from an Fe one by a 3.5 nm thick Cu spacer. Additionally, through the MSHG dependence on the rotation of the fundamental polarization angle, we establish that for large exchange bias values the detected signal originates dominantly from the antiferromagnetic pinned uncompensated spins. This result confirms that the MSHG technique is not only interface-sensitive in general, but it also has the potential for direct observation of the specific antiferromagnetic / ferromagnetic interface. Furthermore, our interface-specific results are consistent with the idea of interface-pinning – the basis of Meiklejohn and Bean's intuitive model for exchange bias.

Moreover, we demonstrate the capability of MSHG to investigate structural and magnetic interface properties. After describing the detection of monolayer roughness at the buried exchange biased Mn/Co interface, we discuss the information that we can extract from our measurements concerning the behavior of the net magnetic moment. Within the IDW-FM model, one expects a difference in magnetization reversal between the AFM/FM interface and the FM bulk, similar to what is observed for a clean Co surface and the Co bulk. However, from our MSHG and MOKE investigations, we establish that the magnetization reversals at the Mn/Co interface and in the Co bulk are collinear.

This experimental observation is therefore quite important in the context of exchange bias since it excludes the possibility of an incomplete domain wall forming in the ferromagnetic material.

Finally, we present preliminary results indicating a rather curious antiferromagnetic / ferromagnetic interface. Our MSHG data reveal the growth of (111) oriented NiO on top of a Ni(001) single crystal. The consequences of such an AFM/FM interface can be dramatic for exchange bias. Indeed, while a NiO(001)/Ni(001) is a compensated interface (i.e. has zero net magnetic moment), NiO(111)/Ni(001) is uncompensated and thus the interface spin order is very different. Further studies elucidating the precise conditions for this growth mode are necessary.

Naturally our investigations were limited in time by the duration of the Ph.D. scholarship. Thus several very interesting questions remain to be addressed and will probably become the topic of future work. Among them, we consider as particularly promising the application of MSHG microscopy to the eventual probing of antiferromagnetic domains and crystallinity at the AFM/FM interface. Additionally, we have discussed the possibility that AFM interface roughness could play a regulatory role between the processes responsible for the loop shift and for the coercivity increase; micromagnetic simulations are likely to shed light on this hypothesis.

# Samenvatting

Exchange bias, oftewel het bestaan van een voorkeursrichting in een ferromagnetisch materiaal onder invloed van de wisselwerking met een anti-ferromagneet, is een wetenschappelijk zeer uitdagend probleem met vele mogelijke toepassingen. Ondanks deze grote wetenschappelijke interesse is er tot op de dag van vandaag geen volledige theoretische verklaring. In dit proefschrift wordt magnetisatie geïnduceerde tweede harmonische generatie, (Magnetization induced Second Harmonic Generation – MSHG) voorgesteld als een veelbelovende en complementaire techniek om exchange bias te bestuderen.

Exchange bias komt voor als een systeem, bestaand uit een ferromagnetisch (FM) laag boven op een antiferromagnetische (AFM) laag, vanaf een temperatuur die beneden de Curie- maar boven de Néel temperatuur ligt, gekoeld wordt tot onder de Néel temperatuur in aanwezigheid van een extern magnetisch veld. De belangrijkste gevolgen van exchange bias zijn een verschuiving van de magnetische hysteresus lus weg van de nulpositie en een verhoging van de coerciviteit. De exacte temperatuur waarbij dit gebeurd wordt de 'blocking temperature' $T_B$ genoemd.

Sinds de eerste pogingen van Meiklejohn en Bean om een theoretisch model voor dit fenomeen te op te stellen zijn er nog enkele andere interessante voorstellen voor een verklaring geweest. Onder andere een recente theorie die gebaseerd is op het idee dat een onvolledige domeinwand (IDW) gevormd wordt in de ferromagneet. Hierbij is het belangrijk op te merken dat elke theorie over de oorzaak van exchange bias ergens veronderstellingen maakt over het grensvlak tussen de ferromagneet en de antiferromagneet. Er is daarom een grote behoefte aan experimentele data die rechtstreeks dit grensvlak betreft.

De grote meerderheid van de bestaande experimentele data bestaat uit metingen van de verschuiving van de hysteresus lus, deze verschuiving is ondertussen bijna synoniem geworden met exchange bias. Toch is er na 50 jaar van metingen aan hysteres verschuivingen nog steeds geen goede verklaring gevonden. Het is daarom noodzakelijk om alternatieve manieren te ontwikkelen om deze 'unidirectional anisotropy' karakteristieken te bestuderen.

De niet lineaire optische techniek MSHG is een grensvlak gevoelige methode met het potentieel om een waardevolle bijdrage te leveren aan de studie van magnetische fenomenen rond een grensvlak. Zeker wanneer het gecombineerd wordt met het lineaire magneto optisch Kerr effect (MOKE). MSHG is speciaal gevoelig voor oppervlakken en grensvlakken en in mindere mate voor bulk eigenschappen terwijl MOKE voornamelijk

gevoelig is voor de bulk. We kunnen dus door de twee te vergelijken een beter inzicht krijgen in het grensvlak.

Om het nut van MSHG aan te duiden als techniek om exchange bias mee te bestuderen, presenteren we twee alternatieven voor het meten van de hysteresus lus verschuiving, namelijk de MSHG asymmetrie en de niet lineaire Kerr rotatie. We laten zien dat deze twee grootheden informatie geven over de magnetische orde aan het grensvlak in situaties waar de hysteresus lus verschuiving dit niet kan. Bijvoorbeeld als een antiferromagnetische CoO laag door een Cu laag van 3.5 nm gescheiden is van een Fe laag. Doordat MSHG afhankelijk is van de rotatie van de fundamentele polarisatiehoek, hebben we vastgesteld dat bij grote waarden van de exchange bias deze voornamelijk te wijten is aan de antiferromagnetische ongecompenseerde bevroren spins. Dit resultaat bevestigt dat MSHG niet enkel een algemene grensvlak gevoelige techniek is maar dat ook het specifieke ferromagnetische/antiferromagnetische grensvlak er mee bestudeerd kan worden. Ook zijn onze grensvlak specifieke resultaten consistent met het idee dat het grensvlak 'bevroren' wordt, wat aan de basis ligt van het intuitieve model van Meiklejohn en Bean voor exchange bias.

Met MSHG kunnen we ook de structurele en magnetische eigenschappen van grensvlakken bestuderen. Nadat we de atomaire ruwheid van het "exchange biased" Mn/Co grensvlak hebben beschreven, bespreken we de informatie die we kunnen halen uit metingen aan het gedrag van het netto magnetisch moment. Binnen het IDW-FM model zouden we een verschil verwachten in magnetisatie omkering tussen het AFM/FM grensvlak en de FM bulk, identiek aan wat we zien bij een zuiver Co oppervlak en de Co bulk. Uit de MSHG en MOKE metingen stellen we echter vast dat de magnetisatie omkeringen aan het Mn/Co grensvlak en de Co bulk colineair zijn.

Deze experimentele waarneming is zeer belangrijk in de context van exchange bias, aangezien hierdoor de mogelijkheid dat er onvolledige domein wanden gevormd worden in de ferromagneet uitgesloten kan worden.

In het laatste hoofdstuk geven we tenslotte de voorlopige resultaten van MSHG metingen die wijzen op een zeer interessant grensvlak, nl. een (111) georiënteerd antiferromagnetisch NiO op een ferromagnetisch Ni (001) kristal. NiO (001) op Ni (001) is een gecompenseerd grensvlak dat wil zeggen, het netto magnetisch moment van al de AFM spins is nul. Echter Ni (111) op NiO (001) is een ongecompenseerd grensvlak. De spinordening op het grensvlak is dus heel anders, wat een zeer groot effect kan hebben op de exchange bias. Verdere studies over de precieze voorwaarden voor deze groeivorm zijn echter nog nodig.

Door de eindigheid van een promotie onderzoek zijn er noodzakelijkerwijs nog enkele zeer interessante vragen blijven liggen voor toekomstig onderzoek. Bijvoorbeeld het bestuderen van antiferromagnetische domeinen en de kristalliniteit van het AFM/FM grensvlak met MSHG microscopie. Ook hebben we de mogelijkheid besproken dat de ruwheid van het AFM oppervlak aan het grensvlak een controlerende rol zou kunnen spelen tussen de processen die zorgen voor de hysterese lus verschuiving en de stijging van de coerciviteit. Micromagnetische simulaties zouden waarschijnlijk licht kunnen werpen op deze hypothese.

# Appendix A
# Summary for non-physicists

## A.1. Exchange bias

Conspiracies typically involve a small number of secretive people, who by working together are able to influence a much larger society. It is then often of great importance to be able to reveal and expose the conspirators, especially if they happen to be foreigners.

A very similar situation occurs in magnetism. It is possible to visualize magnetic order in materials in terms of a collection of small magnetic arrows associated with each individual atom. Each arrow resembles a tiny compass needle with a north and south poles that is called a *spin*. We can then distinguish two main types of magnetic order, just as we could speak of two different human societies. In one of them, called *ferromagnetism*, all the magnetic arrows (or spins) point in the same direction and as a result there are observable magnetic properties (see left panel in Fig A.1). This could be a society of very easy going and social people that work together towards a common goal – magnetism. In the other one, called *antiferromagnetism*, all the spins are directed opposite to their neighbors and consequently, in average, no magnetic properties can be observed (see right panel in Fig. A.1). That would be a society of individuals with their minds set to disagree with everybody on everything just to show how different they are; as it happens, such a society does not accomplish anything.

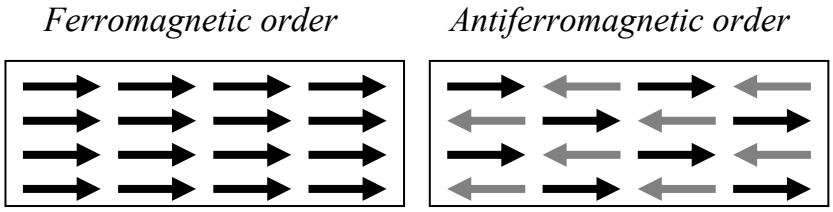


**Fig. A.1** The two main types of magnetic order. The arrows represent the direction of the spins of individual atoms in the materials.

Interestingly enough however, when we put a ferromagnetic material in contact with an antiferromagnetic one, under certain temperature conditions, we can observe that the magnetic properties of the ferromagnet are very strongly modified. In fact, the ferromagnet appears to experience a small magnetic field originating in the antiferromagnet. This phenomenon, known as *exchange bias*, was discovered 50 years ago. Since then, it has found many useful technological applications and nowadays it is at work in almost all computer hard drives in the world.

But how could that be? How is it possible that these antiferromagnetic spins, which are usually too busy arguing with their neighbors to do anything else at all, actually manage to have such an influence over the ferromagnetic ones?

One possible explanation is that a very interesting phenomenon occurs at the interface, which can be envisioned as the border between the two societies. Due to the influence of the ferromagnetic spins, a small number of spins belonging to the antiferromagnet no longer care about directing themselves in an opposite direction to their neighbors but instead align collectively just as if they were ferromagnetic. As they do so, they produce a magnetic field that influences the adjacent ferromagnetic material. The particular direction towards which those few antiferromagnetic spins point out collectively is called the direction of *exchange bias*. Returning to our human society model, it would appear that the disagreeable antiferromagnetic individuals decided to put their differences aside for a common goal – the eventual domination over their neighboring ferromagnetic society.

For most of the past 50 years, this explanation has been just another "conspiracy theory". Studying magnetic interfaces is a challenging task; mainly since they are buried bellow one or even several layers of materials. Thus, without the opportunity to observe and expose the participants in the "antiferromagnetic plot", physicists could only speculate, and understanding of the exchange bias phenomenon remained elusive.

However, recent developments in experimental techniques have changed this situation and for the first time observations of the antiferromagnetic spins responsible for exchange bias were reported. Nevertheless, many questions remain to be answered. For instance, in terms of the human society model, we still don't know exactly how the antiferromagnetic conspirators are organized, do they have collaborators on the other side, etc.

In order to help towards understanding the exchange bias effect (read "completely exposing the conspiracy"), we have made use of an experimental technique that is particularly sensitive to interface magnetism, namely: *Magnetization-induced Second Harmonic Generation*. Behind this arcane appellation there is some really fascinating physics which we will discuss in the next paragraph.

## A.2. Magnetization-induced Second Harmonic Generation

Imagine that you enter a room and that the only light in this room is red. Naturally, as you look around, you would expect all the objects you can see to appear red since there is no other light that they can reflect. However, what might happen in reality is that some of the objects surrounding you could be… blue! This is no optical illusion, in the sense that it is not a trick that your eyes are playing on you; the only light source in the room is red and yet you are seeing genuine blue light. How could *that* be possible?

This phenomenon is called *Second Harmonic Generation* (SHG) and in 1981, the Dutch physicist Nicolaas Bloembergen received the Nobel Prize for developing its theoretical framework.

Second Harmonic Generation is a particular case of the effect called *Sum Frequency Generation* (SFG) in which two or more light waves are mixing. We can represent this by the following equation:

$$I(\omega_1 + \omega_2) \propto I(\omega_1) \cdot I(\omega_2) \tag{A.1}$$

where ω is the wave frequency and *I* is the light intensity.

In the case of SHG, two coherent light waves of the same frequency act together in generating a third light wave that is of the double frequency.

$$I(2\omega) \propto \left(I(\omega)\right)^2 \tag{A.2}$$

Hence, if we chose our initial frequency to be 3.7474 x $10^{14}$ Hz, which corresponds actually to near infra-red, the generated light wave will have a frequency of $2 \cdot 3.7474 \cdot 10^{14} = 7.4948 \cdot 10^{14}$ Hz, which is indeed blue.

Although the observation of blue objects in a red light room is theoretically possible, its experimental realization requires several important conditions. For instance, the red light should be of high intensity, preferably generated by a laser. Lasers have several important characteristics that play a role in SHG: they provide well defined monochromatic light (this is important for Eq. A.2), coherent waves and high intensities.

In the red light room experiment we considered the possibility that some of the objects in the room appear blue. In truth, it could very well be that all the objects do so! This is so, since second harmonic can be generated from every material that has finite dimensions. More specifically, it appears because of symmetry breaking such as at surfaces and interfaces. However, not all materials generate the same amount of second harmonic light and therefore not all the blue light will be really visible. As a matter of fact the observer should have very sensitive eyes since, although conversion factors from $\omega$ to $2\omega$ of up to 80% have been claimed for transmission in some specific crystals, a typical value for this factor after reflection is only $10^{-13}$ %.

Next, imagine that we place an electromagnet with a soft magnetic core in the red light room and we start switching the direction of the magnetization of this device with an AC current every second. If we now look at the blue light that the magnetic core is generating, we will find out that the amount of SHG is changing every second, i.e. the magnet is "blinking".

Magnetism participates in the generation of second harmonic light because it is related to the breaking of time-reversal symmetry. We can consider the spins of atoms in a magnetic material to be the result of small electric current loops around the atoms. Switching the magnetization in the opposite direction is then equivalent to reversing the direction of time so that the current in the electric loops starts flowing in the opposite way.

In order to observe the "blinking" mentioned above, both structural symmetry breaking and time reversal are necessary. In other words, in centrosymmetric materials, *Magnetization-induced Second Harmonic Generation* (MSHG) is produced mainly by the surface of the magnet and therefore it is a useful tool for investigating surface magnetism. Furthermore, if the magnet is coated with a thin film of nonmagnetic material (for instance gold with a thickness smaller than the light penetration depth) MSHG will again occur, this time from the buried magnet/gold interface. It is precisely this physical property – the generation of magnetization-induced second harmonic light from interfaces – that we used in order to help "uncover" the above mentioned "conspiracy."

## A.3. Outcome of this thesis

The "conspiracy" is real! Though we are not the first to claim this experimentally, we believe that our results constitute an important step towards publicly exposing the "plot".

Indeed, probably the foremost conclusion of our work is that MSHG can be successively applied to the study of the exchange bias effect. Although we show that this technique can be delicate to handle, we also demonstrate that it is capable of *directly observing* the antiferromagnetic spins responsible for exchange bias. Quite literally, their presence affects the levels of intensity of the generated blue light, though, in order to "see" them, we make use of optical detectors which are significantly more sensitive than the human eyes.

MSHG is a very new technology with regards to the study of exchange bias, and as Nicolaas Bloembergen said "whenever you use a new technology, new things are ***bound*** to happen"! In this thesis, we thus present two alternatives to the classical ways of studying exchange bias which are able to provide new information on the antiferromagnetic spins when a nonmagnetic spacer is inserted between the antiferromagnet and the ferromagnet. In terms of the human society model, we can say that upon arrival of an international peace force at the border, the antiferromagnetic conspirators keep noticing their ferromagnetic neighbors and therefore again get organized in view of a possible domination scenario, though effectively the peace keepers prevent them from influencing their neighbors. Furthermore, we demonstrate that in the systems that we studied there is no formation of a ferromagnetic domain wall (no ferromagnetic collaborators participate in the antiferromagnetic plot). Finally, we studied the oxidation of a single crystal of nickel (Ni), which is a ferromagnetic material, since the thus obtained nickel oxide (NiO) is antiferromagnetic. Once again, we directed our interest towards the interface. To our surprise, we observed that while at the surface of the crystal the Ni atoms were disposed in a network of squares, those of NiO organized in equilateral triangles! For the time being, the conditions under which nature prefers this counter intuitive assembly to that of a plain superposition of squares on top of other squares remain to be elucidated. Nevertheless, we demonstrate that the neighborhood relations between an antiferromagnetic and ferromagnetic society are just as simple as those that can explain a perfect fitting of an equilateral triangle into a square.

In conclusion, it is our belief that this thesis has only opened the door towards the study of exchange bias with magnetization-induced second harmonic generation and that on this research path many more new things are bound to happen.

# Appendix B
# Résumé pour les non spécialistes

## B.1. Exchange bias

Généralement, dans une conspiration, un petit nombre de personnes travaillent ensemble et en secret pour arriver à influencer une société entière. Il est alors souvent d'une grande importance d'être capable d'identifier et faire connaître les conspirateurs, surtout si ces derniers s'avèrent des étrangers à la dite société. On peut observer une situation très similaire en magnétisme.

Il est possible de visualiser l'ordre magnétique dans les matériaux sous forme d'un ensemble de fléchettes magnétiques, associées à chaque atome. Chacune de ces fléchettes ressemble alors à une minuscule aiguille de boussole, dotée de ses pôles nord et sud, que l'on appelle un *spin*. Dès lors, nous pouvons distinguer deux types principaux d'ordre magnétique, tout comme nous pourrions parler de deux sociétés humaines différentes. Dans le premier, appelé *ferromagnétisme*, toutes les fléchettes magnétique (ou spins) pointent dans la même direction et il en résulte des propriétés magnétiques que l'on peut observer à grande échelle (Fig. B.1 gauche). Ceci serait l'équivalent d'une société de gens très conviviaux qui travaillent ensemble dans un but commun – produire du magnétisme. Dans le second type d'ordre magnétique, appelé *antiferromagnétisme*, tous les spins se positionnent de telle manière que la direction le long de laquelle ils pointent soit l'opposée de celle de leurs voisins. Par conséquence, en moyenne on ne peut observer aucune propriété magnétique à grande échelle (Fig. B.1 droite). Une telle société serait composée d'individus décidés à être en désaccord avec tout un chacun et sur n'importe quel sujet, juste pour montrer à quel point ils sont différents des autres. Naturellement, une telle société ne peut rien accomplir.

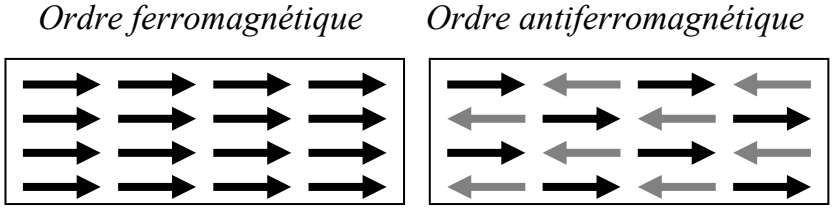


**Fig. B.1** Le deux types principaux d'ordre magnétique. Les flèches représentent la direction des spins de chaque atome dans les matériaux.

Et pourtant… lorsque l'on met en contact un matériau ferromagnétique avec un antiferromagnétique, sous certaines conditions de température, on peut observer que les propriétés magnétiques du matériau ferromagnétique sont fortement modifiées. En fait, le matériau ferromagnétique semble être sous l'influence d'un petit champ magnétique situé

dans l'antiferromagnétique. Ce phénomène, appelé *exchange bias*, a été découvert il y a 50 ans et a trouvé depuis de nombreuses applications technologiques. Par exemple, il est à l'œuvre dans presque tous les disques durs des ordinateurs dans le monde.

Mais comment est-ce possible ? Comment se peut-il que ces spins antiferromagnétiques, qui d'ordinaire sont trop occupés à se disputer avec leurs voisins pour faire quoi que ce soit d'autre, puissent avoir une telle influence sur les spins ferromagnétiques ?

Une explication que l'on pourrait envisager met en cause un phénomène très intéressant se produisant à l'interface, laquelle peut être considérée comme la frontière entre les deux sociétés. Sous l'influence des spins ferromagnétiques, quelques uns des spins appartenant à l'ordre antiferromagnétique cessent de se diriger le long de directions opposées à leurs voisins et, au lieu de cela, ils s'alignent collectivement comme s'ils étaient des ferromagnétiques. En faisant cela, ils produisent un champ magnétique capable d'influencer tous les spins du matériau ferromagnétique adjacent. La direction d'alignement collectif de ces quelques spins antiferromagnétiques s'appelle la direction d'exchange bias. Si l'on revenait à notre image de sociétés humaines, on pourrait dire que certains des personnages antiferromagnétiques et querelleurs ont décidé de mettre leurs différents de côté au nom d'un but commun – la domination finale de la société ferromagnétique voisine.

Pendant les 50 dernières années, cette explication n'était qu'une « théorie de conspiration ». L'étude des interfaces magnétiques est une tache difficile car elles sont enfouies sous une ou même plusieurs couches de matériaux. Ainsi, sans la possibilité de vraiment observer et donc de faire connaître les participants au « complot antiferromagnétique », les physiciens en étaient réduits aux spéculations : la compréhension du phénomène d'exchange bias demeurait élusive.

Cependant, les développements récents des techniques expérimentales ont modifié cette situation et pour la première fois, des observations de spins antiferromagnétiques responsables de l'exchange bias ont été rapportées dans la littérature scientifique. Néanmoins, de nombreuses questions restent sans réponse. Par exemple, pour reprendre l'image des sociétés humaines, nous ne savons toujours pas comment les conspirateurs antiferromagnétiques sont organisés, s'ils ont des collaborateurs du côté ferromagnétique, etc.

Afin de contribuer à la compréhension de l'effet d'exchange bias, (lisez « exposer complètement la conspiration »), nous avons employé une technique expérimentale particulièrement sensible aux interfaces magnétiques, c'est-à-dire : la Génération d'Harmonique Seconde induite par Magnétisme. Derrière cette appellation sibylline on peut trouver un effet physique fascinant que nous allons présenter ci après.

## B.2. Génération d'Harmonique Seconde induite par Magnétisme

Imaginez-vous être dans une pièce éclairée uniquement par de la lumière rouge. Ce pourrait être par exemple un laboratoire de photographie. Normalement, tous les objets que vous voyez devraient alors paraître rouges, puisque c'est la seule couleur qu'ils peuvent refléter. Pourtant, il se pourrait qu'en réalité certains de ces objets soient… bleus ! Il ne s'agit pas ici d'une illusion d'optique, en ce sens que la couleur bleue n'est

pas due à la manière dont vos yeux perçoivent les couleurs. Non, l'unique source de lumière dans la pièce est rouge et pourtant une partie de la lumière qui vous parvient est authentiquement bleue. Comment est-ce possible ? D'où provient cette lumière bleue?

Ce phénomène est appelé la *Génération d'Harmonique Seconde* (GHS) et en 1981, le physicien hollandais Nicolaas Bloembergen qui en développa le cadre théorique reçut le Prix Nobel.

La Génération d'Harmonique Seconde est un cas particulier de l'effet de Génération de Somme de Fréquences dans lequel deux ou plusieurs ondes lumineuses se mélangent. On peut exprimer cela par l'équation suivante :

$$I(\omega_1 + \omega_2) \propto I(\omega_1) \cdot I(\omega_2) \tag{B.1}$$

où ω représente la fréquence de l'onde et *I* indique l'intensité lumineuse.

Dans le cas de la GHS, deux ondes lumineuses de fréquence identiques composent ensemble une troisième onde lumineuse de fréquence double.

$$I(2\omega) \propto \left(I(\omega)\right)^2 \tag{B.2}$$

Donc, si l'on choisit une onde de fréquence initiale 3,7474 x $10^{14}$ Hz, ce qui correspond en vérité à l'infrarouge, l'onde lumineuse générée aura une fréquence double : $2 \cdot 3{,}7474 \cdot 10^{14} = 7{,}4948 \cdot 10^{14}$ Hz , ce qui est effectivement la couleur bleu.

Ainsi, bien que l'observation d'objets bleus à l'intérieur d'une pièce éclairée par de la lumière rouge soit théoriquement possible, dans la pratique, plusieurs conditions supplémentaires sont nécessaires. Par exemple, la lumière rouge devrait être très intense, préférablement produite par un laser. Les lasers ont un certain nombre de caractéristiques importantes qui jouent un rôle dans la GHS : ils fournissent une lumière monochromatique bien définie (ceci est important pour l'équation B.2), des ondes lumineuses cohérentes et de fortes intensités.

Nous avons jusqu'ici mentionné la possibilité que *certains* objets puissent paraître bleus. Mais en vérité il se pourrait bien que *tous* les objets dans la pièce éclairée en rouge le soient ! En effet, l'harmonique seconde peut être générée par chaque matériau aux dimensions finies. Plus précisément, elle apparaît à cause des brisures de symétrie telles les surfaces ou interfaces. Cependant, tous les matériaux ne génèrent pas la même quantité d'harmonique seconde et donc la lumière bleue qu'ils émettent n'est pas toujours bien visible. En fait, l'observateur devrait avoir des yeux très sensibles car, bien que des facteurs de conversion de $\omega$ à $2\omega$ de 80% aient été observés dans certains cristaux spéciaux, les valeurs types après réflexion sont de l'ordre de $10^{-13}$ %.

Allons plus loin ! Imaginons maintenant que nous placions un électroaimant au noyau de fer doux dans la pièce éclairée en rouge et que nous branchions cet appareil sur un courant électrique alternatif qui change de polarité chaque seconde. Cela implique que l'aimantation aussi change de direction chaque seconde. Si maintenant nous regardons la lumière bleue générée par le noyau de l'électroaimant, nous verrons que la quantité de GHS change chaque seconde, autrement dit : l'électroaimant « clignote ».

Le magnétisme participe à la génération d'harmonique seconde parce qu'il est lié à la brisure de la symétrie du renversement du temps. On peut considérer que les spins

dans un matériau magnétique (dont nous avons parlé plus haut) sont le résultat de minuscules boucles de courant électrique autour des atomes. Renverser la direction de l'aimantation est ainsi équivalant à un renversement du sens de l'écoulement du temps ce qui causerait un renversement du sens de l'écoulement du courant dans les boucles électriques.

Afin d'observer le « clignotement » mentionné plus haut, il faut à la fois une brisure de symétrie spatiale et temporelle. En d'autres termes, dans les matériaux centrosymétriques, la *Génération d'Harmonique Seconde induite par Magnétisme* (GHSM) est produite principalement par la surface de l'aimant et donc cette technique expérimentale est un outil utile pour les études des surfaces magnétiques. En outre, si notre électroaimant était plaqué d'une fine couche de matériau nonmagnétique (par exemple de l'or, dont l'épaisseur ne dépasse pas la profondeur de pénétration de la lumière) la GHSM aurait encore lieu, cette fois produite par l'interface aimant/or. C'est précisément cette propriété physique – la génération d'harmonique seconde induite par magnétisme des interfaces – que nous avons utilisée afin de « dévoiler » la « conspiration » décrite auparavant.

## B.3. Résultats de cette thèse

La « conspiration » est bien réelle ! Bien que nous ne soyons pas les premiers à le clamer expérimentalement, nous sommes convaincus que nos résultats contribuent de manière importante à l'exposition publique du « complot ».

En effet, probablement la conclusion première de notre travail est que la GHSM peut être appliquée avec succès à l'étude de l'effet d'exchange bias. Bien que cette technique puisse être difficile à manier, comme nous l'avons montré, elle permet une *observation directe* des spins antiferromagnétiques responsables de l'exchange bias. On peut dire que leur présence à l'interface affecte littéralement la quantité de lumière bleue générée mais pour les « voir » nous avons employé des détecteurs optiques nettement plus sensibles que les yeux humains.

La GHSM est une technologie toute nouvelle en ce qui concerne l'étude de l'exchange bias, et comme l'a dit Nicolaas Bloembergen « lorsqu'on utilise une technologie nouvelle, ***à coup sûr*** de nombreux résultats nouveaux apparaîtront ! » Dans cette thèse, nous présentons deux alternatives aux manières classiques d'étudier l'effet d'exchange bias, qui sont capables de fournir de nouvelles informations sur les spins antiferromagnétiques lorsqu'une couche non magnétique est insérée entre les matériaux ferro- et antiferromagnétiques. En termes de l'image des deux sociétés humaines, on peut dire que lors du déploiement d'une force de paix internationale à la frontière, les conspirateurs antiferromagnétiques gardent leurs voisins ferromagnétiques dans leur ligne de mire et se préparent de nouveau à exercer leurs projets de domination mais, dans la pratique, la force de paix les empêche d'avoir une quelconque influence sur les ferromagnétiques. En outre, nous apportons la preuve que dans les systèmes que nous avons étudiés, il n'y a pas de formation de paroi de domaine ferromagnétique (il n'y a pas de collaborateurs ferromagnétiques dans le complot antiferromagnétique). Finalement, nous avons étudié l'oxydation d'un monocristal de nickel (Ni), matériau ferromagnétique, car l'oxyde de nickel ainsi formé (NiO) est un matériau antiferromagnétique. Ici encore

notre intérêt portait sur l'interface. A notre grande surprise, nous avons observé que tandis que les atomes de Ni étaient disposés en un réseau de petits carrés à la surface du cristal, ceux du NiO se sont organisés en triangles équilatéraux ! Pour l'instant, nous ignorons dans quelles conditions la nature préfère cet assemblage contre-intuitif à la simple superposition de carrés sur d'autres carrés, mais notre résultat a le mérite de démontrer que les relations de voisinage entre les sociétés ferro- et antiferromagnétiques sont aussi complexes que celles qui permettent d'emboîter parfaitement un triangle équilatéral dans un carré.

En conclusion, nous avons la conviction que cette thèse ne fait qu'entrouvrir la porte vers les études de l'effet d'exchange bias au moyen de la génération d'harmonique seconde induite par magnétisme et que sur le chemin de cette recherche, **à coup sûr**, de nombreux résultats nouveaux apparaîtront.

# Appendix C
# Обобщение за не специалисти

## C.1. Обменно предразположение

Всеизвестно е, че в заговорите малък брой хора тайно се споразомяват, работейки заедно, да повлияят на значително по-широко общество. В такива случаи често е твърде важно да се разкрият заговорниците, особено ако те са чужденци.

Много сходна ситуация съществува в сферата на магнетизма. Възможно е да се даде ясна зрителна представа за магнитния порядък във веществата като свържем малка магнитна стрелка с всеки индивидуален атом. Тази стрелка е оприличима на магнитна игла от компас, със северен и южен полюс, която се нарича *спин*. Можем да разграничим два вида магнитен порядък, тъй както бихме могли да обсъдим две човешки общества. В едното, назовано *феромагнетизъм*, всички магнитни стрелки (или спинове) са насочени в една посока и в следствие на това се появяват наблюдаеми магнитни свойства (виж Фиг. C.1 в ляво). Това би било едно много сговорно общество, в което всички работят заедно с общата цел – магнетизма. В другото общество, наречено *антиферомагнетизъм*, всички спинове са насочени в посока противоположна на тази на съседните и следователно, като цяло, никакви магнитни свойства не могат да бъдат забелязани (виж Фиг. C.1 в дясно). Това би било общество, в което всеки индивид е твърдо решен да се противопоставя на всеки друг, по който и да е въпрос, единствено, за да демонстрира колко той самият е различен. Разбира се, такова общество не постига нищо.

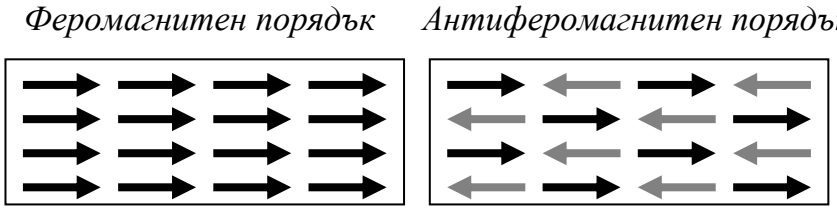


**Фиг. C.1** Двата главни вида магнитен порядък. Стрелките представляват посоката на спиновете на индивидуалните атоми във веществата.

И при все това... когато поставим феромагнитно вещество в контакт с антиферомагнитно, при определени температурни условия, може да наблюдаваме силна промяна в магнитното поведение на феромагнита. В същност изглежда така, като че ли феромагнита е под влиянието на малко магнитно поле породено от антиферомагнита. Това явление, названо *обменно предразположение*, бе открито

преди 50 години и оттогава намери множество технологични приложения. Например, употребява се в почти всички компютърни твърди дискове в света.

Но как е възможно това? Как могат тези антиферомагнитни спинове, които обикновено са прекалено заети със съседски спорове, да съумеят да окажат такова влияние върху феромагнитните спинове?

Едно вероятно обяснение се базира на много интересен ефект, съществуващ на разделящата повърхнина между материалите, която може да си представим като границата между двете общества. Под влиянието на феромагнитните спинове, малък брой спинове принадлежащи на антиферомагнита престават да се насочват в противоположна посока на съседите си и вместо това се подреждат съвкупно, като че ли са феромагнитни самите те. Правейки това, те пораждат магнитно поле, което влияе на близкостоящото феромагнитно вещество. Специфичната посока, към която тези антиферомагнитни спинове са насочват съвкупно се нарича посоката на *обменно предразположение*. Връщайки се към нашата образна представа за човешки общества, изглежда така като че ли намусените антиферомагнитни индивиди са решили да преустановят споровете си в името на една обща цел – господството над близкостоящото феромагнитно общество.

През последните 50 години, това обяснение бе само една теория за наличието на "тайно споразумение". Изследването на магнитни разделящи повърхнини е предизвикателна задача, главно защото те са заровени под един или даже няколко пласта различни материяли. Следователно, без възможността да наблюдават и изложат на показ участниците в "анитферомагнитния заговор", физиците можеха да правят само предположения и разбирането на явлението на обменно предразположение им убягваше.

Скорошните развития на експерименталните техники промениха това положение и за пръв път наблюдения на антиферомагнитни спинове, отговорни за обменното предразположение, бяха докладвани в научната литература. И все пак, множество въпроси остават без отговор. Например, връщайки се към нашите човешки общества, все още е неизвестно как са организирани тези антиферомагнитни заговорници, имат ли те съучастници от другата страната, и т.н.

За да подпомогнем разбирането на явлвнието на обменно предразположение (четете "да изложим на показ наличието на тайния заговор"), ние използвахме експериментална техника, която е изключително чувствителна към магнетизма на разделящи повърхнини, а именно: *Магнитно-предизвикано Пораждане на Втора Хармоника*. Зад това необичайно название се намира истински очарователна физика, която ще обсъдим в следващата част.

## C.2. Магнитно-предизвикано Пораждане на Втора Хармоника

Представете си, че се намирате в стая, в която единствената съществуваща светлина е червена. Например, фотолаборатория. Всички предмети, които виждате около вас би трябвало да изглеждат червени, понеже това е единственият цвят, който те могат да отразят. И все пак, възможно е някои от предметите да се окажат... сини! Това не е оптична илюзия, в смисъл, не става въпрос за измама

породена от вашите очи; единственият източник на светлина в стаята е червен, обаче вие виждате действителна синя светлина. Как е възможно това?

Явлението, за което става въпрос се нарича *Пораждане на Втора Хармоника* (ПВХ) и през 1981 г. холандският физик Николас Блумберген получи Нобеловата Награда за разработване на теорията, която го обяснява.

Пораждането на Втора Хармоника е частен случай на явление, което се назовава *Пораждане на Сбор на Чистоти,* където две или повече светлинни вълни се смесват. Можем да изразим това чрез уравнението:

$$I(\omega_1 + \omega_2) \propto I(\omega_1) \cdot I(\omega_2) \qquad \text{(C.1)}$$

където ω е честотата на вълната и $I$ е светлинната яркост.

В случая на ПВХ, две кохерентни (с еднаква дължина на вълна и фаза) светлинни вълни заедно създават трета вълна, която има двойна честота.

$$I(2\omega) \propto \left(I(\omega)\right)^2 \qquad \text{(C.2)}$$

Следователно, ако изберем началната честота от 3,7474 x $10^{14}$ Hz, което съответства на близо инфра-червено, породената комбинирана светлинна вълна ще има честота от $2 \cdot 3.7474 \cdot 10^{14} = 7.4948 \cdot 10^{14}$ Hz, което отговаря действително на синия цвят.

Въпреки че наблюдението на осветени в червено предмети, които изглеждат сини, е възможно на теория, действителното осъществяване изисква редица важни условия. Например, червената светлина трябва да е много ярка, за предпочитане-излъчвана от лазер. Лазерите имат множество качества, които играят роля в ПВХ: едноцветни излъчвания (това е важно за уравнение C.2), кохерентни вълни и силна яркост.

В експеримента с червеното осветление обсъждахме възожността някои от предметите да изглеждат сини. В действителност, твърде е възможно това да се случи с всички предмети! Причината е, че втора хармоника може да бъде породена от всяко вещество с ограничени размери. По-конкретно, явлението е следствие на нарушения на симетрии, каквито са например повърхностите и разделящите повърхнини. Не всички материали обаче пораждат същото количество втора хармоника и, следователно, синята светлина не е изцяло видима. Всъщност наблюдателят би трябвало да има изключително чувствителни очи. Въпреки че според някои учени фактора на преобразуване от $\omega$ на $2\omega$ в определени материяли е от рода на 80%, типичната стойност за този фактор след отразяване е само $10^{-13}$%.

А сега, представете си, че поставим електромагнит с мека магнитна сърцевина в осветената в червено стая и започнем да променяме посоката на магнетизиране чрез потичане на алтернативен ток всяка секунда. Ако сега погледнем синята светлина, породена от магнитната сърцевина, ще забележим че яркостта на ПВХ се променя всяка секунда, тоест магнитът "мига".

Магнетизмът участва в пораждането на втора хармонична светлина понеже е свързан с нарушението на симетрията за промяна посоката на времето. Спиновете на атомите в магнетизирани вещества могат да бъдат разгледани като следствия на малки единични намотки около всеки атом, през които протича електрически ток в

дадена посока. В такъв случай, преобръщане посоката на магнетизиране е равностойно на промяна в тази на времето, така че електрическият ток да протече в обратна посока.

За да наблюдаваме гореспоменатото "мигане" са необходими симетрични нарушения, както в структурата на веществата, така и в промяната на посоката на времето. Иначе казано, в материали с център на симетрия, *Магнитно-предизвикано Пораждане на Втора Хармоника* (МПВХ) се явява главно поради повърхността на магнита и, следователно, ефекта може да се използва като уред за изследване на повърхностния магнетизъм. Освен това, ако магнитът е покрит с тънък пласт немагнитен материал (например злато с дебелина по-малка от тази на пробивността на светлината) МПВХ ще бъде отново наблюдавана, този път произхождаща от заровената повърхнина разделяща магнита от златото. Ние използвахме точно това физическо свойство – пораждането на магнитно-предизвикана втора хармонична светлина от разделящи повърхности – за да подпомогнем "разкритието" на гореспоменатия "заговор".

## C.3. Резултатите в тази теза

"Конспирацията" е реална! Въпреки че не сме първите, които твърдят това чрез експериментите си, ние сме уверени в значимостта на нашите резултати като важна стъпка към публичното разкритие на "заговора".

Действително, вероятно най-главното заключение от нашата работа е, че МПВХ може да бъде успешно приложено в изследването на ефекта за обменно предразположение. Макар че показваме колко деликатно е боравенето с тази техника, ние също доказваме нейната способност да *наблюдава пряко* антиферомагнитните спинове отговорни за обменното предразположение. Тяхното наличие буквално променя яркостта на породената синя светлина, въпреки че, за да "видим" това, ние ползвахме оптични детектори много по-чувствителни от човешките очи.

МПВХ е много нова технология спрямо изследването на обменното предразположение, и както каза Николас Блумберген, "когато използвате нова технология, нови неща ***непременно*** се случват". В тази теза ние представяме две алтернативи на класическия начин за изследване на обменното предразположение, които са способни да доставят нова информация за антиферомагнитните спинове, когато немагнитен разделящ слой е вмъкнат между анти- и феромагнита. Връщайки се към картината на човешките общества, може да кажем, че след пристигането на интернационална мирна сила на границата, антиферомагнитните заговорници продължават да забелязват близкостоящото феромагнитно общество и, следователно, отново се подготвят за господствен сценарии, но на практика мирните сили им пречат да окажат влиянието си. Освен това, демонстрираме, че в изследваните от нас системи, не съществуват частични феромагнитни доменни стени (няма феромагнитни съучастници в антиферомагнитния заговор). Най-накрая, ние изследвахме окисляването на монокристал от никел (Ni), който е феромагнитен материал, тъй като полученият никелов окис (NiO) е антиферомагнитен. Отново нашето внимание бе насочено към разделящата

повърхнина. С изненада забелязахме че, докато на повърхността на никеловия монокристал атомите бяха разположени в мрежа от квадратчета, тези на никеловия окис се организираха в равностранни триъгълници! За момента условията, при които природата предпочита този противоинуитивен монтаж пред простото съпоставяне на квадратчета върху квадратчета остава неизвестен. При все това ние доказваме, че съседските отношения между феромагнитните и антиферомагнтитните общества са толкова лесно разбираеми, колкото и причините, които могат да обяснят едно идеално нагаждане на равностранен триъгълник в квадрат.

В заключение, можем с увереност да кажем, че тази теза само открехна вратата към изследванията на обменното предразположение с магнитно-предизвикано пораждане на втора хармоника и, че по пътя на тези проучвания, ***непременно*** ще се случат още много нови неща.

# List of publications

- V.K. Valev, M. Gruyters, A. Kirilyuk, and Th. Rasing, "Influence of quadratic contributions in magnetization-induced second harmonic generation studies of magnetization reversal", Phys. Stat. Sol. (b) **242**, No. 15, 3027–3031 (2005)

- V.K. Valev, M. Gruyters, A. Kirilyuk, and Th. Rasing, "Direct observation of exchange bias related uncompensated spins at the CoO/Cu interface", Phys. Rev. Lett. **96**, 067206 (2006)

- V.K. Valev, M. Gruyters, A. Kirilyuk, and Th. Rasing, "Temperature dependence of magnetization-induced second-harmonic generation at buried exchange biased interfaces", Phys. Rev. B **73**, 233101 (2006) (Brief Reports)

- V.K. Valev, A. Kirilyuk, Th. Rasing, F. Dela Longa, J.T. Kohlhepp, B. Koopmans, "Oscillations of the net magnetic moment and magnetization reversal properties of the Mn/Co interface", *submitted*

- Jae-Woo Jeong, V.K. Valev, I. L. Lyubchanskii, Sung-Chul Shin and Th. Rasing, "Direct observation of controlled strain-induced second harmonic generation in $Co_{0.25}Pd_{0.75}$ thin film on $Pb(ZrTi)O_3$ substrate", *submitted*

- V.K. Valev, M. Gruyters, A. Kirilyuk, and Th. Rasing, "Magnetic interface between "nonmagnetic" materials", Physicalia Mag. **28**, n°3, 203 (2006) *(invited contribution)*

- V.K. Valev, A. Kirilyuk and Th.Rasing, "Nonlinear magneto-optical probing of magnetic nanostructures: observation of NiO(111) growth on a Ni(001) single crystal", *submitted*

# Curriculum Vitae

**Name:**
Ventsislav Kolev Valev

**Date of birth:**
31st August 1976

**Place of birth:**
Silistra, Bulgaria

| | |
|---|---|
| 1993 – 1996 | Highschool, *Lycée de l'Hartelolire*, Brest, France |
| 1996 – 2000 | Bachelor Degree in Physics, *Université de Bretagne Occidentale*, Brest, France |
| 2000 – 2001 | Masters Degree in Physics, *University of Wales, Cardiff*, Cardiff, United Kingdom |
| 2001 – 2006 | Ph.D. in Physics, *Radboud University Nijmegen*, Nijmegen, the Netherlands |
| 2006 – present | Post-doc, *Katholieke Universiteit Leuven*, Leuven, Belgium |